

SIMULATIONS OF PLANET MIGRATION
DRIVEN BY THE SCATTERING OF SMALLER BODIES

by

DAVID ROBERT KIRSH

A thesis submitted to the
Department of Physics, Engineering Physics and Astronomy
in conformity with the requirements for
the degree of Master of Science

Queen's University
Kingston, Ontario, Canada
September 2007

Copyright © David Robert Kirsh, 2007

Abstract

Planet migration is an important part of the formation of planetary systems, both in the Solar system and in extrasolar systems. When a planet scatters nearby comet- and asteroid-size bodies called planetesimals, a significant angular momentum exchange can occur, enough to cause a rapid, self-sustained migration (change of semi-major axis a) of the planet. This migration has been studied for the particular case of the four outer planets of the Solar System, but is not well understood in general.

This thesis used the Miranda computer simulation code to perform a broad parameter-space survey of the physical variables that determine the migration of a single planet in a planetesimal disk. A simple model matched well with the dependencies of the migration rate for low-mass planets in relatively high-mass disks:

$$\frac{da}{dt} = \frac{2a \pi \Sigma a^2}{T M_{Sun}} \quad (1)$$

with T the orbital period and Σ the surface density of the planetesimal disk. When the planet's mass exceeded that of the planetesimals within a few Hill radii, the migration rate decreased strongly with planet mass. Other trends were identified with the root-mean-squared eccentricity of the planetesimal disk, the mass of the particles dragged by the planet in the corotation region, and the index of the surface density power law. The issue of resolution was also addressed, and it was shown that

many previous works in this field may have suffered from being under-resolved.

The trends were discussed in the context of an analysis of the scattering process itself, which was performed using a large simulation of massless planetesimals. In particular, a bias in scattering timescales on either side of the planet's orbit leads to a very strong tendency for the planet to migrate *inwards*, instead of outwards.

The results of this work show that planet migration driven by planetesimal scattering should be a widespread phenomenon, especially for low-mass planets such as still-forming protoplanets. The simple model provided here, augmented by many more subtle effects, will prove essential to any future work in this underestimated field.

Acknowledgements

I would like to thank my supervisor, Martin Duncan, for many interesting discussions, several debates (it's not damped migration!), and for keeping me on track without applying any stress. I would also like to thank Douglas McNeil for a great deal of help in the early stages of my research, and for presentation advice. I would also like to acknowledge the financial support of the Natural Sciences and Engineering Research Council of Canada. Finally, this work could not have been done without the personal support of Amanda Schwartz, thank you!

Table of Contents

Abstract	i
Acknowledgements	iii
Table of Contents	iv
List of Tables	vii
List of Figures	viii
Chapter 1:	
Introduction and background	1
1.1 Motivation	1
1.2 Epochs of planet-disk interaction	2
1.3 Keplerian orbits	4
1.4 The three-body problem	8
1.5 The Jacobi integral	9
1.6 Hill radius and the feeding zone	12
1.7 Horseshoe orbits and mean motion resonances	18
1.8 Jacobi integral asymmetry	21
1.9 Synodic Period	23

1.10	Structure of the thesis	25
Chapter 2:		
	Previous work	26
2.1	Early work	26
2.2	Ida, Bryden, Lin and Tanaka 2000	29
2.3	Gomes, Morbidelli and Levison 2004	32
2.4	Works using planetesimal-driven migration	34
Chapter 3:		
	Simulations	36
3.1	SyMBA	36
3.2	Setup and initial conditions	39
3.3	Parameter space	41
Chapter 4:		
	The scattering process	43
4.1	Growth of wings	44
4.2	Horseshoes and resonances	62
4.3	Angular momentum transfer	64
4.4	Dependence on wing height	68
4.5	Imbalance	72
Chapter 5:		
	Planet migration	78
5.1	Baseline rates	78

5.2	Resolution	86
5.3	Planet mass	90
5.4	Eccentricity	101
5.5	Horseshoes	105
5.6	Initial semi-major axis	111
5.7	Final mass trend	113
5.8	Planet mass growth	121
5.9	Variation in the Hill radius and wing mass	124
5.10	Self-heated initial conditions	126
5.11	Surface density power law index	128
 Chapter 6:		
	Discussion and conclusions	139
6.1	Trends	139
6.2	The interpretation of the fiducial rate	144
6.3	Resolution	145
6.4	Migration direction	147
6.5	The one-scatter limit	150
6.6	Future work	152
 Bibliography 154		
 Appendix A:		
	Supplementary information	158
A.1	Maximum eccentricity change	158

List of Tables

- 5.1 Delay and direction of migration for a gap in the planetesimal disk of several Hill radii inside and outside of the planet's semi-major axis. . . 98

List of Figures

1.1	The orbital angles Ω the longitude of the ascending node, ω the argument of pericentre, and i the inclination are shown for an orbit compared to a reference plane and a reference direction. [22]	7
1.2	Curves of constant Tisserand parameter are shown, with four C_T values calculated at four points: $a = 0.95, 0.96, 0.98, 1; e = 0; i = 0$. Each of these values of C_T has curves on both sides of the planet at $a_P = 1$. Also shown is a dotted line interior to the planet corresponding to apocentre Q at the planet, and exterior to the planet corresponding to pericentre q at the planet. Both plots are identical except for the eccentricity scale.	11
1.3	The particle P orbits G the guiding centre on an elliptical orbit of semi-major axis $2ae$ while the guiding centre is on a circular orbit of radius a about the star at focus F . [22]	15
1.4	Two planets are shown on elliptical orbits about the large central star, at various stages in their orbits, on a 2:1 resonance where the inner planet completes 2 orbits for every 1 orbit of the outer planet. Conjunctions occur at a large distance, ensuring no close encounters will ever occur. [22]	19

1.5 Two horseshoe orbits a low-mass particle orbiting the star μ_1 will experience when having a semi-major axis within $1R_H$ of the planet μ_2 , with the helical case having an eccentricity and the smoother case having a very low eccentricity. Two Lagrange points are marked. [22] 20

2.1 Change in planetesimal eccentricity and angular momentum, normalized to the Hill factor and $v_P R_H$ respectively, for circular orbits on their first encounter with a planet. The changes are shown as a function of the distance to the planet in Hill radii. From Ida *et al.* 2000 [15]. 30

4.1 Snapshots of Jacobi wing growth at six values of time, in multiples of the planet's period. Particles all started at $e = 10^{-4}$, distributed evenly from 22.85 to 27.15AU. Particles in mean motion resonances outside of the wing produce jagged spikes. 46

4.2 Particles with eccentricity $e < 0.01$ were counted in 1000 equally spaced bins of semi-major axis. The resulting surface number densities are shown in units of the Hill radius from the planet. The inner edge of the inner wing and the outer edge of the outer wing are marked. . . . 48

4.3 The average eccentricity for particles in the inner and outer wings, where the wings are defined to range from $1R_H$ from the planet to a maximum value of $C_T^{feed}(a, e) = C_T(a_P + 3.5R_H, 0)$. Both particle sets rapidly go to higher eccentricity, with the outer wing proceeding higher than the inner. 50

4.4 The absolute distance of the centre-of-mass for each wing is shown in units of the Hill radius, where the wings are defined as in figure 4.3. Both wings move away from the planet, with the outer wing moving farther. 51

4.5 The number of particles in each wing is traced in the top panel, where the wings are defined as in figure 4.3. The bottom panel shows the percentage difference between the wings, with the outer wing starting with more than the inner and gaining from there. Absolute particle number drops due to planetary accretion. 52

4.6 Fractions binned by Tisserand parameter C_T . The lines in the bottom panel show the fraction of particles in each wing, by C_T bin that have a $\Delta e > \chi/10$ during one planetary period. The line fit to it is what would be expected if every particle had an interaction once a synodic period, where the synodic period is calculated from the C_T value's corresponding a at $e = 0$. The green and blue dotted lines are the fraction, of those that have an interaction, that switch wings and therefore cross the planet's orbit. Crossing "out" would imply starting interior to the planet and ending exterior, and vice versa. 56

4.7 The distribution of scattering events by their change in planetesimal eccentricity, displayed logarithmically. Only wing particles ($C_T < C_T^{feed}$, $|a - a_P| > 1R_H$) are included. Each frame displays the distribution averaged over a certain number of orbits stated in the top left. Scatterings that stay in the outer or inner wing upon scattering are segregated. 59

4.8	The distribution of scattering events with respect to the change in eccentricity of the planetesimal. Each frame displays the distribution averaged over a certain number of orbits stated in the top left. Scatterings crossing outwards or inwards are segregated.	61
4.9	The average change in eccentricity (in Hill units) is displayed as a function of Tisserand parameter C_T over 150 bins in that parameter. The changes are averaged over the bin and over a number of orbits stated in the top left. Scatterings crossing outwards or inwards are segregated. The zero line has been indicated by a dotted line when necessary. Values of C_T for which no Δe is plotted had no crossing events recorded in the bin throughout the interval indicated.	63
4.10	Angular momentum differences counted for four types of scattering: particles that stay in the inner/outer wings in the bottom frame; particles that cross between the wings in the middle frame. The absolute value of the summed differences of these categories are shown, with the particles that stayed in and the particles that crossed in actually producing a negative change in angular momentum. The difference between the two curves in each frame are shown in the top frame, and these are further summed to give the net angular momentum change for the entire disk.	66
4.11	Angular momentum changes between timesteps were integrated for various intervals of time for particles binned by C_T in 150 bins. Particles were grouped by the four in/out stay/cross categories, to show where the strongest kicks to the planet would be coming from.	69

4.12	The percentage of crossings from a given e -bin (out of 150 bins) and wing, per the number of scatterings that occurred in that bin. The eccentricity is expressed in Hill units. The bottom panel shows the percentage difference between the crossing probability in the outer and inner wings.	71
4.13	Total numbers of particles within the defined planetary wings were counted as a function of time in the upper plot. In the lower plot the percentage difference between the counts are shown, and can be seen to level off.	73
4.14	The initial and final percentage differences of the particle number counts in inner/outer wings are plotted for varied planet mass (plotted in terms of the Hill factor), with the fit to the initial set by equation 1.26. Also shown is a curve of three times the result of equation 1.26.	75
5.1	The factor f varies the planet/planetesimal mass fraction and the number of particles per Hill radius, increasing the resolution of the planet's migration from 25AU.	89
5.2	Migrations are shown for indicated planet masses in a constant-mass disk. Best-fit lines are also shown with the data to demonstrate the accuracy of constant migration rates.	92
5.3	Migrations are shown for indicated planet masses in a constant-mass disk, along with best-fit lines.	93

5.4 Four to six migration rates (in units of the $n\sigma v$ value) are plotted for each value of M_P/M_{Wing} , with a line drawn along the average values. The light red vertical line indicates the change from low \tilde{e} to high \tilde{e} . The blue line indicates the one-scatter limit, which is satisfied only on the left of this line. 95

5.5 Migration rates in units of the fiducial rate for runs in which the disk root-mean squared eccentricity was set to 10^{-4} (red points) and twice the Hill factor (green points). The lines connect the averages for each value of the planet mass. 102

5.6 Migration rates in units of the fiducial value are shown for runs at multiple values of the root-mean-squared Hill eccentricity of the disk, with a fit provided by equation 5.26. 104

5.7 Migration rates in units of the fiducial rate as a function of the mass ratio between one Jacobi wing and the horseshoe zone, with a fit provided by equation 5.27. 107

5.8 An example of horseshoe-damped migration, with an oscillation period of ~ 5000 years ($T_{syn}(1R_H)$), for the case with $M_{hs} = 4.8M_{wing} = 6.7M_P$, for four runs. 108

5.9 The fraction of the original horseshoe particles that remain in the horseshoe region after 7×10^4 years for the various values of M_{wing}/M_{hs} . Only the slowest migrators, dragged down by the highest horseshoe masses, manage to retain any particles. 110

5.10 Migration rates divided by the fiducial rate for four runs at each studied value of the planet’s semi-major axis a_P . Averages for the first four and last three a_P values are separated, but no real trend is apparent (note the small vertical scale). 114

5.11 Migrations are shown in a dynamically cold disk with no horseshoe particles, with a planet of mass $M_P = 4.5M_E$, for a varied mass disk (indicated by the value of M_P/M_{wing} in the upper corner of each migration). When possible, two constant-rate fits have been applied to the first and second phase of the migration, as described in the text. One higher resolution run is shown for $M_P/M_{wing} = 100$ in black. . . 118

5.12 More migrations are shown, now with values of M_P/M_{wing} close to or less than one. 119

5.13 Migration rates in units of the fiducial rate for several runs at each of various values of the planet’s mass to the wing mass. These runs include no horseshoes, and a dynamically cold initial disk. Most runs have early (and short-lived) migration rates that are faster than the later rate, and in those cases both values are shown. High planet mass cases are estimates, as the migration is unlikely to be well-described by a constant rate. 120

5.14 Migration for the case $M_P/M_{wing} = 5$, extended to 5×10^5 years, with constant migration rate fits displayed. 122

5.15 Change in the planet’s mass, relative to its initial mass of $4.5M_E$, for six values of M_P/M_{wing} taken from the M1 runs. The faster migrators, at the bottom, reach the edge of the disk before the end of the simulation. 125

5.16 Migrations shown for the M2 runs, replicating M1 runs except for a period of massless heating before the migration was begun. The M2 runs are shown in red, green, blue and pink, while the M1 runs are shown in black, grey, orange and light blue. The inward green line for $M_P/M_{Wing} = \frac{2}{3}$ was heated for five times longer. 129

5.17 Migrations were fit with equation 5.39, using least-squared methods to determine the factor f . The factors are shown separately for the outwards and inwards migrations as a function of the surface density index k . The averages for each group are also shown as horizontal lines. The bottom panel also shows the initial mass difference between the wings as a function of k 133

5.18 Migrations shown are for the inward-migrating cases with surface density power law index k indicated, and the best-fit line from equation 5.39 also shown. The $k = -3$ case breaks at the edge of the disk, while 'bends' are visible in the $k = 0$, $k = +1$ cases which are likely due to the migrations following below the one-scatter limit. . . 135

5.19 Migrations shown are for the outward-migrating cases with surface density power law index k indicated, and the best-fit line from equation 5.39 also shown. All breaks are due to the planet reaching the edge of the disk. The bottom-right panel shows two runs for $k = 3$ which had expanded disks to allow longer migrations. 136

5.20 The ratio of the planet mass to the wing mass (calculated using $M_{wing} = 4\pi\Sigma_0 R_H a_P (a_P/a_0)^k$ for several runs with different surface density power law indices k . An increase in this fraction beyond 1 would tend to slow/damp the migration. 138

Chapter 1

Introduction and background

1.1 Motivation

Observations of extra-solar systems have shown that planets are not always arranged as they are in our Solar System. Gas giants with masses of roughly a tenth to ten Jupiter masses have been found closer to their stars than Mercury is to the Sun (earning them the name Hot Jupiters) and this has been a surprise (Mayor and Queloz, 1995 [20]). While exoplanets have been found at larger distances, and smaller masses (more than 200 exoplanets have been found, see *exoplanets.org* for a frequently-updated list), our understanding of Hot Jupiters in particular provides an intriguing mystery. Early solar system evolution models suggested that planets formed *in situ*, but not enough material would exist so close to the star to allow such formation of Hot Jupiters. This meant that new models had to be explored where planets are able to *migrate* and change their orbital distance from their central stars. Additionally, there is increasing evidence based on the orbits of small icy bodies beyond Neptune that migration has occurred in our own Solar System (Malhotra,

1993 [19]).

Migration schemes commonly utilize angular momentum exchange with the gas left over from the star's formation to propel planets to new orbits. This migration turns out, however, to often be too fast to easily explain the survival of planets, and they could end up thrown into the star. This remains one of the largest problems in planetary astrophysics: how do planets move? This thesis will explore the problem using a simple mechanism often overlooked: planetary interactions with small bodies similar to comets and asteroids.

1.2 Epochs of planet-disk interaction

During the initial collapse of a protostar, much of the material from the original gas cloud does not fall directly in, but is pulled into a gas disk about the star as it conserves angular momentum. This gas disk will survive for about three to ten million years after the star's formation (Haisch *et al.* 2001 [10]), and it is within this disk that planet formation begins.

Two main competing models exist for giant planet formation. One model has the gas in the disk form gravitational instabilities that directly collapse into a gas giant, on timescales of orbital periods (Boss 2001 [1]). However, this model may require overly high gas densities, and does not explain the rocky terrestrial planets. The second model is the core accretion model (Pollack *et al.* 1996 [26]), which has the solid component of the gas disk (silicates, carbon, oxygen etc.) condense out of the gas and form dust and icy bodies. The dust aggregates, and clumps, and eventually the solid component becomes comet- and asteroid-size objects called planetesimals. These are about a kilometre in scale, and some may survive throughout the entire

planet formation process to remain in the current Solar System.

Planetesimals will collide and stick together and grow over time, eventually reaching the runaway accretion phase (Kokubo and Ida, 1995 [18]). At this point, the bigger an object is the faster it will grow, and so an object that is slightly larger than the others will grow faster, and become even bigger, and ultimately 'run away' in mass from all the others. Eventually this phase will transition to the oligarchic phase, where protoplanets begin to gravitationally dominate their neighbourhood (Wetherill and Stewart, 1993 [33]). At this point many protoplanets have formed, but are regularly spaced apart as any pair that come close together will scatter each other and/or collide. Protoplanets in the oligarchic phase continue to accrete planetesimals, but it is in this phase as well that those in the outer regions may have attained enough mass to attract and hold a gaseous envelope. As they now accrete gas, they may again reach a runaway phase where their growing mass allows them to attract even more gas. In some cases gas giants can form, and in others rocky or icy planets (protoplanets that never managed to accrete much gas) will also be present in the system.

Throughout planet growth, the gas disk has been dissipating, with the inner region being drawn into the star, and the outer region being blown away. After the approximately three to ten million year depletion time, all that is left is the planets and the disk of planetesimals. This leaves time (several billion years for our Solar System) during which these two components will interact. The planets will scatter and accrete planetesimals, and this process will not only continue to change their mass, but will also alter their orbital elements, in particular their distance to the star as we shall see.

1.3 Keplerian orbits

The orbits of planets and planetesimals about the Sun were identified as ellipses by Johannes Kepler in 1609 to 1619, using empirical techniques. This section will describe these orbits and define the relevant physical quantities that describe them, mainly using Murray and Dermott (1999) [22]. The ellipses are stable orbits with the Sun at one focus of the ellipse, and barring interplanetary interactions they will remain unchanged. The two most fundamental measures of an orbit are the semi-major axis a and the eccentricity e . The semi-major axis is half the length of the long axis, while the eccentricity measures the departure from circularity. Zero eccentricity therefore gives a circular orbit where the semi-major axis is the radius. Eccentricity of 1 gives a parabola, larger than 1 gives a hyperbola and $0 < e < 1$ is the regime of ellipses. While the semi-major axis describes the average distance of the planet from the Sun, two other measures are often more useful: the maximum distance from the sun, the apocentre Q ; and the minimum distance from the sun, the pericentre q . Respectively, these can be expressed easily as:

$$Q = a(1 + e) \tag{1.1}$$

$$q = a(1 - e) \tag{1.2}$$

One full rotation about the sun, say from apocentre to apocentre, is given by the orbital period T . Using units based on the terrestrial year, and using the semi-major axis of the Earth to be one astronomical unit (1 AU) and using that as the unit of distance from a star of one solar mass, the period can be expressed as:

$$T^2 = a^3 \tag{1.3}$$

and this was Kepler's third law. Using the period, the mean motion of the planet can be defined, which is the angle it sweeps out per year:

$$n = \frac{2\pi}{T} \quad (1.4)$$

and this is in fact the angular speed for a circular orbit. The speed of the planet will vary along its elliptical orbit, and can be derived in particular at the apocentre Q and the pericentre q as:

$$v_Q = na\sqrt{\frac{1-e}{1+e}} \quad (1.5)$$

$$v_q = na\sqrt{\frac{1+e}{1-e}} \quad (1.6)$$

Two other useful measures of a Keplerian orbit are the angular momentum and the energy. The specific angular momentum $h = \vec{r} \times \dot{\vec{r}}$, which is per unit mass, comes out to be:

$$h = na^2\sqrt{1-e^2} = 2\pi\sqrt{a(1-e^2)} \quad (1.7)$$

while the energy (potential plus kinetic) of the orbit is derivable as

$$E = -\frac{\pi}{a} \quad (1.8)$$

In a system with multiple planets, or even a system with one planet and many planetesimals, the coordinate system requires more than just a and e to specify an orbit. This is because the problem is three dimensional, as not all orbits will be in the same plane or oriented in the same direction (where the direction of an orbit can be chosen as the line connecting peri/apocentre). Defining a reference plane, then, the third dimension can be specified using the inclination i , which gives the angle between the orbital plane and the reference plane.

In order to fully characterize a planet's location and velocity instantaneously, three positional coordinates and three velocity values would be required. For Keplerian orbits, however, the three orbital values a, e, i are sufficient as long as the direction of the orbit and the planet's position *within* its orbit is also specified. Three orbital angles are used for this: Ω the longitude of the ascending node; ω the argument of pericentre; and M the mean anomaly. The angle Ω is from some reference direction on the reference plane to the point where the orbit crosses the reference plane. This crossing occurs at two nodes on either side of the orbit, but the *ascending node* is the one where the orbit crosses from below to above the reference plane in the sense of the planet's motion. The angle ω is up from the reference plane along the orbital plane to the pericentre. The angle M is the fraction (from zero to 2π) of the orbit from the pericentre that the planet has moved as a function of time. The mean anomaly can therefore be expressed as: $M = n(t - \tau_{peri})$ where t is the time since τ_{peri} , the time of pericentre passage. The angles Ω , ω and i are shown in figure 1.1 from Murray and Dermott (1999) [22].

Keplerian orbits can be derived from gravitational forces, which give for the relative motion of two masses m_1 and m_2 :

$$\frac{d^2\vec{r}}{dt^2} + \mu\frac{\vec{r}}{r^3} = 0 \quad (1.9)$$

where \vec{r} is the distance vector between the two masses and $\mu = G(m_1 + m_2)$ with G the gravitational constant. Taking the vector product of \vec{r} with this and integrating gives the specific angular momentum $\vec{h} = \vec{r} \times \dot{\vec{r}}$. It can be shown that \vec{h} is a constant, which tells us that the motion of the masses lies in a plane: the orbital plane. The equation can be solved in polar coordinates to give:

$$r = \frac{h^2/\mu}{1 + e \cos \theta - \varpi} \quad (1.10)$$

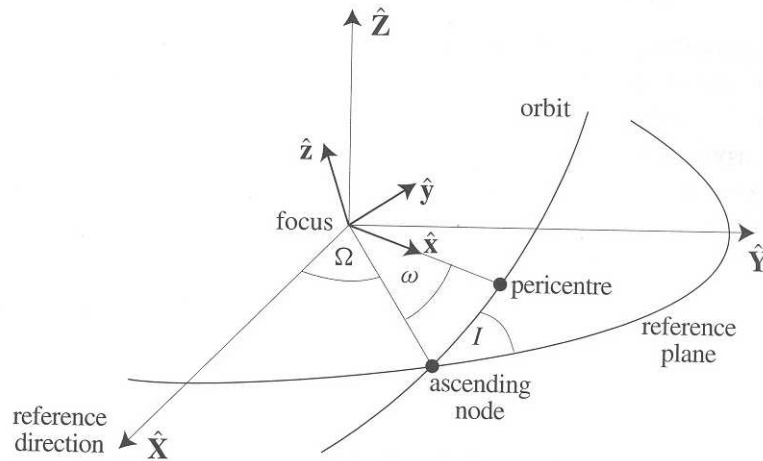


Figure 1.1: The orbital angles Ω the longitude of the ascending node, ω the argument of pericentre, and i the inclination are shown for an orbit compared to a reference plane and a reference direction. [22]

with a phase ϖ . This is the general equation of a conic, and an ellipse for $0 < e < 1$, with the mass m_1 at one focus and the other focus empty. From this result the orbital period can be calculated to be, in SI units:

$$T^2 = \frac{4\pi^2}{\mu} a^3 \quad (1.11)$$

which reduces back to $T^2 = a^3$ for the terrestrial units described above, in which $\mu = 4\pi^2$.

These equations do not contain an explicit time dependence, which makes solving for the position of m_2 difficult. The mean anomaly M , however, can be measured as a function of time and used to solve for an angle E , called the eccentric anomaly and related by $M = E - e \sin E$, Kepler's equation. The (x, y) positions, or the distance r can then be calculated from E . Kepler's equation is transcendental in E , complicating the solution. Nonetheless, the fact that the two-body problem can be

solved provides the foundation for most of orbital mechanics.

1.4 The three-body problem

While the two-body problem has an analytic solution with closed, regular orbits, adding even one more mass to the system changes everything. The simplest case, known as the circular restricted three-body problem, has two massive bodies on circular, coplanar orbits about their centre of mass, and a third object that is too small to influence these orbits. The motions of the massive bodies, the star and a planet say, are predictable; that of the third body, the planetesimal, is not. There is no analytic solution for the planetesimal's orbit, and in fact there are infinite possibilities to what it could do: everything from a stable orbit to an ejection from the system. Except for several constrained cases that can be solved in more detail, investigating this problem requires numerical integration of the full equations of motion.

The focus of this thesis will be on a generalization of the three-body problem. One planet will be immersed in a sea of planetesimals which will have individual masses much less than the planet's, and will not interact with each other. Chapter 4 will focus on the case where the planetesimals effectively have zero mass, such that every planetesimal is involved in its own three-body interaction. The results of this chapter could be viewed as a hundred thousand solutions to the three-body problem. Chapter 5 will infuse the planetesimals with mass, enough that the entire collection will in most cases outweigh the planet. In this situation each planetesimal will be instantaneously experiencing an approximation to the three-body problem, but the planet will be so perturbed that it will not remain on a constant circular orbit.

The following sections will describe several quantities and qualities of orbits in the

circular, restricted three-body problem.

1.5 The Jacobi integral

Neither the energy nor the angular momentum of a particle is conserved in the circular restricted three-body problem, but a conserved quantity does exist in the form of the Jacobi integral, also called the *integral of relative energy*. In a non-rotating inertial frame centered on the center-of-mass of the system, this integral is of the form:

$$C_J = E - \vec{n} \cdot \vec{L} \quad (1.12)$$

where E is the energy and \vec{L} the angular momentum of the planetesimal, and \vec{n} is the orbital velocity of the planet. As this integral is the only conserved quantity, the problem has no exact solution, which leads to the need for simulation. Provided the planet is much less massive than the star, and that the planetesimal is not too close (within the Hill sphere, see section 1.6) to the planet, the integral can be simplified using known expressions for the relevant quantities. This leads to the useful dimensionless Tisserand parameter that is expressed relative to the planet's semi-major axis a_P as:

$$C_T = \frac{a_P}{a} + 2\sqrt{\frac{a}{a_P}}\sqrt{1 - e^2} \cos i \quad (1.13)$$

This parameter is used in the Solar System to characterize and identify comets, as a comet will retain the same characteristic value relative to Jupiter before and after a scattering event (a strong interaction with Jupiter that can greatly alter various other orbital parameters). For small i , this simplifies to what will be used for the majority of this thesis:

$$C_T = \frac{a_P}{a} + 2\sqrt{\frac{a}{a_P}}\sqrt{1 - e^2} \quad (1.14)$$

1.5.1 Jacobi wing structure

Scattering events, when a planetesimal passes close to a planet (normally occurring near *conjunction*: when the planet and the planetesimal are on a line along with, and on the same side of, the sun) and has its orbit perturbed, tend to increase a planetesimal's eccentricity, especially for nearly circular orbits. The conservation of the Tisserand parameter then tells us what new orbital parameters the planetesimal can obtain. If the semi-major axis and the eccentricity are the two most important of these, it makes sense to trace the orbital change in the $a - e$ plane. The question becomes: what do lines of constant Tisserand parameter look like in the $a - e$ plane?

Examples of the curves of constant Tisserand parameter are shown in figure 1.2 for two ranges in eccentricity. The curves begin (at zero eccentricity) at inward displacements from the planet (at $a = a_P = 1AU$) of $\Delta a_{in}(e = 0) = 0, 0.02, 0.04, 0.05AU$, and the identical value of C_T is also shown outside of the planet (the corresponding outward displacement is slightly different). A planetesimal that started at one of these initial displacements and had its eccentricity increased would therefore move up and away from the planet in this plane. One curve on each side of the planet exactly corresponds in C_T to another on the other side, however, so planetesimals that conserve C_T can also cross between the wings. A planetesimal crossing between wings would therefore be crossing the planet's orbit as well, in that its semi-major axis (and angular momentum) would be changing from greater than the planet's to less than the planet's or vice versa.

A useful analogy to the wing-crossing interaction is also presented in figure 1.2, in the form of the dotted line. This dotted line presents curves of (a, e) for which the apo/pericentre is located directly at the planet's semi-major axis, $Q = a_P$ and

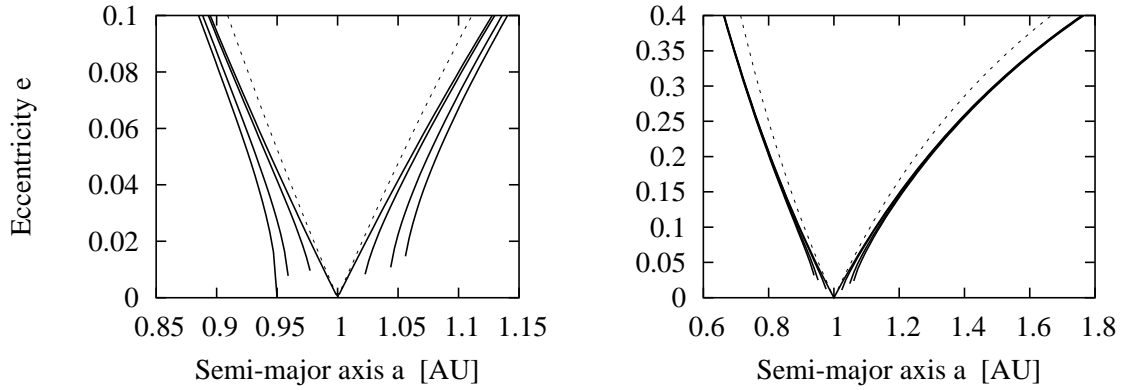


Figure 1.2: Curves of constant Tisserand parameter are shown, with four C_T values calculated at four points: $a = 0.95, 0.96, 0.98, 1$; $e = 0$; $i = 0$. Each of these values of C_T has curves on both sides of the planet at $a_P = 1$. Also shown is a dotted line interior to the planet corresponding to apocentre Q at the planet, and exterior to the planet corresponding to pericentre q at the planet. Both plots are identical except for the eccentricity scale.

$q = a_P$. The apocentre is the inner curve and the pericentre is the outer curve. These curves roughly approximate the conserved- C_T curves, especially in slope. This implies that a planetesimal staying in the inner wing would be approximating an apocentre that stays directly at the planet's semi-major axis. A further implication is that if a planetesimal crosses from the inner wing to the outer wing during a scattering event, its initial apocentre (at the planet's orbit) would become its new pericentre. This approximation could be refined with a small offset such that $Q_{init} = a_P - \delta \rightarrow q_{final} = a_P + \delta$, but is suitable to first order for later purposes.

In the region close to the planet, planetesimals will very quickly move up these curves, producing a wing-shaped structure in the $a - e$ plane, and will supply the angular momentum that will fuel the planet's migration. These curves therefore trace a very important population, and are referred to as Jacobi wings. While all particles conserve exactly C_J (and very closely C_T), the Jacobi wing particles in particular are

in a well-defined region about the planet, which will be discussed in the next section.

Several qualities of the wings are visible in the figure. At low eccentricity (on the same scale as the Δa at $e = 0$) the wings are very steep, implying that early excitation of the eccentricity will not induce much semi-major axis change in the planetesimals. At higher eccentricity the constant- C_T curves converge, narrowing the wing in a , and the outer wing begins skewing to much higher Δa than the inner wing. This last implies that at high eccentricities, planetesimals in the outer wing will be much farther from the planet than those in the inner wing.

1.6 Hill radius and the feeding zone

Far from a large planet, planetesimals will orbit the sun on very regular Keplerian orbits. It is when they near the planet that major perturbations will occur. This region, where the pull of the planet is as important as the star's tidal influence, is set by the approximate size of the planet's potential well in the reference frame of the restricted three body problem that is rotating with the planet, calculated by Hill (1878) [14] to be:

$$R_H = a_P \left(\frac{M_P}{3M_{Sun}} \right)^{\frac{1}{3}} \quad (1.15)$$

which is the Hill radius of a planet of mass M_P . The Hill radius therefore defines a vital sphere of influence for the planet, as planetesimals passing near or within the Hill sphere of a planet will experience a very strong scattering. Also of great use and importance is the dimensionless value of R_H/a_P , which is called the Hill factor χ :

$$\chi = \left(\frac{M_P}{3M_{Sun}} \right)^{\frac{1}{3}} \quad (1.16)$$

The range in planetesimal semi-major axis a compared to the planet's semi-major

axis a_P over which strong scatterings can occur is known as the feeding zone. The range is, at zero eccentricity, between $1R_H$ and $3.5R_H$ from the planet's semi-major axis. It is this zone from which the Jacobi wings will rise on the $a - e$ plane, and it is this zone from which most of the planet's accreted material will have come (hence the term 'feeding').

The inner bound of $1.0R_H$ represents the fact that planetesimals with a semi-major axis within one Hill radius of the planet's semi-major axis (Goldreich and Tremaine, 1982 [6]) occupy 'horseshoe' orbits that are stable and will not strongly scatter (see section 1.7). The outer bound of the feeding zone, at $3.5R_H$, is calculated from dynamical considerations in the circular restricted three-body problem that ensure orbits beyond this will not cross the planet for all time (Gladman, 1993 [5]). This number was also calculated by Ida and Makino (1993) to be $2\sqrt{3}R_H$ [17]. The extent of the feeding zone is actually set not by a range in a but by a limit on the Jacobi energy, which can be related to the Tisserand parameter to give the approximately equivalent condition that a crossing planetesimal have a C_T within:

$$C_T^{max} = 3 + 3^{\frac{4}{3}} \left(\frac{M_P}{M_{Sun}} \right)^{\frac{2}{3}} \quad (1.17)$$

determined by Henon (1969 [12], 1970 [13]). This gives a limiting distance slightly different from $3.5R_H$ is at zero eccentricity, as it is an approximation to first order in the mass ratio. As will be discussed in section 1.8, $3.5R_H$ is actually the value at the *outside* of the planet's orbit, and the distance on the inside is slightly smaller. Both of these comments are dealt with by specifying the outer edges of the feeding zone to be the value of C_T as calculated at $a = a_P + 2\sqrt{3}R_H$, which gives a value that can be used interior and exterior to the planet. This also ensures that particles at high- e , where the wings widen in a , will not be excluded as they would be if the region was

simply taken to be $3.5R_H$ wide.

Outside of this zone activity can still occur: a chaotic zone extends farther from the planet than the feeding zone (for planets more massive than $18M_{Jupiter}$ this reverses) as it is calculated by $R_c = 2a_P \left(\frac{M_P}{M_{Sun}} \right)^{\frac{2}{7}}$ [5]. In this zone resonances overlap and can pump eccentricity quite a lot, but planetesimals will nonetheless never cross the planet (assuming zero eccentricity and constant semi-major axis for the planet, and no planetesimal-planetesimal interaction). The edge of this zone is also more 'fuzzy' than the edge of the feeding zone, as it owes to overlap of resonances. For a planet that eventually moves, this means that the disk has been pumped to higher eccentricity beyond the range of the material it will have already strongly scattered. This will be key in the initial migration behaviour to be explored later.

1.6.1 Hill eccentricity

For a high eccentricity planetesimal with a semi-major axis within the range $(a_P, a_P + 3.5R_H)$, a conjunction with the planet at apocentre would give it a distance from the sun of $Q = a + ae$. If the radial excursion ae is greater than a few Hill radii, the planetesimal could actually be *farther* from the planet than the a -width of the feeding zone, and out of the range of the planets ability to cause a strong scattering. This could also occur for a conjunction at pericentre, and in fact if e is high enough it could occur for a conjunction at almost any point in the orbit. The Hill eccentricity $\tilde{e} = e/\chi$, eccentricity in units of the Hill factor, is therefore a good indicator of the ability of a planetesimal to 'miss' the planet during its conjunction. Another useful way to consider this is with the guiding centre approximation.

The guiding centre approximation says that a planet on an orbit with a, e can

be decomposed into a circular orbit convoluted with an elliptical one. The 'guiding centre' will be on a circular orbit about the star at semi-major axis a , and the planet will orbit the guiding centre, like a moon, on an elliptical orbit with semi-major axis $2ae$. For a planetesimal with $\tilde{e} > 1$, this means that the elliptical orbit could actually enclose the entire Hill sphere of the planet it is passing. For a planetesimal with $\tilde{e} < 1$, the elliptical orbit would penetrate the Hill sphere, making a scattering far more likely. Figure 1.3 shows a schematic view of the guiding centre approximation from Murray and Dermott (1999) [22], with the guiding centre marked by an empty circle G that is circularly orbiting the star, a distance a away at focus F (the other focus F' is empty), and the particle P orbiting G on the dotted ellipse.

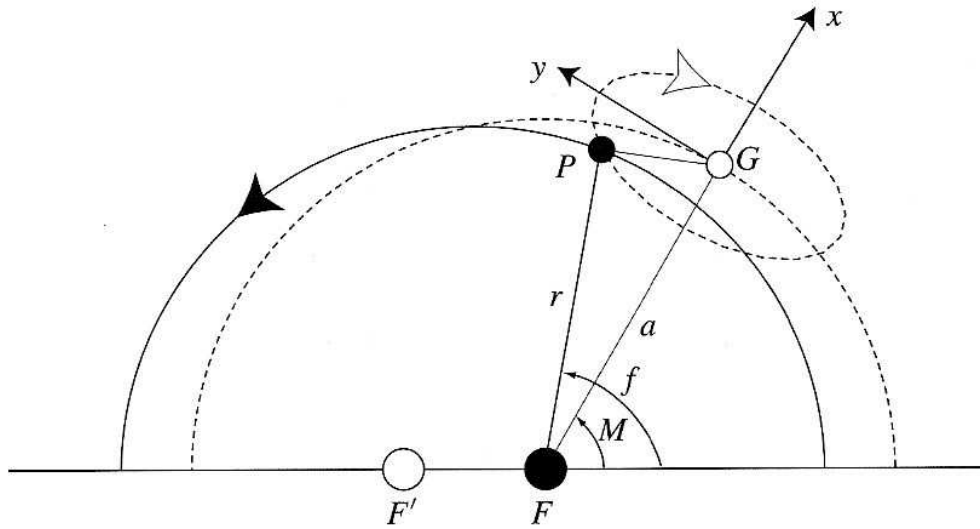


Figure 1.3: The particle P orbits G the guiding centre on an elliptical orbit of semi-major axis $2ae$ while the guiding centre is on a circular orbit of radius a about the star at focus F . [22]

Low Hill eccentricities in the planetesimal disk will be referred to as dynamically

'cold', because relative velocities between the planet and the planetesimals will be mostly set by the shear across the disk due to the difference in Keplerian orbital speeds ($v \propto a^{-\frac{1}{2}}$). This is also referred to as a shear-dominated regime. A disk of planetesimals with high Hill eccentricity will be referred to as a dynamically 'hot' disk, and a situation where the disk is dispersion-dominated. This is because relative velocities between the planet and the planetesimals will be determined more by the eccentricity than the Keplerian shear.

1.6.2 Wing mass

If the feeding zone is the source of the planetesimals that will drive migration, then an important dynamical variable will be the mass of planetesimals within the feeding zone. This is called the wing mass, named for particles within the feeding zone that will move up the lines of constant Tisserand parameter and look like wings on the $a - e$ plane (a clear visualization will be presented in figure 4.1). Two methods will be used to calculate the wing mass throughout this work: summation of particles, and theoretical surface density.

In order to count the particles within a wing, the Tisserand parameter can be calculated at a given time for every particle, in reference to the current semi-major axis of the planet a_P . The maximum Tisserand parameter is given by calculating C_T at $a = a_P + 3.5R_H$ and $e = 0$, and the minimum by a C_T calculated at $a = a_P + 1R_H$ and $e = 0$. Particles with a value of C_T within those bounds is therefore within the wing. They can then be separated into counts for the inner wing and the outer wing simply by seeing if their semi-major axis (or angular momentum) is less than or greater than the planet's, respectively. A slight variation on this would modify the

'minimum' extent simply by ensuring that $|a - a_P| > 1R_H$ to exclude the horseshoes.

The wing mass can also be calculated from the *initial* surface density profile of the planetesimal disk. This may be useful in cases where the planet has migrated a good deal and all that is desired is an estimate of the wing mass that it *would* have had if it had started in the new location. The wing mass in this case would be $M_{wing} \approx 2\pi a_P da \Sigma(a_P)$ where the surface density of the planetesimal disk Σ is normally expressed as a power law of index k normalized to the initial location of the planet a_0 . This power law treatment of the disk, normally with $k \sim -1.5$, has been in use since Hayashi (1981) [11]. The width of a wing, da , is from 1 to 3.5 Hill radii, but as 1.3 is sometimes used [15] for the edge of the horseshoe zone, and 3.25 for the inner edge of the wing (see section 1.8), it is taken to be approximately $da \approx 2R_H \approx 2\chi a_P$. This gives:

$$M_{wing} = 4\pi a_P^2 \chi \Sigma_0 \left(\frac{a_P}{a_0} \right)^k \quad (1.18)$$

where the surface density $\Sigma = \Sigma_0 \left(\frac{a_P}{a_0} \right)^k$ uses the subscript 0 as 'the initial planetary semi-major axis' and the subscript P as the planet's current semi-major axis. The value $\pi \Sigma a_P^2$ is taken to be a measure of the mass of the disk, so that the term $M_{disk} = \pi \Sigma a_P^2$ will often be used. In this case, the wing mass can be expressed simply as $M_{wing} = 4\chi M_{disk}$ and is thus a small fraction of the disk mass (the Hill factor for Earth is $\chi_E \sim 0.01$, and for Jupiter is $\chi_J \sim 0.07$).

As the main supply of the strongly-scattered planetesimals, a Jacobi wing can be regarded as the 'fuel' of migration. For this reason, the ratio of planet to wing mass M_P/M_{wing} will be often referred to as an indication of whether or not the planet has enough fuel to affect migration.

1.7 Horseshoe orbits and mean motion resonances

In the feeding zone discussion of section 1.6, a gap of $1R_H$ on either side of the planet was implied where scatterings would not occur. This means that the feeding zone is actually two distinct bands on either side of the planet's orbit from $1.0 \rightarrow 3.5R_H$. Planetesimals within this $a = a_P \pm 1R_H$ zone do not scatter strongly because they are in stable 'horseshoe' orbits, a particular kind of mean motion resonance that shelters them from close approaches to the planet.

Mean motion resonances are orbits for which the period of the planetesimal and the period of the planet are in certain whole-number ratios, for example $T_{in}/T_{out} = i/(i + j)$ for an inner and outer body, where i and j are integers. Resonances are often specified as 2:1, 3:2, etc., where the first would imply that the inner object completes 2 orbits for every 1 orbit of the outer object. These can provide very stable situations, for example with a 2:1 resonance that has a conjunction with the inner object at pericentre when the outer object is at apocentre (the maximum separation possible for a conjunction), the inner object would be at pericentre again when the outer object was at pericentre on the other side of the star, and the next conjunction would repeat the initial configuration exactly. In this way, no close encounter can ever occur. Figure 1.4 shows an 'overhead' view of the planets in this orbital configuration from Murray and Dermott 1999 [22]. While particles in resonance can be sheltered from close encounters, they can also have their eccentricity forced to higher values. This will be shown in section 4.2.

Horseshoe particles in particular are at the 1:1 *corotation* resonance, because their a is so close to a_P . This resonance is different from the others, in part for being extremely stable over very long (but not indefinite) times. With periods so similar,

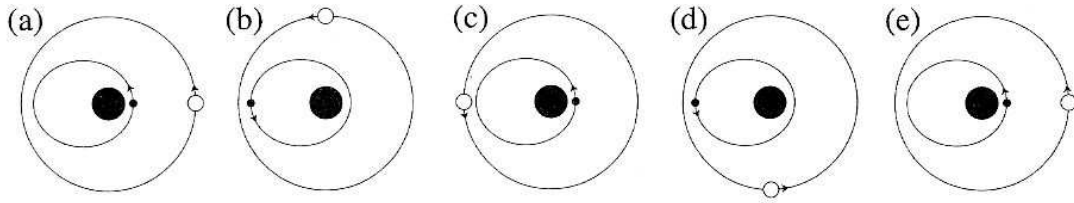


Figure 1.4: Two planets are shown on elliptical orbits about the large central star, at various stages in their orbits, on a 2:1 resonance where the inner planet completes 2 orbits for every 1 orbit of the outer planet. Conjunctions occur at a large distance, ensuring no close encounters will ever occur. [22]

the time between conjunctions becomes very long (this is the synodic period to be discussed in section 1.9). These orbits in the reference frame of the planet will librate about a_P , performing a helix shape wrapped about the planet's orbit. They will slowly approach the planet but will stop short of reaching the Hill sphere, instead turning around and reversing the helix. The 'horseshoe' name comes from the fact that, in this frame, they do not complete a full orbit but leave a gap near the planet where they keep turning away. Two examples of horseshoe orbits, one helical, the other very smooth and more representative of the 'horseshoe' shape, are shown in figure 1.5 from Murray and Dermott 1999 [22].

Resonances can be very stable, and this stability can induce 'trapping', where the planetesimal will remain in the resonance even if the planet migrates and the position of the resonance varies over time. The horseshoe resonance, being the widest resonance, is also the most important in this regard because it will contain the most mass (assuming the mass is distributed evenly in a). The effect of this trapping is that the planet must drag resonantly trapped planetesimals along with it, increasing its inertial mass. The direct effect of dragging the horseshoes in particular will be

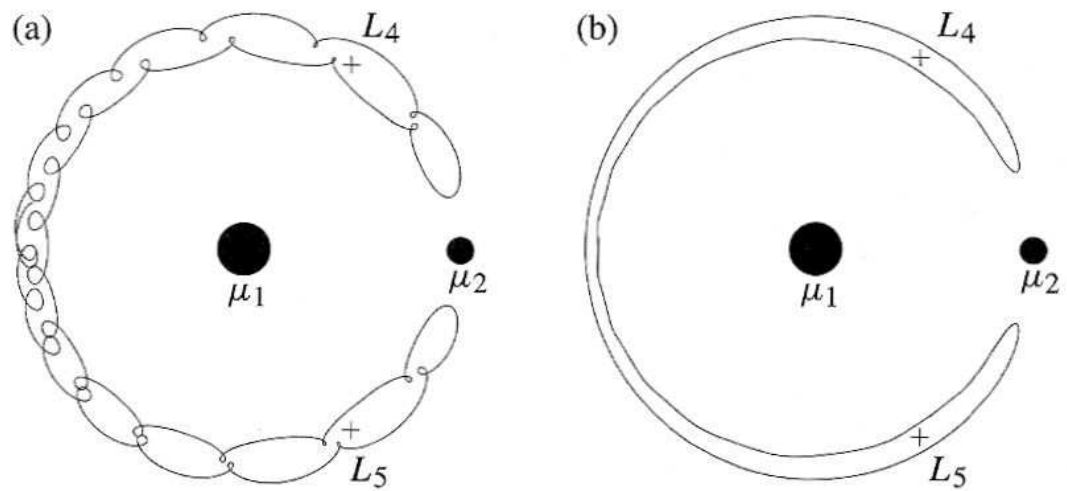


Figure 1.5: Two horseshoe orbits a low-mass particle orbiting the star μ_1 will experience when having a semi-major axis within $1R_H$ of the planet μ_2 , with the helical case having an eccentricity and the smoother case having a very low eccentricity. Two Lagrange points are marked. [22]

investigated in section 5.5.

1.8 Jacobi integral asymmetry

The Jacobi integral is asymmetric in semi-major axis relative to the planet's position, even at zero eccentricity. A feeding zone actually extends to a certain value of this integral, so this leads to an asymmetry in the a -width of the feeding zone on either side of the planet. Assuming a dynamically cold disk with $e, i \approx 0$, and $a_{in} = a_P(1 - \delta_{in})$ and $a_{out} = a_P(1 + \delta_{out})$, the Tisserand parameter can be calculated for a displacement inside the planet's orbit and a displacement outside. Equating these parameters allows us to solve for what displacement outwards must be taken to reach the same parameter as a given displacement inwards. This is expressed as:

$$C_{in} = \frac{1}{1 - \delta_{in}} + 2\sqrt{1 - \delta_{in}} \quad (1.19)$$

Similarly, the Tisserand parameter for a δ_{out} would be:

$$C_{out} = \frac{1}{1 + \delta_{out}} + 2\sqrt{1 + \delta_{out}} \quad (1.20)$$

Expanding these for small δ gives:

$$C_{in} \approx 3 + \frac{3}{4}\delta_{in}^2 + \frac{7}{8}\delta_{in}^3 \quad (1.21)$$

$$C_{out} \approx 3 + \frac{3}{4}\delta_{out}^2 - \frac{7}{8}\delta_{out}^3 \quad (1.22)$$

Equating these two Tisserand parameters $C_{in} = C_{out}$ then gives the relation between the two displacements that will lead to the same ability by the planet to scatter planetesimals at those displacements.

$$\frac{3}{4}\delta_{in}^2 + \frac{7}{8}\delta_{in}^3 = \frac{3}{4}\delta_{out}^2 - \frac{7}{8}\delta_{out}^3 \quad (1.23)$$

Expressing $\delta_{out} = \delta_{in}(1 + x)$ for the outer displacement a small amount x larger than the inner displacement, the right hand side of the equality becomes:

$$= \frac{3}{4}\delta_{in}^2(1 + 2x + x^2) - \frac{7}{8}\delta_{in}^3(1 + 3x + 3x^2 + x^3) \quad (1.24)$$

Taking only the terms to first order in x (the biggest x^2 term is still multiplied by δ_{in}^2 , itself a small number)

$$\frac{7}{4}\delta_{in}^3 \approx \frac{3}{2}\delta_{in}^2x - \frac{21}{8}\delta_{in}^3x \quad (1.25)$$

Now rearranging and expressing x as the difference of δ_{out} and δ_{in} leaves us with:

$$\frac{\delta_{out} - \delta_{in}}{\delta_{in}} \approx \frac{7}{6}\delta_{in} \left(1 + \frac{7}{4}\delta_{in} - \frac{49}{16}\delta_{in}^2 \right) \quad (1.26)$$

and this can also be done to compute the step inwards in terms of the step outwards:

$$\frac{\delta_{out} - \delta_{in}}{\delta_{out}} \approx \frac{7}{6}\delta_{out} \left(1 - \frac{7}{4}\delta_{out} + \frac{49}{16}\delta_{out}^2 \right) \quad (1.27)$$

The asymmetry is therefore seen to be dependent on the width of the zone in question: the bigger the zone gets, the bigger the differential between the outer and inner edges. The outer feeding zone is out to $\sim 3.5R_H$, and so the asymmetry is proportional to the Hill radius, and therefore to the cube root of the planet's mass. For the Earth ($R_H \approx 0.01AU$ at $1AU$) the extent of the inner feeding zone would be 3.8% less than the extent of the outer zone, while Jupiter has a differential of 21%. For displacements at the same non-zero eccentricity the differential would be even larger, as is apparent from the high-eccentricity ends of the constant-Tisserand parameter lines in figure 1.2. In the case of a disk with surface density proportional to a^{-1} , this translates directly to the amount of mass in each feeding zone. There is an immediate bias to the situation, with more mass available to the planet on the outside of its orbit. This bias will grow over time, instead of equalizing, as will be discussed in section 4.5 where this approximation will also be confirmed.

1.9 Synodic Period

Another essential parameter to the problem is the synodic period. This is the amount of time between conjunctions of planetesimal/planet, the beat period, and is determined by comparing the mean motions of the planet ($n_P = \frac{2\pi}{T_P}$) and the planetesimal ($n_{pl} = \frac{2\pi}{T_{pl}}$). The time for a full revolution of this relative angular speed would be $T_{syn} = \frac{2\pi}{|\Delta n|}$, giving:

$$T_{syn} = \frac{2\pi}{\left| \frac{2\pi}{T_{pl}} - \frac{2\pi}{T_P} \right|} \quad (1.28)$$

$$T_{syn} = \frac{T_{pl}}{\left| 1 - \frac{T_{pl}}{T_P} \right|} \quad (1.29)$$

The synodic period is a highly variable quantity, as will be evident throughout this thesis. A particle, once scattered, will move to a different synodic period, often by a large amount. The synodic period will vary across the wing region, meaning that a wing does not have a *single* timescale that describes the entirety of it, and even if it did the timescale would rapidly change *while the particles are scattered*. This is something to keep in mind whenever the quantity is discussed: its value is highly variable. Nevertheless, it is the best timescale indicator available.

Another asymmetry becomes evident between the inner and outer feeding zone of a planet if we take displacements inside and outside the planet's orbit. With $a_{in} = a_P(1 - \delta)$ and $a_{out} = a_P(1 + \delta)$ we can compute the synodic period for a equal displacements of two Hill radii (roughly the centres of the wings), or $\delta = 2\chi$. The period of a body is $T = a^{\frac{3}{2}}$, so the planetesimals will have $T_{pl} = a_P^{\frac{3}{2}}(1 \mp \delta)^{\frac{3}{2}}$ for inward and outward displacements respectively. The synodic periods are therefore:

$$T_{syn} = \frac{(1 \mp \delta)^{\frac{3}{2}}}{\left| 1 - (1 \mp \delta)^{\frac{3}{2}} \right|} T_P \quad (1.30)$$

This can be approximated for small δ to be:

$$T_{syn} \approx \frac{1 \mp \frac{3}{2}\delta}{\left|1 - (1 \mp \frac{3}{2}\delta)\right|} T_P \quad (1.31)$$

$$T_{syn} \approx \left(\frac{2}{3\delta} \mp 1\right) T_P \quad (1.32)$$

The outer synodic period is therefore $2T_P$ larger than the inner. For the Earth, displacements of $\delta = 2\chi$ would give synodic periods of 32 years on the inside, and 34 years on the outside. Another useful indicator of the timescale difference on either side of the planet is the *relative* synodic period, which is the synodic difference of the synodic periods. This would be:

$$\Delta T_{syn} = \frac{2\pi}{\left|\frac{2\pi}{T_{syn}^{in}} - \frac{2\pi}{T_{syn}^{out}}\right|} \quad (1.33)$$

and can be thought of as the time between instances of *both* planetesimals reaching conjunction at once. Using the result for the synodic periods gives:

$$\Delta T_{syn} = \frac{T_{syn}^{in} T_{syn}^{out}}{\left|T_{syn}^{in} - T_{syn}^{out}\right|} = \left(\frac{2}{9\delta^2} - \frac{1}{2}\right) T_P \quad (1.34)$$

For the Earth the relative synodic period is therefore 555 years. This is how long it would take the Earth to fully feel the timescale bias which causes it to overtake the inner material more frequently than it is overtaken by the outer material.

The displacements discussed so far have been equally interior and exterior to the planet's semi-major axis, but as was discussed in section 1.8 the centre of the outer wing is farther from the planet than the centre of the inner wing. Moving farther from the planet reduces the synodic period, such that for the equivalent location in the outer wing as a δ from the planet in the inner wing:

$$T_{syn}^{out} \approx \left[\frac{2}{3\delta} \left(1 - \frac{7}{6}\delta - \frac{49}{24}\delta^2\right) + 1\right] T_P \quad (1.35)$$

$$\Delta T_{syn} \approx \left(\frac{4}{11\delta^2} - \frac{7}{363\delta} - \frac{343}{726} \right) T_P \quad (1.36)$$

which, for the Earth, give values of 33.5 years and 907 years respectively for $\delta_{in} = 2\chi$, with this last value suffering only 0.1% error from the full calculation. The relative synodic period has greatly increased despite the small change in T_{syn} .

This timescale difference on either side of the planet will prove critical in determining the net scattering rate, and the ultimate migration direction of the planet. This will be explored further in section 4.5, and throughout this thesis.

1.10 Structure of the thesis

Thus far the physical quantities that describe planetary systems have been introduced. Chapter 2 will explore the concepts behind planetesimal-driven migration and how they have evolved in the literature, bringing us to the work that will be done in this thesis. Chapter 3 will introduce the simulation software and basic parameters that will be used to follow the evolution of the planet-planetesimal system. Using simulation, chapter 4 will then return to the basic question of how planetesimals are scattered by a planet. In particular, how the semi-major axes and eccentricities of planetesimals change, and what populations experience the largest changes will be investigated, as well as how the angular momentum of the system changes. Chapter 5 will then put all of this together and determine trends of planetary migration for the various physical quantities of the system such as mass, eccentricities, etc. The results of all the simulations of that chapter will be summarized in chapter 6, in the context of the ideas presented in this chapter and developed in chapter 4, to give a final analysis of the process of planetesimal-driven migration.

Chapter 2

Previous work

Planet migration owing to planetesimal scattering has been investigated many times, but often as a side-effect of accretion and primarily in the early Solar System. Early work assumed that the planets were too large to be moved simply by scattering much smaller bodies, and that it was effects from the gas disk that accounted for any motion. Integrating orbits to the precision accomplished in this work was also far beyond the early reach. As computing technology improved, however, and more abstract solar system configurations were explored, planetesimal scattering as a source of angular momentum exchange began to be acknowledged. This chapter will introduce many of the previous papers and results that have laid the ground-work for this field.

2.1 Early work

The first paper to introduce the idea that planets could have migrated a substantial distance due to planetesimal scattering was from Fernandez and Ip (1984) [4]. This paper explored the accretion and scattering by Jupiter, Saturn, Uranus and Neptune

when they had nearly reached their final states, using a few thousand particles and scattering estimates based on two-body formulations from Öpik (1951) [24]. Previous ideas had estimated that any angular momentum transport from scattering was due to each planet completely ejecting planetesimals from the system (e.g. Safronov 1969 [27]), but their results showed a more complex process that dynamically coupled the giant planets: while Jupiter easily ejects planetesimals and therefore loses angular momentum, migrating inwards, the other planets find it easier to pass material to Jupiter than to eject it. By passing material inwards to Jupiter, the giants gain angular momentum and migrate outwards. This result has been the primary viewpoint of scattering-based migration ever since.

Using a mixed-variable symplectic (MVS) algorithm (see section 3.1), the basis for the algorithm used in this work, Malhotra (1993) [19] more rigorously followed orbits of planets and planetesimals in an effort to prove that this mode of migration occurred in our Solar System. That work imposed a migration scheme on Neptune using an analytic drag force, in order to approximate the migration observed by Fernandez and Ip, and showed that Pluto could be caught in the 3:2 resonance with Neptune. Indeed the process pumps Pluto’s eccentricity up, and allows an estimate of how far Neptune had moved once Pluto was caught from the dynamical equation:

$$e_{final}^2(Plu) - e_{initial}^2(Plu) \approx \frac{1}{3} \ln \frac{a_{final}(Nep)}{a_{initial}(Nep)} \quad (2.1)$$

giving at least 5AU of change in Neptune’s semi-major axis in order to drive Pluto’s eccentricity from around zero to its current value of 0.25. Her simulations backed up this result, cementing the idea that planetesimal scattering could be a critical force for the architecture of the outer solar system.

Hahn and Malhotra (1999) [9] also explore the giant planet migration scenario

for the Solar System, using several disk masses with 1000 particles of a fraction of an Earth mass and an MVS code. They found approximately the same results as Fernandez and Ip. A great deal of stochasticity still existed in the migration of the planet, with quick excursions of ~ 10 AU during which Neptune migrates out and returns rapidly. This stochasticity is induced by the (unphysically) large mass of each individual planetesimal, and as the ultimate migration of the planet was only approximately three times this excursion distance, the trends are only true in generality. This work also explored the resonance trapping of Pluto, expanding the concept to the production of the Oort cloud and the Kuiper belt. The Kuiper belt is the group of planetesimals beyond Neptune of which some are trapped in resonances that, similar to the Pluto case, imply Neptunian migration.

Murray *et al.* (1998) [23] explored planet migration from a different angle, using two-body approximations and not N-body simulation. They emptied the feeding zone entirely, assuming that it had been mostly accreted to form the planet in the first place, and explored the effect of the resonances. Planetesimals trapped in resonances are pumped to higher eccentricity, eventually entering the Hill sphere despite having very large distances from the planet in semi-major axis. For high mass planets (such as Jupiter) the planetesimal would then be ejected after a few random scatterings, and finally the planet would begin to migrate inwards. This model uses very low-mass disks and requires a great deal of time relative to the simulations in this thesis. This makes the model a possible candidate for further migration on longer timescales than are discussed in this thesis. This work was important for being among the first to explore the most simple situation: one planet. It also noted that planetesimals would not exist very close to the star, having never formed or even sublimating, and this

produces a natural cut-off to planetesimal-induced migration. This cut-off is very much desired as a reason for the hot Jupiters to have migrated close to their stars without falling in.

2.2 Ida, Bryden, Lin and Tanaka 2000

The first paper to present self-consistent migration of a single planet due to planetesimal scattering was from Ida, Bryden, Lin and Tanaka (2000) [15], hereafter referred to as IBLT. In an effort to investigate the migration of Neptune and the formation of the Kuiper belt, they explored migration due to interactions with the gas disk, migration due to planetesimal scattering, and resonant trapping during migration.

In IBLT section 3, on planetesimal scattering, they began by exploring the scattering behaviour of nearby planetesimals similar to chapter 4 in this work. Planetesimals on initially circular orbits were integrated as a function of their distance to a single planet scaled by the Hill radius (here referred to as the Roche radius, with 'R' subscripts) $b_R = (a_{pl} - a_P)/r_R$. They identified horseshoes as extending out to $|b_R| \approx 1.3$ and strong scatterings as extending out to $|b_R| \approx 3.1$. The eccentricity (in Hill units) and angular momentum changes (scaled by $v_P R_H = n_P a_P R_H$, or $\Omega a r_R$ in their notation) that they found are shown as a function of b_R in figure 2.1.

They then integrated the angular momentum changes from $3.1 \rightarrow \infty$ for the 'distant' encounters and from $0 \rightarrow 3.1$ for the close encounters and strong scatterings. They found that the distant encounters produced a total angular momentum change of less than an order of magnitude as strong as the close encounters' total change; the latter had a rate of change of the angular momentum from Neptune to zero- e

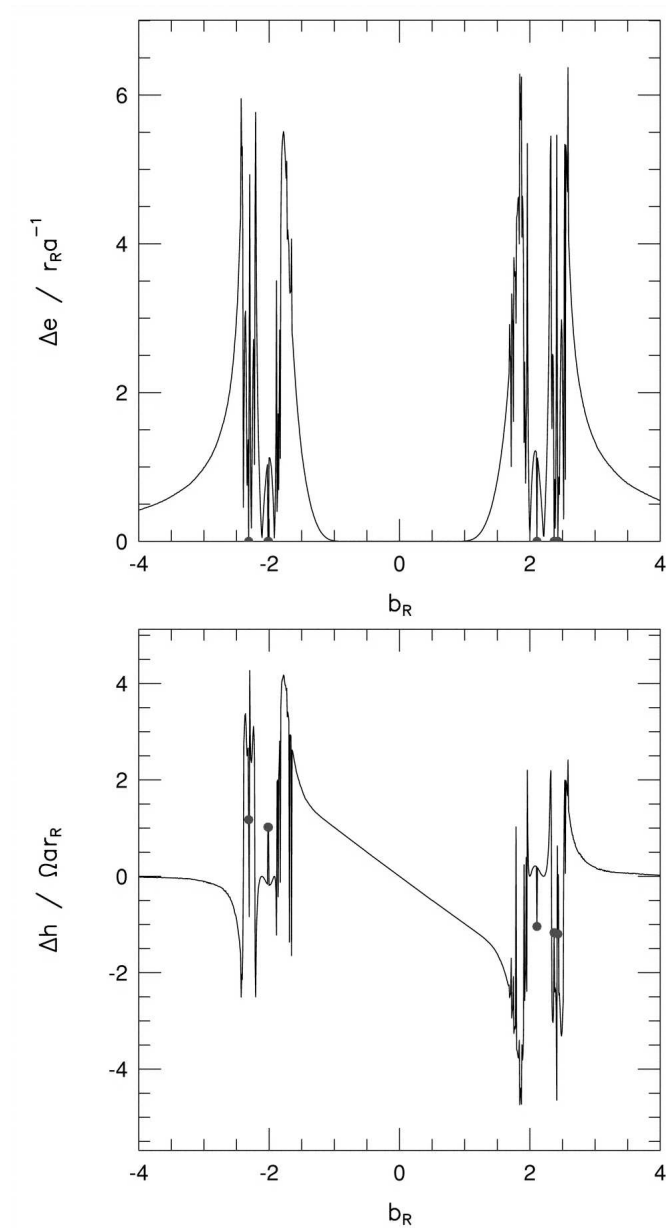


Figure 2.1: Change in planetesimal eccentricity and angular momentum, normalized to the Hill factor and $v_P R_H$ respectively, for circular orbits on their first encounter with a planet. The changes are shown as a function of the distance to the planet in Hill radii. From Ida *et al.* 2000 [15].

planetesimals of:

$$\dot{L} \approx -4.7\Sigma n_P^2 a_P r_R^3 \quad (2.2)$$

where the sign implies that the planet gained angular momentum and was thus *attracted* to the outer wing particles. The distant encounters were *repulsive*, and the inner populations were opposite in sign to their corresponding outer populations. This is only valid in the first encounter for each value of b_R , and thus is harder to measure experimentally as particles quickly change distances and synodic periods (rate of encounter).

In order to replenish scattered planetesimals, and not continuously interact with the same population, Ida *et al.* argued that either the planetesimals would need another mechanism to move them, or the planet itself would have to move. In particular, the planet would have to move by its encounter zone in one synodic period (measured at the edge of that zone), which gives (using equation 1.32) a limiting migration rate of $b_R r_R / (2T_P / 3b_R r_R)$:

$$\frac{da_P}{dt} > (b_R \chi)^2 \frac{3a_P}{2T_P} \quad (2.3)$$

where b_R is the number of Hill radii (~ 3.5 in this case) and χ now refers back to the Hill factor.

They calculate a migration rate from equation 2.2, their integrated angular momentum exchange rate, of:

$$\frac{da}{dt} \approx \frac{4\pi\Sigma a_P^2}{M_{Sun}} \frac{a_P}{T_P} \quad (2.4)$$

which will be compared to a fiducial rate calculated using simple approximations in section 5.1. This would be the migration rate assuming equation 2.3 is true, so every 'first' encounter with a planetesimal has the planetesimal at zero eccentricity.

The paper also estimates migration rates in a dynamically hot disk, where planetesimals have a finite e_{pl} . After assuming that the average eccentricities and inclinations have the relation $e \sim 2i$ (a common trait of dynamically relaxed disks, as in Ida and Makino (1992) [16]) they find that the migration rate in a disk with eccentricity e would be reduced, as discussed in section 1.6.1, such that:

$$\frac{da}{dt} \approx \left| \frac{da}{dt} \right|_{e=0} \left[1 + \left(\frac{e}{\chi} \right)^3 \right]^{-1} \quad (2.5)$$

and this will be compared to simulation results in section 5.4.

A 'migration instability' is discussed in the paper wherein a slight imbalance of planetesimals on either side of the planet will lead to sustained migration, and outward migration is suggested to be the most common. No prediction is made as to which direction of migration (outward or inward) is favoured, however. A simulation is performed using 2500 particles spread over $a_P \pm 25R_H$ from a planet of mass $0.3M_{Nep}$, and noisy outward migration is the result.

2.3 Gomes, Morbidelli and Levison 2004

The self-sustained migration of a planet in a planetesimal disk was explored by Gomes, Morbidella and Levison (2004) [8] as an exponential runaway process. They proposed a toy model of coupled differential equations which, while not suited to offering initial numerical estimates, predicts a migration rate which is either a damped or forced exponential in time depending on the resupply of planetesimals to the constantly-depleted feeding zone. This can be contrasted to the simple model which will be developed in section 5.1 which gives immediate results and will be invaluable as a comparison for all simulations in this work.

The particle count used for their simulations was 10^4 (we have thus far seen a progression in state-of-the-art resolution of hundreds to a thousand, to 2500, and now 10,000 particles, but this is still orders of magnitude below the number of planetesimals the Solar System would have had), particles which were spaced over the Solar System (a disk width of $\sim 30\text{AU}$) to allow further tracking of Neptune's migration. Their migrations again showed quick excursions that subsequently reversed themselves, excursions over almost the entire disk in this case, and a good deal of noise. They attempted a long range migration by removing the other giant planets once Neptune had begun migrating, and allowing the migration to continue over a more extended disk. They found that the migration would end at the disk edge, and normally reverse itself (and head back inwards), but in the case with a very wide disk (the edge was at 200AU) the planet reversed by 120AU . They also noted several occasions where the migration seemed to stop briefly before continuing outwards. These results will be discussed further in section 6.3. The paper claims a satisfactory resolution based on several migrations arriving at the same endpoint in a certain time, despite their widely differing paths. Indeed, in figure 5.1 of this work and in the larger planets of the M0 runs to be described in section 5.3, such convergences are also seen in under-resolved runs. However, the convergences are several AU away from the endpoints that are converged upon by multiple runs that are all well-resolved with higher particle counts. Convergence alone is therefore not a guarantee of proper resolution.

The placement of an Earth-mass planet outside Neptune's orbit was also explored. The expected result was that it would be captured by Neptune upon the latter's migration, and pushed along, but the actual result was that it migrated much faster

than Neptune. The expectation was influenced by the previous bias towards the "Jupiter in, the rest out" view of migration where it is the planet's ability to pass planetesimals to Jupiter, and Jupiter's ability to eject planetesimals, that produces most of the effect. However, as pointed out by IBLT, any planet no matter its ability to eject planetesimals can undergo self-sustained migration. The migration rate as a function of planet mass will be explored in section 5.3, and it will be seen that this 'surprising' result is very much to be expected when comparing high- and low-mass planets in the same disk.

2.4 Works using planetesimal-driven migration

Several other papers have utilized planetesimal-driven migration, mainly in the Solar System context and often as a mechanism to produce the arrangement of the giant planets and the Kuiper Belt (e.g. Thommes *et al.* 1999 [29], Gomes 2003 [7]). These simulations have tended to max out at 10^4 particles and resolutions that are, in some cases, less than a hundredth of what is achieved in this thesis. The main reason for this is not computing power but rather the length of the run: for Solar System studies the disk is not very massive and migration requires tens of millions of years. Most runs in this thesis will require less than a hundred thousand years. The impact of low resolution will be seen in sections 5.2, 5.3, 5.5 and 5.7, and will be discussed in the context of previous work in section 6.3.

One model that has received a great deal of attention is the 'Nice' model, originating in a paper by Tsiganis, Gomes, Morbidelli and Levison (2005) [32]. This model assumes that after the gas disk has dissipated Saturn is left within a few tenths of an AU from the 1:2 resonance with Jupiter, and the ice giants Uranus and Neptune

are at roughly 13AU and 17AU respectively (with their order perhaps switched). It is also assumed that a residual disk of planetesimals of total mass $\sim (30 - 50)M_{Earth}$ spread from just outside the planets to ~ 35 AU will slowly 'leak' planetesimals into the giant planet zone as resonances pump up their eccentricities. Scattering of the leaked planetesimals slowly drives Saturn away from Jupiter and into the resonance, which quickly excites its eccentricity and throws the ice giants into chaotic orbits. The ice giants cross into the remnant planetesimal disk, a population that has never been depleted as no planet has ever migrated into it before, and they migrate out to their present positions. Not only does this model address several concerns on the semi-major axes of the giants, it also produces roughly correct eccentricities and inclinations. The model places some constraints on masses and initial separations, but as before it may be affected by low resolution, and such constraints in particular could be improved with more particles. This mechanism (the passing of planetesimals inwards to Jupiter and Saturn) differs from the more local scattering that will occur in this thesis, and thus the extent of resolution required here may not be the same as that required in these models. Furthermore, the authors acknowledge the desire for more particles, but the integration is too long to permit such particle counts as will be used here. Nonetheless, the Nice model, being one of the current favourites for the formation of the Solar System, is one of many theories that could greatly benefit from information acquired for this thesis.

While Solar System formation is a key subject, system formation in general is of growing importance; especially with the developing ability to observe extra-solar systems. This thesis will not only inform migration models in our system, but become an essential step in the modelling of any planetary system.

Chapter 3

Simulations

This chapter will introduce the tool that will be used to explore planetesimal scattering and planet migration: computer simulation. The software will be discussed, in more detail than is truly required, and the basic components of setting up an individual simulation will also be introduced. The software itself has been utilized and tested in many previous papers, and thus will not be heavily tested in this work.

3.1 SyMBA

The simulation software used for this thesis was Miranda (McNeil *et al.*, 2005 [21]), a parallelized implementation of SyMBA (Duncan *et al.*, 1998 [3]). SyMBA is a symplectic integrator, which is an algorithm specific to Hamiltonian systems that enforces exactly certain conservation laws characteristic of Hamiltonian dynamics (Saha and Tremaine, 1992 [28]). The integrator solves an approximate Hamiltonian exactly, and this bounds the absolute value of the energy error at a low value. The integrator is also time reversible. SyMBA uses a 'democratic heliocentric' method

with multiple time steps.

The basic symplectic integrator (Wisdom and Holman, 1991 [34]) avoids treating the star as just another body in an N-body problem by acknowledging that in a planetary system each timestep is mainly a Keplerian orbit about the star perturbed by other interactions. Since the two-body problem can be solved exactly, it would be unnecessary to calculate a planet's interaction with its star in the same manner as an interaction with a planetesimal. Using the knowledge that any given timestep will include changes in position and velocity due to the orbit and changes due to the other interactions, the full operator giving the evolution over a timestep τ can be broken into two operations on velocities and positions:

$$E_1 \left(\frac{\tau}{2} \right) E_0(\tau) E_1 \left(\frac{\tau}{2} \right) \quad (3.1)$$

which is equivalent to applying a kick to the momentum of each body due to every other body (the operator E_1) for a time $\tau/2$, then evolving the positions of the bodies along their Keplerian orbits (the operator E_0) set by their updated momentum for a time τ , and then again applying momentum kicks at the new positions for a time $\tau/2$. This scheme is referred to as 'kick-drift-kick', and when applied repeatedly it would be a continuous series of half-timestep-offset kicks and drifts. This is also equivalent to a 'leapfrog' scheme where the position is evolved for a time τ using a velocity calculated in the middle of that evolution. The drift would be calculated from the Keplerian Hamiltonian and the kick from the interaction Hamiltonian. The basic symplectic integrator is sometimes referred to as a mixed-variable symplectic (MVS) integrator [28] because it has to switch between variables natural to the two-body problem and cartesian coordinates.

The original scheme of Wisdom and Holman (1991) [34] employed a set of spatial

coordinates in which each particle's origin is at the centre-of-mass of all the particles *internal* to it. This is done, technically, to avoid cross-products in the Hamiltonian and keep it as the sum of only two pieces: the Keplerian and the interaction operators. One problem with this scheme is that the sun is not at the centre of the orbit (as it is not the centre-of-mass) but it is the heliocentric positions that are desired, and there are issues when bodies cross each others' orbits, changing their order from the sun and thus who is internal to whom. The other problem is that no adaptive timestep is permitted because varying the timestep in repeated applications of equation 3.1 destroys the symplectic nature of the integration [3]. The solution to the first problem is with the democratic heliocentric method, and the solution to the second is the multiple timestep method described below.

The democratic heliocentric (DH) method modifies the problem so the canonical positions are heliocentric while the canonical momenta are barycentric. This makes the resultant Hamiltonian the sum of three pieces and requires the addition of a linear drift to the Keplerian and interaction operators. The DH method removes the need for specific ordering, allowing planets to cross orbits. The multiple timestep (MT) method addresses the need for an unchanging Hamiltonian by breaking the existing Hamiltonian into short-lived pieces. Cutoff radii are set at certain distances from a planet, the gravitational force decomposed into those zones, and the operators recursively applied over short times. Essentially this results in an object entering subdivided 'shells' as it approaches a planet. In each shell the number of elements of the decomposed force it feels (and thus the number of operators) increases, and the timestep over which each is applied decreases, better resolving the motion over short times. All particles will always feel all the shells, but the shells they are outside

of will have no effect on them; nonetheless the Hamiltonian is unchanged and the symplectic nature of the integrator is unbroken.

Although only one planet is used for this thesis, the Miranda implementation of SyMBA with the DH and MT methods ensures that planetesimals will feel well-resolved scatterings very close to the planet and that the planet responds self-consistently. As these scatterings will often present the strongest changes in angular momentum, they are critical to ensuring an accurate migration process.

3.2 Setup and initial conditions

The physical quantities required to run a simulation include data on the planets and planetesimals in the system, and data on the timescales to be investigated. All simulations used one planet. Planets and planetesimals require the same physical input: mass, radius, Hill radius, semi-major axis, eccentricity, inclination, and the three orbital angles Ω , ω and M .

In order to utilize units of length in astronomical units (AU) and time in years, G is set to 1, the star's mass in the system is set to $(2\pi)^2$, and planet/planetesimal mass is scaled by that factor. These settings can be seen from the definition of the orbital period in equation 1.11 to cancel the constant factors such that $4\pi^2/GM_{Sun} \rightarrow 1$. Jupiter, at 10^{-3} Solar masses (318 Earth masses), is therefore 0.04 in simulation mass units. The unit of the physical radius, Hill radius and semi-major axis is the astronomical unit. The eccentricity of an object is dimensionless, and the last four parameters are in radians. These parameters are input through two files, `pl.in` and `field.in`, which includes the number of planets/planetesimals respectively and then a list of the physical quantities for each such object.

The third input file is `param.in`, which specifies the timing values, all measured in years. The first input times are the start and stop times. The next three are intervals: the timestep length, the time between outputs, and the dump time. The timestep is normally chosen to be at most 2% of the smallest orbital period for the objects in the simulation. Time between outputs is chosen to give a reasonable number of snapshots of planet migration (normally around 100 outputs), or to resolve the process of planetesimal scattering (a fraction of a synodic period at $2R_H$). The dump time is the time between which a set of data files containing all relevant information to the simulation is output. These dumps enable a complete restart of the simulation should it fail during the run. The dump time is chosen to be less than the output time, but does not affect the simulation results.

The surface density profile of the planetesimal disk was, unless otherwise stated, $\Sigma \propto a^{-1}$. Practically, this means that the spacing between each planetesimal's semi-major axis is equal throughout the disk, and that the system can be thought to have an initially uniform linear density of planetesimals/AU. High-resolution runs tended to use around 1000 particles per Hill radius in the disk. To keep any migration smooth the ratio of planetesimal-planet mass was also well-resolved, usually by at least 600-to-1. This, and the extent of the disk, would determine the necessary planetesimal number for a simulation. Disk extent was usually chosen to be $25R_H$ inside and outside the planet, which allowed for enough migration to get a trend, and ensured that the planet did not initially feel the edge of the disk. For runs with very high particle number ($\sim 10^6$) the disk was truncated closer to the planet in the direction it would not migrate, so as to not waste time computing orbits that would never approach the planet. Strong interactions do not occur past $3.5R_H$ from the planet,

so this closer truncation was normally kept to greater than $5R_H$ (which also normally allows inclusion of the chaotic zone).

Planetesimals all had the same mass unless otherwise stated. Their eccentricities and inclinations were randomly chosen from a Rayleigh distribution (e.g. Tremaine, 1998 [31]) which is the natural state of a dynamically relaxed disk. A particular value of e could then be determined using a random number x from 0 to 1 by:

$$e = e_{RMS} \sqrt{-\ln(1-x)} \quad (3.2)$$

where the root-mean-squared value of the eccentricity e_{RMS} was chosen for each simulation, and the RMS inclination was set to half of that value. This follows from the result (e.g. Ida and Makino, 1992 [16]) that the process of runaway growth leading to planet formation will leave the planetesimal population with, on average, $e \approx 2i$. The orbital angles for each planetesimal were chosen randomly, from zero to 2π .

3.3 Parameter space

The main parameter that was explored in this thesis is the relative mass between the planet and the disk. In order to keep a proper resolution, this results in planets that are between 0.01 and 10 times the mass of their Jacobi wings. This ratio was varied by changing the planetesimal mass, the planetesimal density, or the planet mass itself.

The eccentricity of the disk was also explored, normally in terms of \tilde{e} the Hill eccentricity. Most simulations were started with disk eccentricities of 0.01 or 10^{-4} , however, as these numbers were generally comparable to or much less than the Hill factor respectively. This results in runs with relatively hot disks, or cold disks.

Other simulations also varied initial semi-major axis, surface density and subsets of the mass ratio (horseshoe mass, wing mass, etc.). Runs with test particles were performed for cases where no migration was desired, and runs with mass on only one side of the planet were performed as extreme cases. A common approach to avoid horseshoe orbiters was to simply remove all of the planetesimals within one Hill radius on each side of the planet.

Simulations use as few as several thousand particles, up to one million particles. The effects of varying temporal and spatial resolutions were also explored, where spatial resolution is set by the number and mass of particles chosen to give a fixed planetesimal surface density.

Chapter 4

The scattering process

This chapter will introduce several concepts that will be used to explain effects seen in the migrations of the next chapter. The methods developed here serve as a useful diagnostic of the interaction process. However, much of this chapter will not be essential in the understanding of migration. The key results of this chapter will be seen in sections 4.1.1, 4.1.3, 4.4 and 4.5.

The process of scattering planetesimals causes a transfer of angular momentum that shifts the orbit of a planet. The angular momentum received by or removed from the planet will be in proportion to the mass fraction of planetesimal to planet. Massless particles will therefore not be felt by the planet, and it will not move; this is known as the restricted three-body problem. This situation is useful for studying the effect of scattering on a single particle, or an ensemble, because each passage will encounter a planet in the same planetary orbital configuration as the last passage. Changes in distance to the planet, or angular momentum relative to the planet, take on more meaning when the planet's orbit is not altered during the change. For this reason, several simulations were done with massless planetesimals.

The main simulation (called D0) referenced in the following sections utilized 10^5 particles spread over five Hill radii on either side of the planet. The planet had a mass in units of the stellar mass of 1.5×10^{-5} ($4.5M_E$), and was located at 25AU, giving it a Hill radius of approximately 0.43AU. The planet had zero eccentricity and inclination. The disk was initialized with a $\Sigma \propto a^{-1}$ surface density, giving a uniform spacing between particles of 4.3×10^{-5} AU. The planetesimals were actually given a finite mass, of 10^{-69} , but any shift in the planet's orbit that this amount of mass could cause would be far below numerical resolution. The eccentricities and inclinations of the planetesimals were Rayleigh-distributed with a root-mean-squared eccentricity of 10^{-4} , and an RMS inclination of half of that. Orbital angles (see section 1.3) were chosen randomly between zero and 2π . The simulation ran for 10^5 years, or 800 planetary orbits (800×125 years), using a timestep of 1 year and output intervals of one planetary orbit.

4.1 Growth of wings

Scatterings result in the growth of planetesimal eccentricities along paths of constant Tisserand parameter that form Jacobi wings. These wings are roughly equivalent to lines of constant apo/pericentre in the $a - e$ plane (see section 1.5.1). Several snapshots of the planetesimal distribution in this plane are shown at several times (in units of the planet's orbital period) in figure 4.1. It is clear that as planetesimals are pumped up the wings, they are not only moving to higher average eccentricity, but they are moving to greatly different distances from the planet. The inner wing contains planetesimals that move to smaller orbital periods, while the outer wing contains planetesimals moving to larger orbital periods. This also changes the synodic

period for each planetesimal by a great deal (see section 1.9).

The planetesimals conserve their Tisserand parameter C_T , and thus it is useful to consider ensembles based on this parameter. Particles placed in bins based on their value of C_T will be gathered up with particles that shared very similar initial semi-major axes. The Tisserand parameter can therefore be considered the proxy for 'distance to the planet' for particles that have been pumped up the wings: it tells us where, when projected back down to zero e , they would be relative to the planet. However, the same value of C_T can be found inside the planet's orbit as well as outside, and this results in an important distinction: planetesimals may stay on their original 'side' of the planet, or they may switch sides. For several sections of this chapter, averaging over particles binned by C_T requires first distinguishing these groups within the set of all the particles in the bin. Furthermore, as the synodic period (the time between conjunctions) is many orbital periods, and many output times, only a fraction of the particles in each bin can undergo an encounter between each output.

The extent of the wings as calculated from C_T^{max} (equation 1.17) was checked by looking at the low-eccentricity particles remaining on either side of the planet at the end of the D0 simulation. Particles with eccentricity less than 0.01 were counted in 1000 bins of semi-major axis throughout the disk zone simulated. The surface number density of particles in each bin is shown in figure 4.2. Gaps are clearly evident on either side of the planet, corresponding to the zones that have been pumped to higher eccentricities within the wings, so that after many synodic periods (many scatterings), no particles are left at low- e within each feeding zone.

The extent of the outer wing is theoretically $3.464R_H$, or $2\sqrt{3}R_H$, as from Ida and

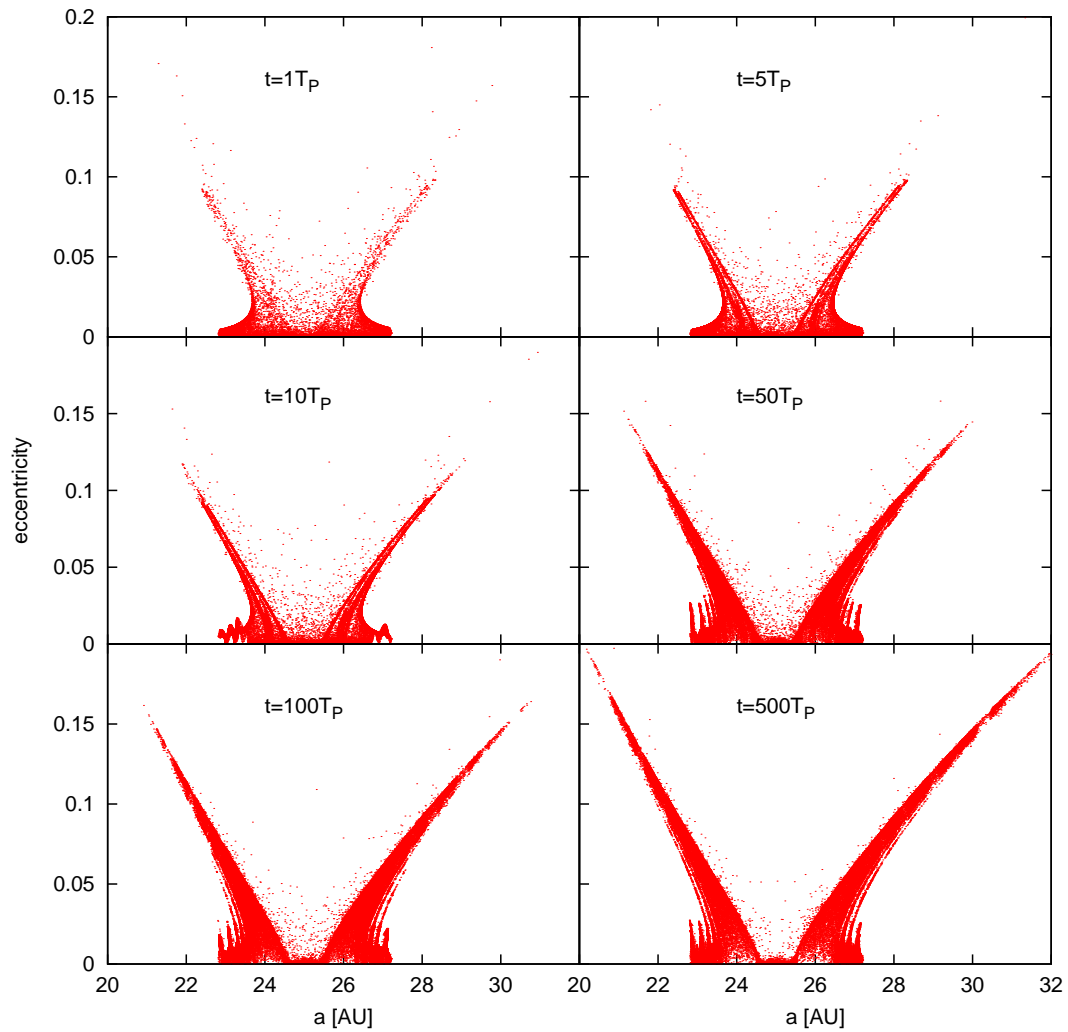


Figure 4.1: Snapshots of Jacobi wing growth at six values of time, in multiples of the planet's period. Particles all started at $e = 10^{-4}$, distributed evenly from 22.85 to 27.15AU. Particles in mean motion resonances outside of the wing produce jagged spikes.

Makino (1993) [17], and the observed value is $3.481 \pm 0.004 R_H$ where the error is given by the bin spacing. Calculating the inner gap width using the theoretical inner value from equation 1.27 gives a prediction of the inner wing extending to $3.277 R_H$, whereas the observed value is approximately $3.281 \pm 0.004 R_H$. The observed asymmetry is therefore 6.1% in terms of $(\delta_{out} - \delta_{in})/\delta_{in}$, as opposed to the 5.7% expected, which is very good for the purposes of this paper. The extent of the feeding zone is therefore well approximated by the theory given thus far. As mentioned earlier, however, the extent does not quite match that predicted by C_T^{max} . To be specific, for this planet $C_T^{max} = 3.00265$, C_T calculated at $a = a_P + 3.464 R_H$ is 3.00248 and the values of C_T at the inner and outer observed edges are 3.00255 and 3.00250 respectively. The overprediction of the wing width using C_T^{max} means that for the majority of this chapter a different C_T limit will be used:

$$C_T^{feed} = C_T(a = a_P + 3.464 R_H, e = 0, i = 0) \quad (4.1)$$

which is simply the value of the Tisserand parameter calculated at the outer edge of the wing defined by the feeding zone width of $2\sqrt{3}R_H$.

The difference between C_T^{max} and C_T^{feed} is likely due to the difference between C_J the Jacobi integral and C_T the Tisserand parameter, which is merely an approximation in terms of $\mu^{\frac{1}{3}}$, with μ the mass ratio of planet to sun. The approximation is therefore valid within the third power of this small term. The Jacobi integral is computed using barycentric coordinates whereas the Tisserand parameter is expressed in heliocentric coordinates. Since these coordinates differ by terms of order μ , the size of this discrepancy is not a surprise. The value of C_T^{feed} matches well with the D0 results, and that is enough for now.

The inner edges of the gaps are at $1.170 \pm 0.004 R_H$ on *both* sides of the planet,

whereas equation 1.26 would have predicted an asymmetry of 2.4%. The horseshoe zone is not as well-defined in the theory, however (see Gladman (1993) [5] for a brief overview) and for the purposes of this work it is enough to say that they extend roughly symmetrically to $1R_H$ on either side of the planet.

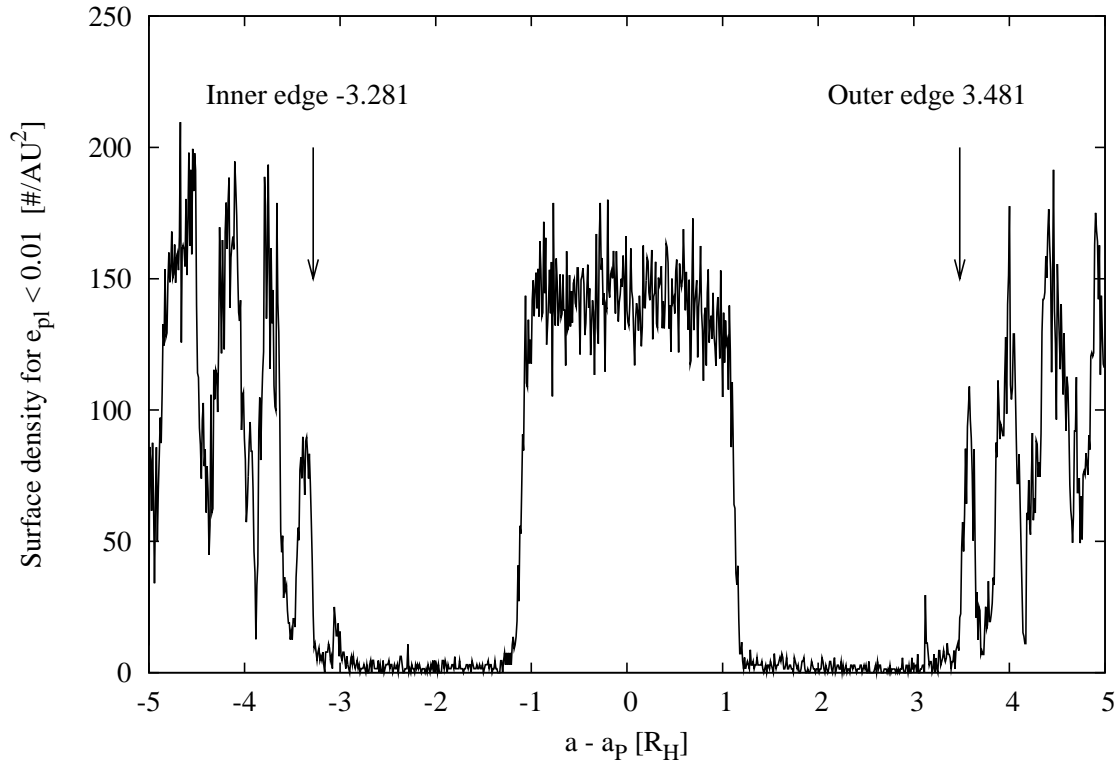


Figure 4.2: Particles with eccentricity $e < 0.01$ were counted in 1000 equally spaced bins of semi-major axis. The resulting surface number densities are shown in units of the Hill radius from the planet. The inner edge of the inner wing and the outer edge of the outer wing are marked.

4.1.1 Average growth

The first analysis of scattering behaviour in the wings consisted of tracing the average eccentricity and semi-major axis of each wing. The wings were defined as the regions

within C_T^{feed} and farther than $1R_H$ from the planet, while the Tisserand parameter for each particle was calculated using equation 1.14. Comparing particles' C_T with the C_T^{feed} ensures that the wing 'reach' asymmetry (section 1.8) is not overlooked, as it would be if wings simply extended $3.5R_H$ on either side of the planet. The eccentricities (in units of the Hill factor χ) are shown as a function of time (in units of the planet's orbital period) in figure 4.3. The averages grow up to a few χ over the course of the simulation, with the most growth occurring in the first hundred periods. The semi-major axes for each wing are expressed as the distance to the planet in units of the Hill radius R_H in figure 4.4. These distances grow by a couple of Hill radii, again with the most growth occurring in the first hundred periods. This timescale can be compared to the synodic time in the *original* centre of the wing (roughly $2R_H$ from the planet) which is approximately given by equation 1.32 to be twenty periods. The majority of the growth therefore occurs in the first $\sim 5T_{syn}(2R_H)$. It should be remembered, however, that the synodic period is greatly changing while wing growth occurs, for individual particles as well as for the average wing quantities.

4.1.2 Wing populations

While the wings grow through the scatterings of the planetesimals, the populations in each wing will be changing. Not all scatterings result in a planetesimal staying in the same wing it began in, many will cross over to the other side of the planet. Figure 4.5 shows the numbers of planetesimals in each wing as a function of time. The outer wing is initially more populated due to the extra 'reach' of the planet to the outside, as was discussed in section 1.8, and this bias increases over time. The bias will be further discussed for varied planet masses in section 4.5. Both populations drop,

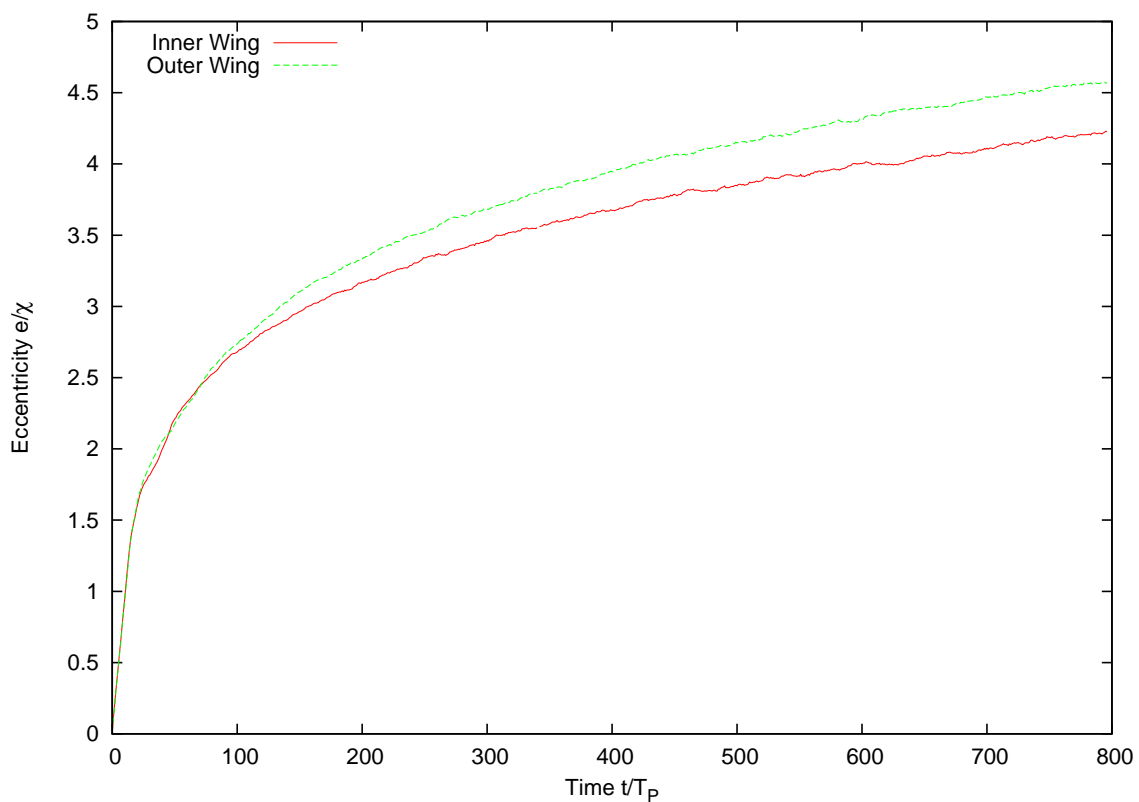


Figure 4.3: The average eccentricity for particles in the inner and outer wings, where the wings are defined to range from $1R_H$ from the planet to a maximum value of $C_T^{feed}(a, e) = C_T(a_P + 3.5R_H, 0)$. Both particle sets rapidly go to higher eccentricity, with the outer wing proceeding higher than the inner.

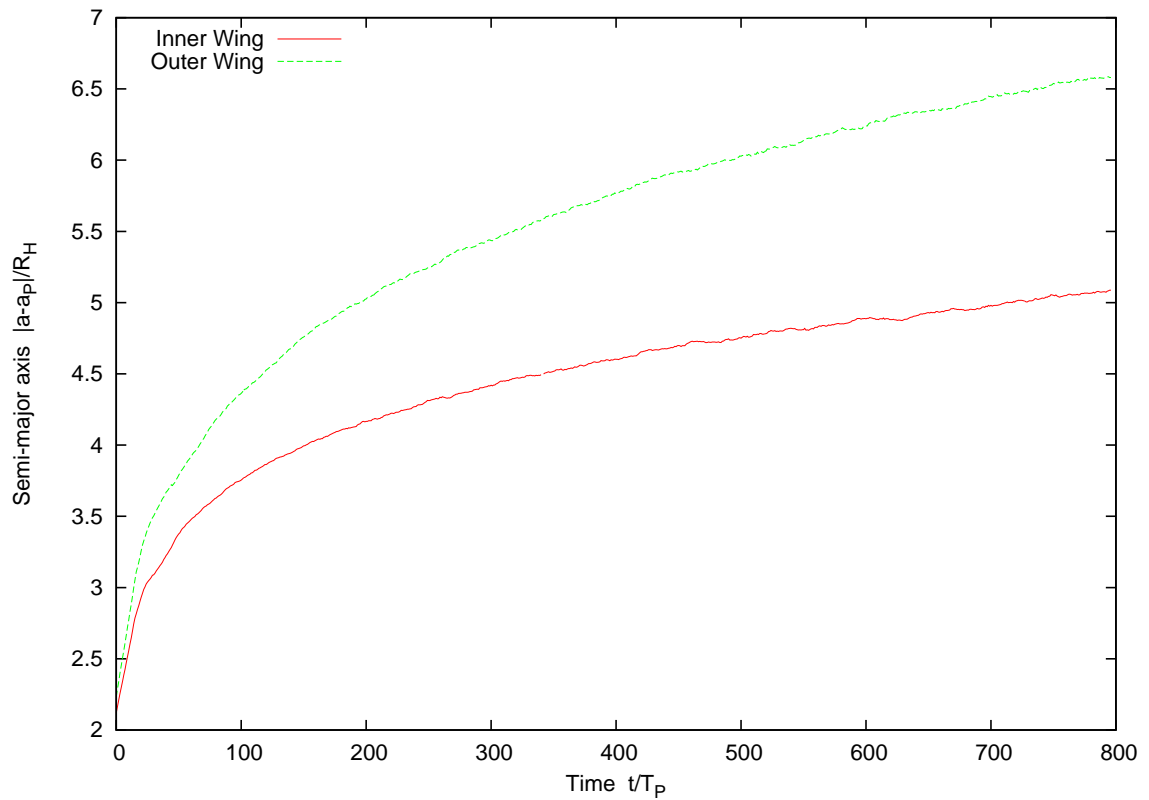


Figure 4.4: The absolute distance of the centre-of-mass for each wing is shown in units of the Hill radius, where the wings are defined as in figure 4.3. Both wings move away from the planet, with the outer wing moving farther.

however, owing mainly to particles being accreted by the planet: the net particle number in the simulation drops by 8.5% during the run.

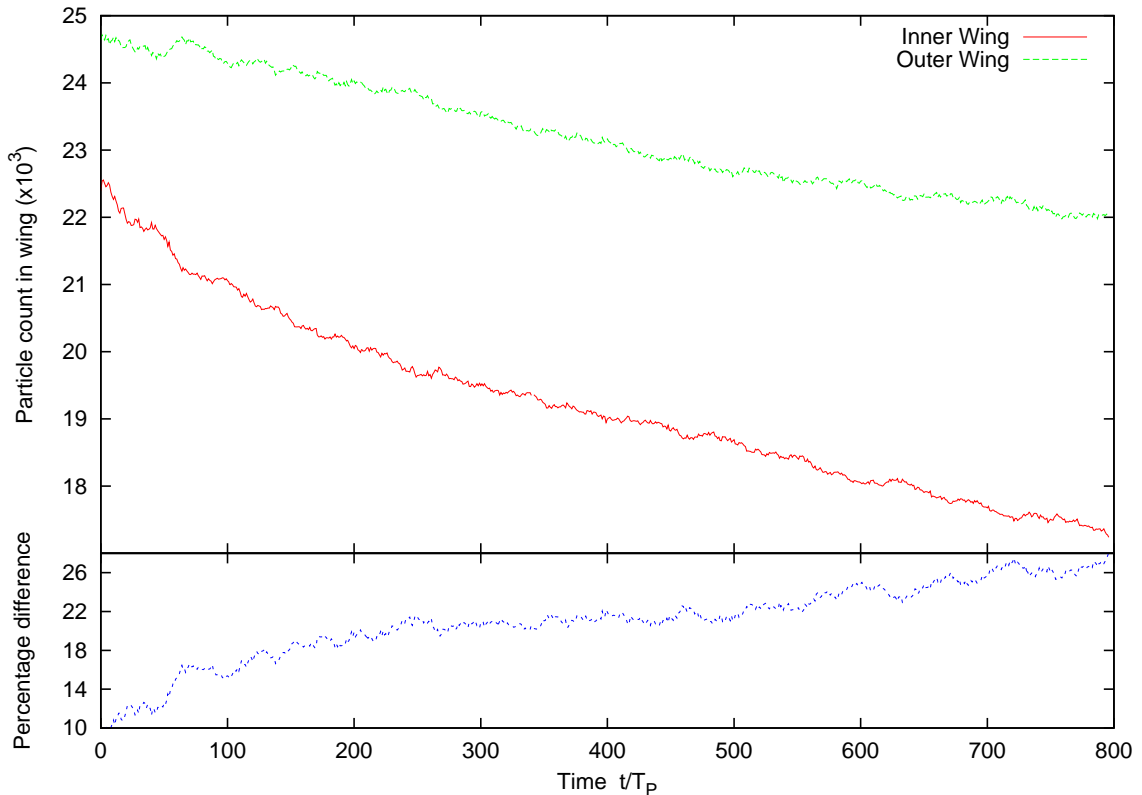


Figure 4.5: The number of particles in each wing is traced in the top panel, where the wings are defined as in figure 4.3. The bottom panel shows the percentage difference between the wings, with the outer wing starting with more than the inner and gaining from there. Absolute particle number drops due to planetary accretion.

4.1.3 Scattering probabilities

Planetesimals are constantly interacting with the planet, resulting in three possible orbital changes for a particle per output: staying in its original wing; crossing to the other wing; or not having a strong encounter with the planet at all. As discussed earlier binning the particles by C_T is the best option (as the wing is extended and

warped in $a - e$ space), but for one output time ($t_{out} = T_P = 125$ years) a significant fraction ($1 - T_P/T_{syn}$) of the particles in a given bin will not be near enough to the planet to have any interaction at all. It is important that these not be confused with particles that have interacted and 'stayed put', so the requirement that $\Delta e > 0.002$ will be applied to the 'stay' category. This is $1/10^{th}$ of the Hill factor, and it is anticipated that the Hill factor will be the unit of any eccentricity change (as will be shown in the next section). Therefore, anything with such a low Δe is likely not at conjunction. This section will investigate for each wing how many particles experience a conjunction within the 125 year output interval, and how many of those cross between the wings. This will give interaction probabilities (related to the synodic period) and crossing probabilities. The analysis here will be followed-up on in section 4.5 for various-massed planets.

The bottom panel of figure 4.6 shows the fraction of particles that suffered an orbital change of greater than $\Delta e > \frac{\chi}{10}$ between output times, out of the number of particles in that C_T bin originally. This is therefore the probability of having an interaction in one period as a function of C_T . The top panel of figure 4.6 shows the fraction of particles that started in the inner (outer) wing in each C_T bin and crossed to the outer (inner) wing, out of the set of particles in the inner (outer) wing in that C_T bin that had an interaction between outputs. This is therefore the probability of crossing during an interaction from a given wing, as a function of C_T . This has been integrated from $t = 200T_P$ until the end of the run.

The crossing curves show that if a particle *has* an interaction, the interaction is far more likely to cause that particle to switch wings if it is at low Tisserand parameter, and therefore close to the planet. Furthermore, the two curves for particles originating

in the inner/outer wings are nearly identical, showing that the crossing probability is well determined as a function of C_T , in which it is symmetric to both sides of the planet. The probability of crossing during an interaction is, from $\sim a_P - \frac{3}{4}R_H$ to $\sim a_P - 3R_H$, well fit by the curve shown:

$$P \propto \frac{1}{C_T - 3.0} \quad (4.2)$$

The probability is $\sim 30\%$ at $a_P - 1R_H$, already down to $\sim 10\%$ at $a_P - 2R_H$ and $\sim 2\%$ at $a_P - 3R_H$. For reference, the number of Hill radii interior to the planet to reach a corresponding C_T is shown at the top of the figure. The horseshoes, within $1R_H$, cross the orbit of the planet at every interaction as discussed in section 1.7, so this implies that the horseshoe interaction lasts a few periods.

The bottom panel of figure Figure 4.6 shows a simple fit to the interaction probability: the fraction is just the ratio T_P/T_{syn} , such that all the particles experiencing conjunction with the planet *during* the output interval will experience some interaction with $\Delta e > \chi/10$. Using the simplest assumptions, with the wing at zero eccentricity: $C_T = \frac{a_P}{a} + 2\sqrt{\frac{a}{a_P}}$ and $T_{syn} = \frac{2}{3\left(1-\frac{a}{a_P}\right)}$, the result to second order is: $\frac{T_P}{T_{syn}} = \sqrt{\frac{9}{5}(C_T - 3.0)}$, and this is what is shown. The probability of interaction is clearly higher than this, by a factor of two or so. This is likely due to the average synodic period for wing particles reducing (*i.e.* scatterings become more frequent and therefore more likely per output interval) as particles are driven to larger distances from the planet (*i.e.* up the wing). This nonetheless makes a good case for most particles experiencing an interaction of $\Delta e > \frac{\chi}{10}$ at every conjunction.

The probabilities in the bottom panel are shown separately for particles which start their interaction (or didn't interact at all) in the inner and outer wings, and there is a clear disparity. Indeed, if these curves simply give the interaction timescale,

then the timescales for both wings are very regular across each wing, but the outer wing has a *longer* time of interaction. The difference between the curves averages to approximately 20%, roughly equivalent to the final difference in the wings' populations as seen in figure 4.5. This difference in the interaction probability per period, most likely due to the difference in the timescales, is therefore the most likely cause of more particles ending up in the outer wing than in the inner. This would seem to conflict somewhat with figure 4.4 which showed that the outer wing particles are farther from the planet on average than the inner wing particles, which should lead to a shorter synodic period. This calls into doubt the use of the synodic period as the exact value of the interaction timescale. The results of section 4.4 will show that the eccentricities of the wings also play a role in the value of the interaction timescale. These points will be returned to and expanded on in section 4.5.

4.1.4 Eccentricity change without crossing

The growth of the wings in eccentricity clearly implies that the average scattering event increases the eccentricity of the planetesimal. The next two sections will investigate what that average increase is, and how it depends on the Tisserand parameter.

The first subset of scatterings to be investigated will be the planetesimals that do not cross between the inner and outer wings between the beginning and end of an individual scattering. These particles therefore stay in their original wing. The main complication with this grouping is that it includes planetesimals that, between outputs, did not have an interaction at all; for example planetesimals in opposition to the planet. The last section excluded planetesimals that experienced an interaction with $\Delta e < \chi/10$, but it is uncertain that these interactions would not be just as valid

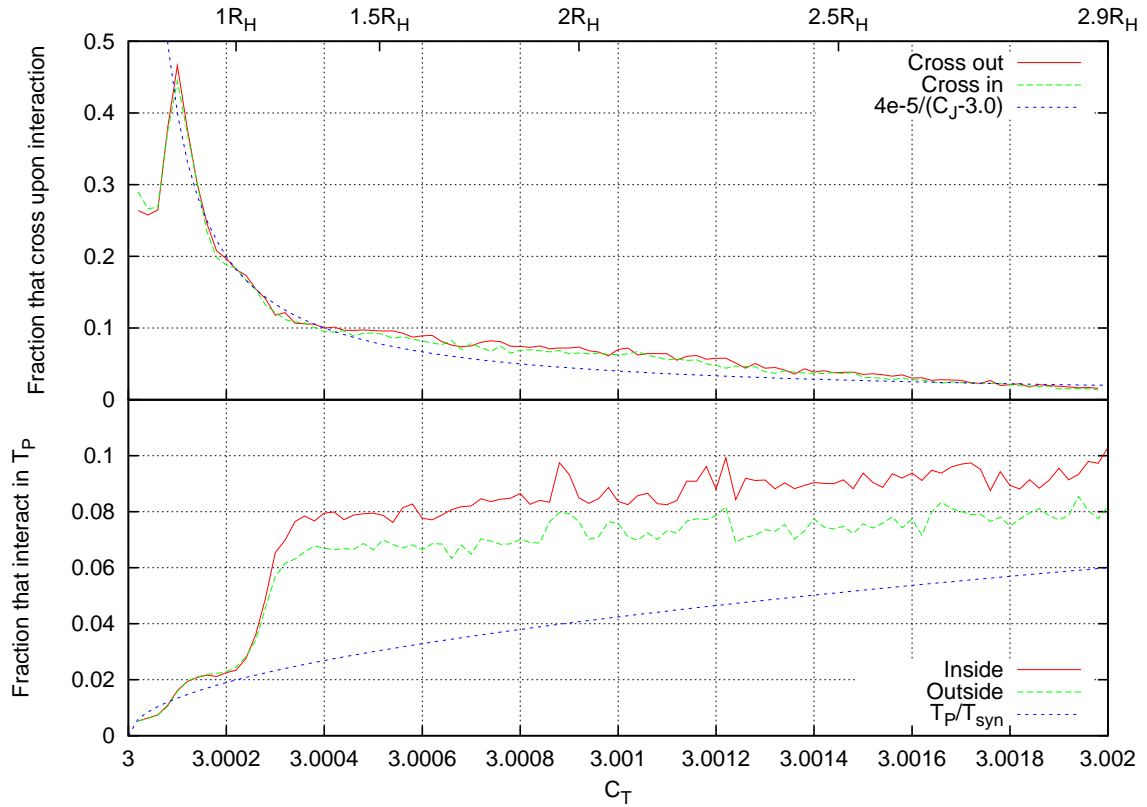


Figure 4.6: Fractions binned by Tisserand parameter C_T . The lines in the bottom panel show the fraction of particles in each wing, by C_T bin that have a $\Delta e > \chi/10$ during one planetary period. The line fit to it is what would be expected if every particle had an interaction once a synodic period, where the synodic period is calculated from the C_T value's corresponding a at $e = 0$. The green and blue dotted lines are the fraction, of those that have an interaction, that switch wings and therefore cross the planet's orbit. Crossing "out" would imply starting interior to the planet and ending exterior, and vice versa.

as an interaction with $\Delta e \sim \chi$.

To investigate this, the change in eccentricity was measured for particles that, between outputs, did not cross to the other wing. To be specific, if they started with less angular momentum than the planet, they ended with less, and if they started with more than they ended with more. In order to ensure that no horseshoe particles (which stay at low eccentricity) were counted, the requirement was set that $a > a_P + 1R_H$ for particles in the outer wing, and $a < a_P - 1R_H$ for particles in the inner wing. The requirement was also set that $C_T < C_T^{feed}$ to ensure that no particles outside of the wings (all of which do not cross) were counted. The Δe values were then binned in 150 bins, ranging from -2χ to $+2\chi$. These counts were integrated over various times, such that the changes in the Δe distribution would be visible in figure 4.7. This figure shows the distribution of Δe averaged over several intervals: the first 10 orbits; the next ten orbits; 80 orbits after that; 100 more orbits; and the remaining 600 orbits in the run.

The counts are displayed logarithmically as the central peak is orders of magnitude higher than the wings of the distribution: the central peak contains all particles that didn't have an interaction at all, and from figure 4.6 this is close to 90% of the particles at every output. A second peak is evident in the first ten orbits at $\Delta e \sim \frac{3}{4}\chi$, and during this interval the distribution of Δe is strongly asymmetric to positive eccentricity changes. This is why the wings grow vertically in the $a - e$ plane, and for the particles that stay in their original wings the contribution to the growth is fairly small, only on the order of $\Delta e \sim \chi$. For later times, when the wings are higher and particles have eccentricity to lose, the Δe is symmetric at zero, implying that equilibrium has been reached and, at least from particles that stay in their original

wing, not much more wing growth will be evident. This seems to take ~ 20 orbits, which is roughly one synodic period at $a = a_P - 2R_H$, the 'centre' of the wing.

The inner and outer wings are segregated in the figure, but show no substantial difference except for a possible slight tendency for the outer wing to have larger Δe , which fits with the fact that the outer wing attains a higher average eccentricity (as seen in figure 4.3).

4.1.5 Eccentricity change upon crossing

The change in eccentricity was also measured for particles that, between outputs, changed wings. The requirement that $a > a_P + 1.2R_H$ for particles crossing from the outer wing, and $a < a_P - 1.2R_H$ for particles crossing from the inner wing was held in order to exclude horseshoes. Horseshoes *do* cross the planet's orbit, but are not the type of scattering we are interested in here, and thus it is important enough to exclude them that the limit was extended beyond the usual $1R_H$ to $1.2R_H$ (the limit identified in figure 4.2), which may even shave off a few close wing particles. No requirement was needed for the outer extent of the wing, as any particle that crosses the planet's orbit must by definition be a wing or horseshoe particle. The Δe values for all the crossings were then binned in 150 bins, ranging from -6χ to $+6\chi$. These counts were integrated over varied times as in the last section. Figure 4.8 shows the distribution of Δe averaged over the various intervals. Aside from the resolution changing as more scatterings are counted for longer times, two other changes are immediately evident.

The main peak in Δe drops from $\sim 2\chi$ down to $\sim 0\chi$, such that the initial scatterings are obviously far more asymmetric to large positive Δe , reflecting the growth of the wings in e , whereas later scatterings tend to have just as many *decreases*

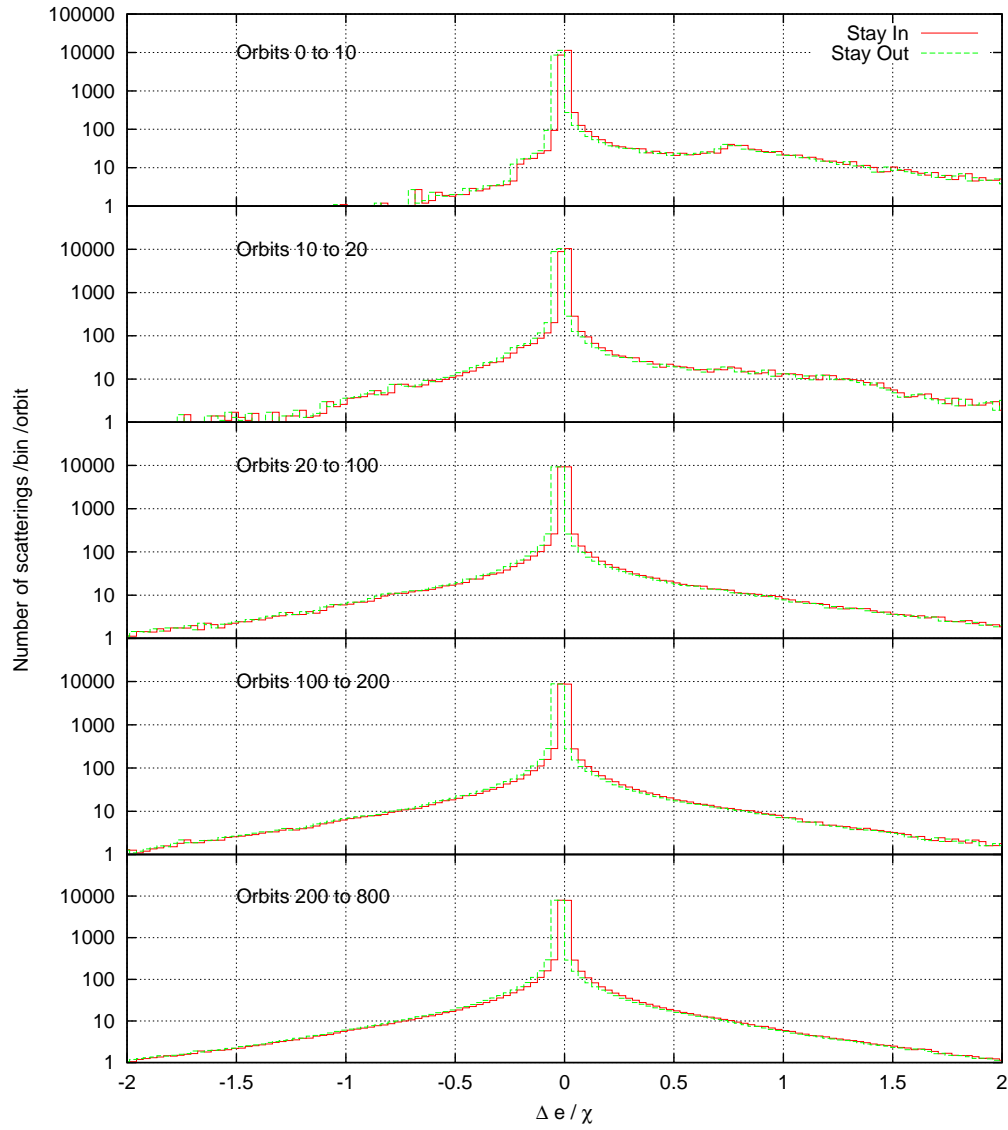


Figure 4.7: The distribution of scattering events by their change in planetesimal eccentricity, displayed logarithmically. Only wing particles ($C_T < C_T^{feed}$, $|a - a_P| > 1R_H$) are included. Each frame displays the distribution averaged over a certain number of orbits stated in the top left. Scatterings that stay in the outer or inner wing upon scattering are segregated.

in e as a given increase. This is another indicator of equilibrium being reached towards the end of the simulation, as the particles would be shifting within the wings without increasing the average e of the wings.

A second peak in Δe is apparent at early times at high values ($\Delta e \sim 5.5\chi$), but this dissipates and is mostly gone by the end of the run. This is most likely a build-up at the edge of the distribution reflecting the upper limit of the planets ability to impart a Δe (see section A.1 for an approximate determination of this limit). This limit can also be seen as the upper range of the eccentricity changes in the figure 2.1 from IBLT. The strongest changes in e therefore occur at early times, and are double-peaked.

At several points in the distribution, especially at high Δe at the early times, and at zero Δe at late times, the Δe is slightly higher for particles crossing outwards than inwards. This contributes to the fact that the wing is slightly higher on the outside, seen in figure 4.1

Using the same routine that tracked scattering probabilities by C_T for the last section, the average Δe for all particles that crossed from a certain C_T bin was also calculated. This allowed a determination of where the highest kicks were occurring, specifically for particles crossing between the wings. Figure 4.9 shows what the average Δe looks like as a function of C_T for the same intervals as used in the previous section's analysis. For the close particles the action occurs mostly in the first twenty orbits (about one synodic period at the wing centre), and after that they mostly average to zero. For the farther particles, no data was recorded for the first twenty orbits at all, as they did not have the eccentricity required to come closer to the planet and cross. After that, however, they start experiencing large changes in eccentricity. Regions of the plots near zero would indicate equilibrium has been reached

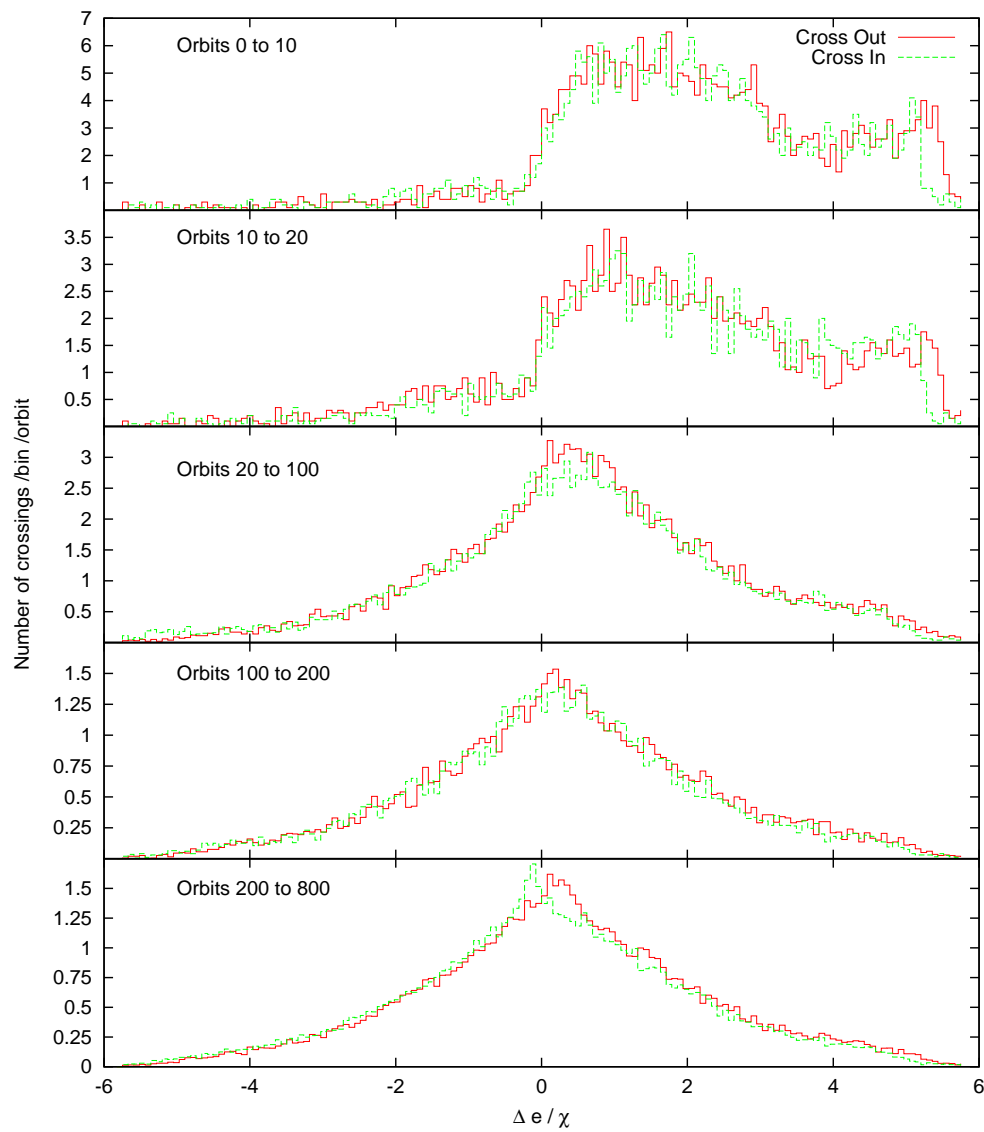


Figure 4.8: The distribution of scattering events with respect to the change in eccentricity of the planetesimal. Each frame displays the distribution averaged over a certain number of orbits stated in the top left. Scatterings crossing outwards or inwards are segregated.

for that C_T , which shows that the early particles equilibrate very fast despite their very large synodic period, and the farther particles require more time, despite their much shorter synodic period. However, as figure 4.6 shows, the crossing probability is much lower at high C_T , and therefore the noise due to averaging over only a few scatterings would be higher, and this explains much of the spikiness in the final frame at high C_T .

4.2 Horseshoes and resonances

In the previous sections, horseshoes were excluded from the main groups of interactions, and resonances were ignored. Horseshoes, as evidenced from figure 4.1, tend to drift about in the $a_P \pm 1R_H$ region without changing their eccentricities. Furthermore, since they are so close to the planet, their synodic period is very long. Horseshoes exchange angular momentum with the planet at every conjunction when they 'switch sides' and reverse their direction in the corotating frame, but exchange an equal and opposite amount at the next conjunction, making their net effect nearly zero. However, as they are trapped in the 1:1 mean motion resonance with the planet, the planet will drag them along with it if it tries to migrate, and this increases its effective mass. This makes horseshoes a very different population from the wings (which fuel migration), and their effect on migration will be specifically discussed in section 5.5.

Resonances, as also seen in the $a - e$ plane of figure 4.1, tend to increase their eccentricity without changing their semi-major axis very much, producing jagged spikes. They will then oscillate vertically in the $a - e$ plane within these spikes. The spikes are only up to $e \sim \chi$ in the timescales presented here, and thus are unlikely



Figure 4.9: The average change in eccentricity (in Hill units) is displayed as a function of Tisserand parameter C_T over 150 bins in that parameter. The changes are averaged over the bin and over a number of orbits stated in the top left. Scatterings crossing outwards or inwards are segregated. The zero line has been indicated by a dotted line when necessary. Values of C_T for which no Δe is plotted had no crossing events recorded in the bin throughout the interval indicated.

to provide any strong angular momentum transfer. They may become important, however, if they are pumped high enough that particles which *were* unable to cross the planet's orbit begin to rise up into the wings, where they can cross and experience stronger interactions. This process was discussed in Murray *et al.* (1998) [23]. This introduces a new population of particles into the wing, and represents one of the few 'stochastic' processes in the whole disk-planet interaction, as they can provide bursts of available mass at varying times and locations. They are nonetheless slow to achieve this, and do not contain much mass, so this process was not heavily investigated for this thesis.

4.3 Angular momentum transfer

Scatterings have been investigated for their characteristics in a and e , but for the purposes of studying planetary migration it is the change of angular momentum that is the driving factor. This section will explore the angular momentum exchange from particles that cross wings, or stay in a wing, as a function of C_T and on average, in order to determine what populations would propel the planet and how they would do it. As the particles in this section are massless, what is truly being discussed is the specific angular momentum $h \propto \sqrt{a(1-e^2)}$ which does not depend on mass. The specific angular momentum change for the planet would be the specific angular momentum change for all the particles multiplied by the factor m_{pl}/M_P which is basically a constant during a scattering.

Planetesimals crossing outwards will gain specific angular momentum, which is proportional to $a^{\frac{1}{2}}$, while planetesimals crossing inwards will lose specific angular momentum. Planetesimals staying in a wing but moving away from the planet will gain

for the outer wing and lose for the inner wing. This brief summary neglects the fact that the eccentricity is also changing, which complicates the issue, as specific angular momentum is also proportional to $\sqrt{1 - e^2}$. Properly evaluating angular momentum changes as particles are driven up the wings, or cross, is therefore difficult analytically, but simple using the results of the D0 run.

The initial analysis of angular momentum transfer will look at net changes in angular momentum over time, due to crossings and due to 'stationary' particles. Particles which switched, between outputs, from having angular momentum $h < h_P$ to $h > h_P$, or vice versa, were considered to cross, and particles with an unchanged inequality were considered to stay. Horseshoes were not excluded, as they undergo such small net changes over time that they should not contribute anyway. Similarly, particles outside the wing were still counted, as they should mostly cancel and they will be part of the disk regardless, and therefore are of interest for this *net* change analysis.

The Δh for each particle was summed within its category (cross/stay in/out) to give, for every timestep, the total change of angular momentum due to that category of scattering. The changes were added cumulatively, so that the total change up until a certain time could be tracked. The result is shown in figure 4.10, with the bottom frames showing the cumulative change in angular momentum due to scatterings of particles that remain in their initial wings (with the inner/outer populations separated, and the inner one is actually negative), or cross between the wings (with the particles crossing from the outer to the inner wing being negative). The top frame shows the differences from each of those populations between the two wing populations, and these differences add to give the net change in angular momentum that

has occurred due to all scatterings.

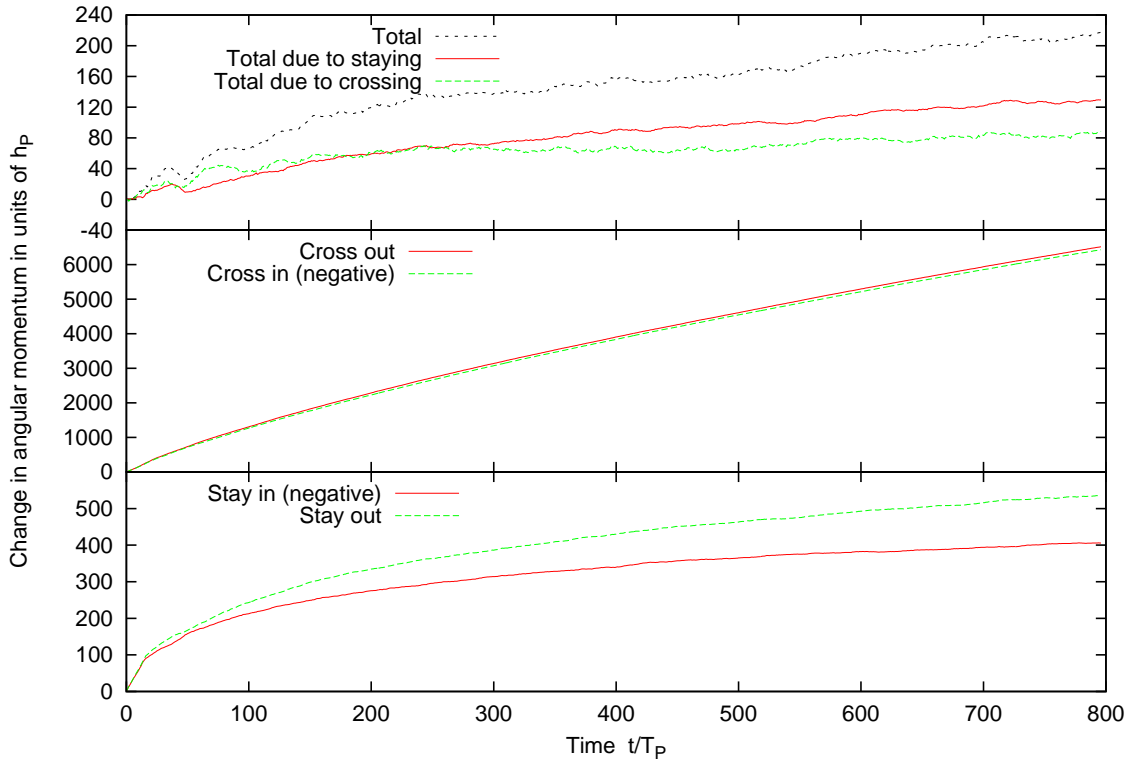


Figure 4.10: Angular momentum differences counted for four types of scattering: particles that stay in the inner/outer wings in the bottom frame; particles that cross between the wings in the middle frame. The absolute value of the summed differences of these categories are shown, with the particles that stayed in and the particles that crossed in actually producing a negative change in angular momentum. The difference between the two curves in each frame are shown in the top frame, and these are further summed to give the net angular momentum change for the entire disk.

The net angular momentum exchange is positive for the disk, and therefore the planet would be losing angular momentum and migrating in if the disk had any mass. The particles that stay in the outer wing and the particles that cross to the outer wing are the two groups that contribute the most angular momentum. The differences between the staying and the crossing particles, displayed as two of the

lines in the top frame, are very even, with both approximately contributing half of the net exchange. This is despite the angular momentum exchange from the crossings being much larger than the exchange from the stationary particles. At early times it is the crossing particles that gain the most angular momentum, with the staying particles eventually overtaking that gain. The net angular momentum imparted to the disk continues growing even by the end of the simulation, implying that a true equilibrium has not been reached, and may never be reached.

The population that stays in the wing never produces strong angular momentum changes, but as the figure shows, it is the *difference* between the in/out populations that produced the net angular momentum change, and in this difference the staying population is as important as the crossing population. This may not be as true for a migrating planet, however, which moves relative to the position of the wings at any given instant. The simple model that will be used to describe the migration process, to be defined in section 5.1, will be based mostly on the crossing population. It should be remembered that the staying population may still provide as much angular momentum as the crossing population.

4.3.1 Angular momentum transfer by C_T

The angular momentum changes for scatterings were then explored as a function of C_T , in order to see which part of the wings contributed the most. It has already been seen that the low- C_T (the near part of the wing) are scattered more frequently (see figure 4.6), but particles crossing between the wings at the inner edges of the wings have the least distance Δa to cross, and therefore should have a smaller angular momentum change. The angular momentum changes across timesteps for particles

falling in the usual four categories (crossing/staying in the inner/outer wing) were summed in 150 bins in C_T , and were integrated in the five time slices utilized in the previous sections. The results are shown in figure 4.11.

The highest angular momentum changes come from about $1.5R_H$ from the planet, at the inner edge of the wing where crossings are most common. A deficit exists just inside $2R_H$ from the planet, at the early stages, but by the late stages the entire region is fairly smooth past $1R_H$. It can be seen that the angular momentum transfer is minimal beyond $\sim 2.2R_H$, which is the value that will be used in section 5.1.2 as the 'middle' of the wing.

4.4 Dependence on wing height

The wings grow vertically in the $a - e$ plane over time, reaching higher eccentricities, but in some disks the planetesimals may already be heated to a few χ at the start of the simulation. The question then arises: how does the population scattered at high eccentricities differ from that scattered at low eccentricities? If the e is higher than a few χ it could be expected that particles would 'miss' the planet's Hill sphere (see section 1.6.1), and this should reduce the probability of scattering.

The number of scatterings between outputs was counted from orbit 400 until the end of the simulation, when the run is mostly equilibrated and the wings are at their highest. Included scatterings were limited to a Δe of $\chi/10$, and were required to be outside of $1R_H$ from the planet to exclude horseshoes, and have $C_T < C_T^{feed}$ to include only wing particles. The number of particles in a given e -bin that switched from the outer wing to the inner wing was divided by the total number of particles that registered a scattering event from that e -bin in the outer wing, to give the

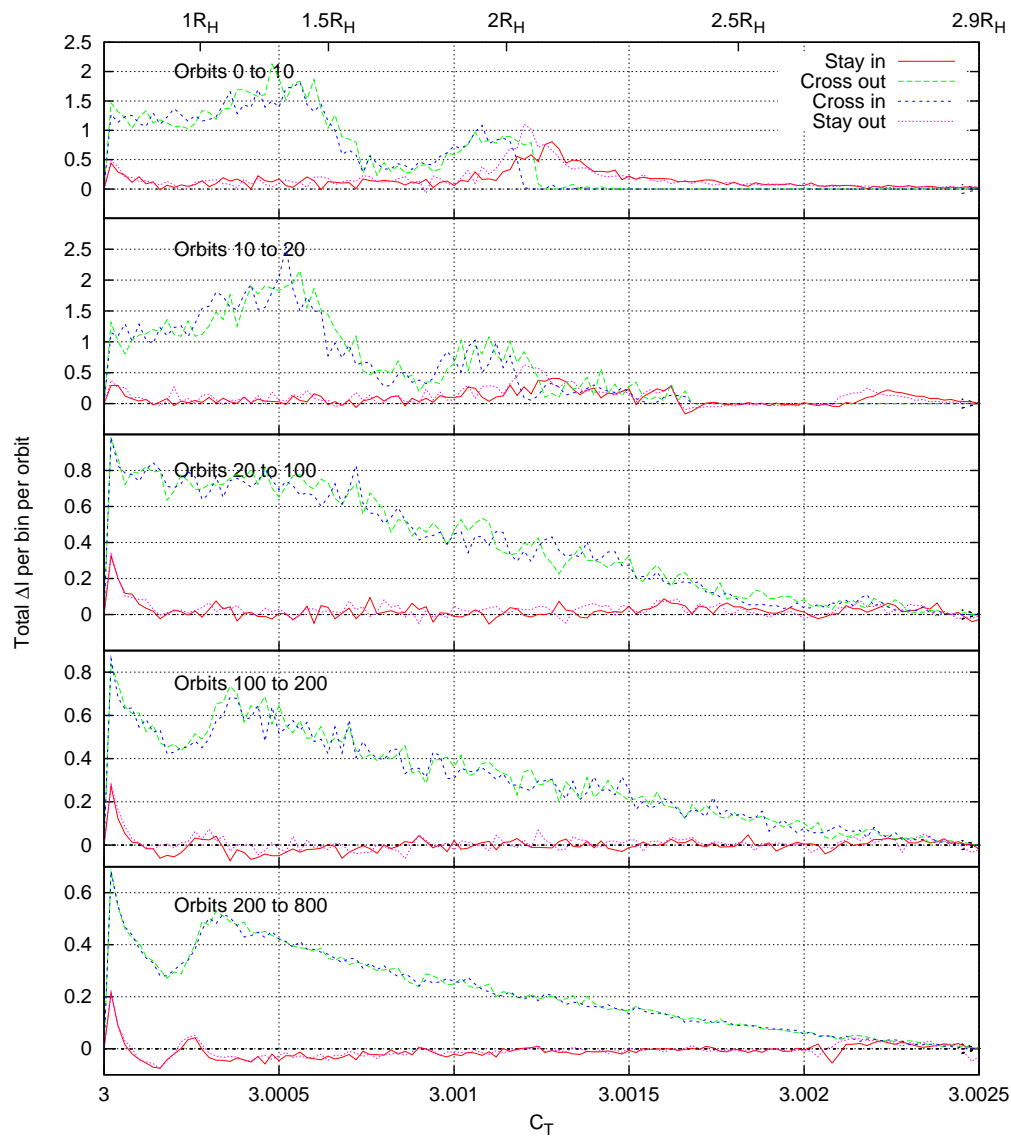


Figure 4.11: Angular momentum changes between timesteps were integrated for various intervals of time for particles binned by C_T in 150 bins. Particles were grouped by the four in/out stay/cross categories, to show where the strongest kicks to the planet would be coming from.

probability of crossing inwards during a scattering. Similarly, the number of particles in a given e -bin that switched from the inner wing to the outer wing was then divided by the total number of particles that registered a scattering event from that e -bin in the inner wing, to give the probability of crossing outwards during a scattering. The resulting probabilities are shown in figure 4.12.

It can be seen that the probability of crossing the planet's orbit during a scattering is small at low eccentricity, when the particles far from the planet would not have enough eccentricity to cross its orbit. The probability peaks around $e/\chi \sim 1$, dropping as the eccentricity grows and allows the particle to miss the planet's Hill sphere during conjunction. The drop proceeds even more rapidly past $e/\chi \sim 4$, and bottoms out around $e/\chi \sim 6$. However, even in a very hot disk, it is unlikely that the entire population be at such high eccentricity. Simulations with a Rayleigh-distributed planetesimal eccentricity centered at a root-mean-squared eccentricity of such a high value would still have particles at lower eccentricity, and the process of scattering will also bring particles to lower e , so such cases of zero crossings would be unlikely to last long. However, it is clear that particles of such high e will not cross unless their e eventually decreases.

The drop in the crossing probability is extremely fast past $\sim 4\chi$, and can be approximated with a factor of $1 + \left(\frac{e}{4.5\chi}\right)^9$. The IBLT factor in the reduction of angular momentum exchange due to high eccentricity was $1 + \left(\frac{e}{\chi}\right)^3$, much slower, leaving the exact dependence of the probability on the eccentricity hard to predict. The fast drop may be an important part of the reason for the difference in the interaction timescales of the wings (which have different average eccentricities) as discussed in section 4.1.3 and as will be discussed further in the next section.

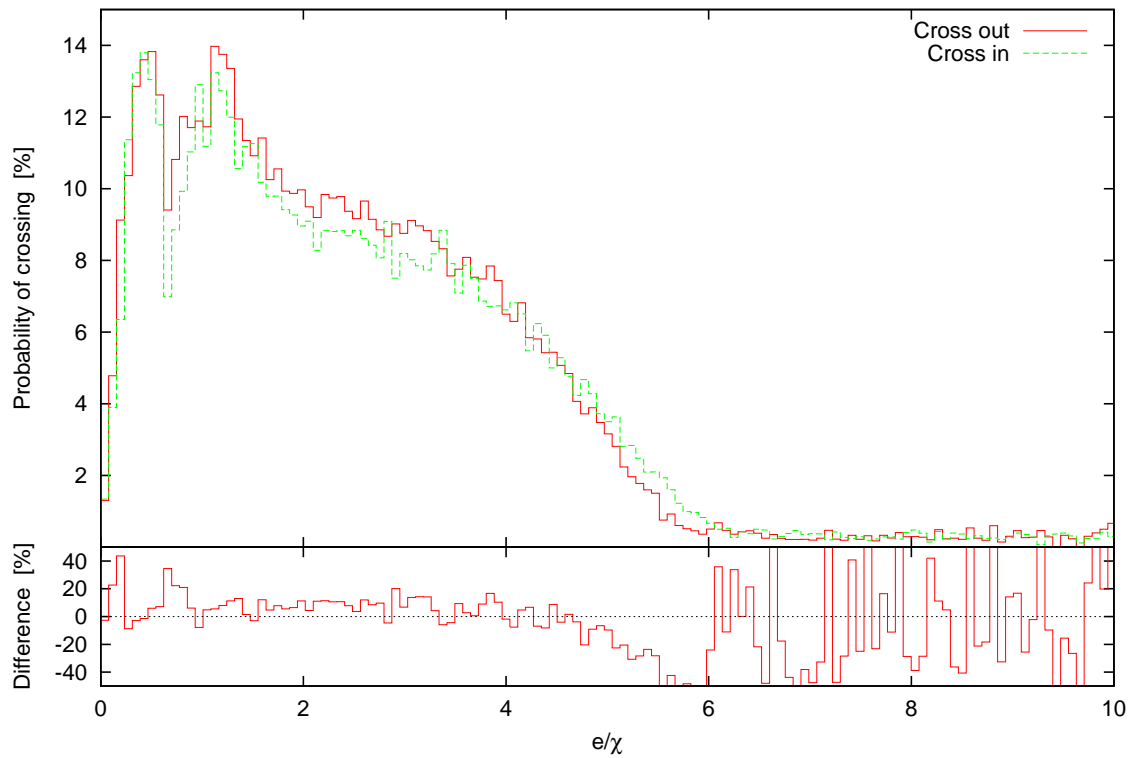


Figure 4.12: The percentage of crossings from a given e -bin (out of 150 bins) and wing, per the number of scatterings that occurred in that bin. The eccentricity is expressed in Hill units. The bottom panel shows the percentage difference between the crossing probability in the outer and inner wings.

4.5 Imbalance

Which way will the planet migrate, inwards or outwards? The IBLT paper stopped short of providing a prediction, but already (section 4.1.2) we have seen that the ratio of outer-to-inner populations of planetesimals grows with time, implying a push to the planet to migrate inwards. In order to further test the asymmetries in general scattering described in sections 1.8 and 1.9, and further characterize the population imbalance just described, a set of simulations was run with a planet of varied mass located at $a_P = 25AU$ in an unvaried massless disk. The disks were composed of 2×10^4 particles distributed evenly (ie. $\Sigma \propto a^{-1}$) from $a_P - 6R_H$ to $a_P + 6R_H$, with eccentricity $e_{RMS} = 0.01$. The systems were run for 10^5 years (800 planet orbits). Any particle with Tisserand value less than C_T^{feed} and with a distance from the planet of greater than $1R_H$ was counted as a wing particle.

Shown in figure 4.13 is a comparison of the population of planetesimals in the inner and outer wings for a planet of $37.5M_{Earth}$. The top panel shows the net number of particles in the two wings and the bottom panel shows the percentage difference between the two wings. The differences are reaching equilibrium after about 4×10^4 years, which is ~ 320 orbits or $\sim 4\Delta T_{syn}$ (as calculated for $\delta = 2\chi$ from equation 1.36). This is similar to figure 4.5 which performed this analysis for the D0 run, except here the eccentricities were set to $e_{RMS} = 0.01$ and this likely leads to less accretion and particle loss.

The final difference (after reaching an approximate equilibrium) and the initial difference in wing count were recorded for all the runs, and are shown in figure 4.14 versus the Hill radius value for each simulation's plane. There was substantial oscillation in the count differences in the lower masses, as the asymmetry (see section 1.8

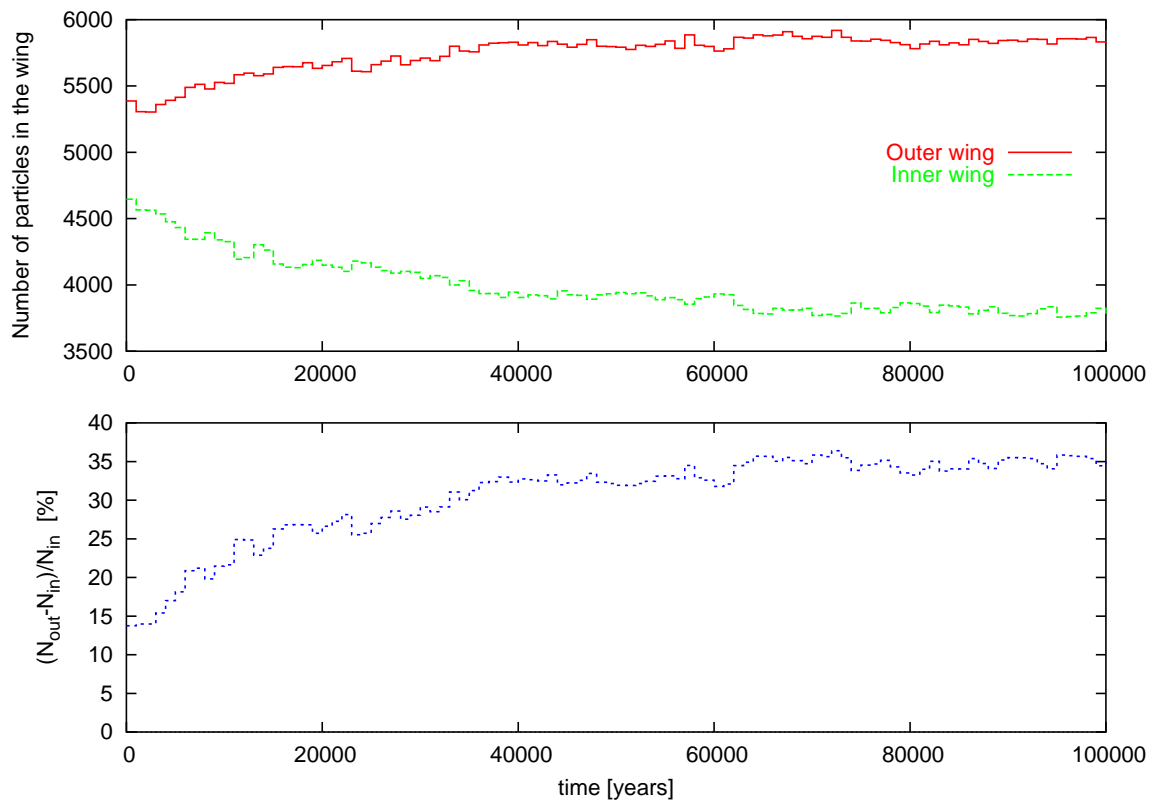


Figure 4.13: Total numbers of particles within the defined planetary wings were counted as a function of time in the upper plot. In the lower plot the percentage difference between the counts are shown, and can be seen to level off.

for the wing reach asymmetry) should be smaller and the synodic period longer for these planets, so error-bars are also shown to indicate the variation in the final difference. The lower error is the smallest difference that occurred after one synodic period (normally it occurred near $2T_{syn}$, as this is when the first scattering will have been largely reversed by the second scattering), while the upper error is simply the largest difference that occurred.

The initial difference is fit very well by equation 1.26 with a δ_{out} of $3.464R_H$, which was the δ used in calculating the limiting C_T , with a correction factor of 1.44 to account for the conversion of wing width to number of particles excluding horseshoes. This merely confirms the approximations used in that derivation. The final difference is close to thrice as large as the initial value, perhaps owing to the fact that inner particles are scattered on a shorter timescale, as described in section 1.9. If these particles had carried substantial angular momentum relative to the planet's, the planet would therefore have lost angular momentum in moving the planetesimals to wider orbits, and it would have migrated inwards.

A timescale analysis will now be done to see if it can be determined why the initial population imbalance is increased by a factor of three. For particles being scattered from one reservoir to another, the equilibrium condition for the population ratios can be described as a diffusion proportionality by:

$$\frac{n_{out}}{n_{in}} = \frac{T_{out}}{T_{in}} \quad (4.3)$$

so that an inner timescale shorter than the outer one will cause more frequent scatterings to the outside, and therefore a build-up of material there.

The initial timescales chosen to represent T_{out} and T_{in} were the synodic periods, as defined by equation 1.28. The question becomes where should the synodic periods

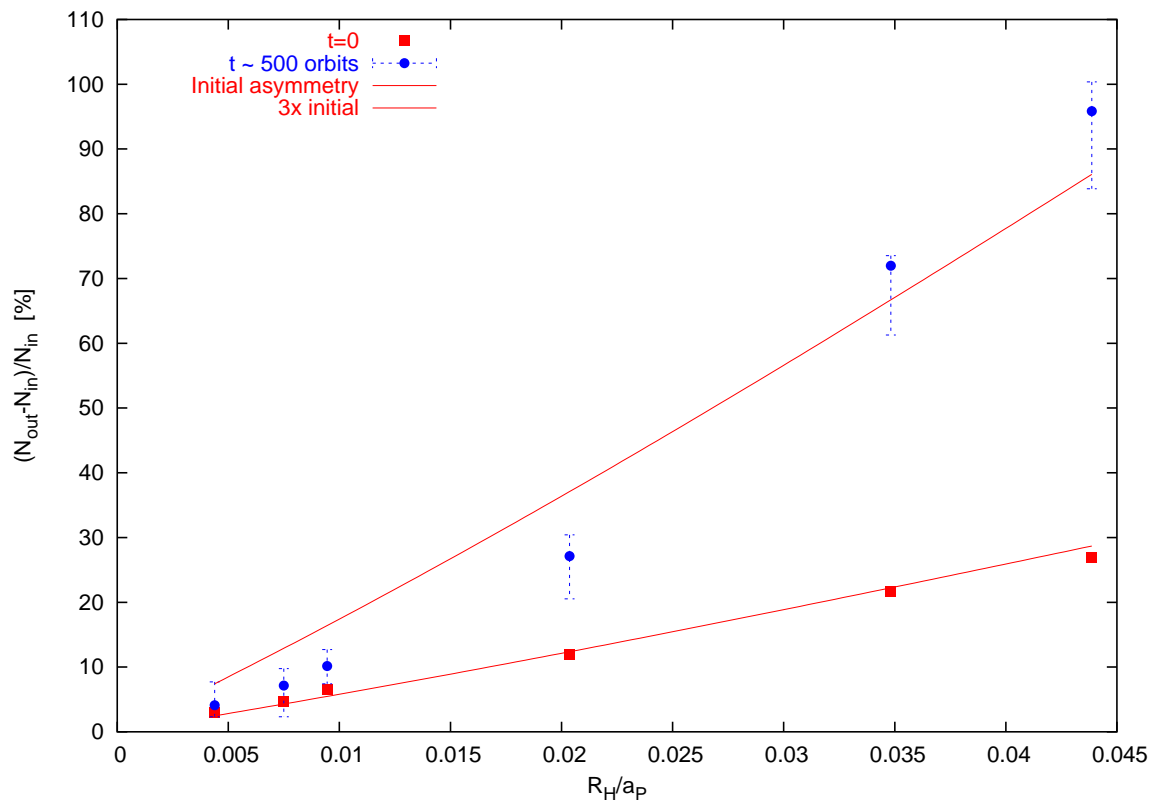


Figure 4.14: The initial and final percentage differences of the particle number counts in inner/outer wings are plotted for varied planet mass (plotted in terms of the Hill factor), with the fit to the initial set by equation 1.26. Also shown is a curve of three times the result of equation 1.26.

be measured: the outer edge or the middle of the initial wing boundaries, or perhaps the centre-of-mass semi-major axis for the wings at equilibrium? The trouble is that the inner wing does not move as far from the planet as the outer wing (see figure 4.4), and this means that the outer synodic period becomes much *smaller* than the inner, wherever it would be measured. For example, the $37.5M_{Earth}$ planet described earlier has centre-of-masses for the wings at $\delta_{in} = 3.5\chi$ and $\delta_{out} = 6.7\chi$ at equilibrium, and a ratio of the synodic periods at these displacements of 0.85, meaning that material should be scattered faster *from* the outside *to* the inside. However, the average eccentricity in the outer wing is also higher (see figure 4.3) and as figure 4.12 shows, particles with high eccentricity have a much smaller probability of crossing. This is because, as discussed in section 1.6.1, eccentricities higher than one Hill eccentricity can move wing particles outside of the feeding zone at conjunction. The synodic period is therefore not a complete descriptor of the interaction timescale for high- e particles, but it remains the simplest measure.

The final (after 800 orbits) differences in the average distance of the wings to the planet, and the average eccentricities of the wings, depend on the planet mass. The $0.75M_{Earth}$ planet had a difference in the average distances of about a Hill radius between the wings, and a difference in the eccentricities of a fraction of a Hill factor. The $75M_{Earth}$ planet, on the other hand, had a distance difference of about $6R_H$ and an eccentricity difference of about 1.5χ . As both factors influence the relative *interaction timescales* of the wings, if not the actual synodic period which only depends on Δa , then there is certainly reason to believe that it is the timescales that determine the wing population imbalance, and its dependence on planet mass. The interaction probability as shown in figure 4.6 for the D0 run indeed showed that the

timescale (if that is simply dependent on the inverse of the probability) was larger for the outer wing, which would cause a pile-up of material there. It is the exact form of the timescale on the distances and eccentricities, which are both dependent on the Hill factor, that remains a mystery for now. Nonetheless the population imbalance contributes to a crucial bias in the migration direction of planets, and will be discussed further throughout this work, especially in sections 5.11 and 6.4.

Chapter 5

Planet migration

This chapter will delve into the process of planetary migration driven by planetesimal scattering. A toy model will be used to produce a fiducial migration rate, a point of comparison for the simulation results. Resolution issues in simulation will be explored, and then the many simulation sets that were used to investigate trends with various physical quantities will be described. These trends will be explained, but for the most part not heavily modeled, using the results from the previous chapter on the scattering process. This will all be summarized in the next chapter, the discussion.

5.1 Baseline rates

The scattering rate of a planet passing through a planetesimal disk can be estimated in a simple manner using an $n\sigma v$ argument, and this in turn can be used to estimate the angular momentum exchange rate and the migration rate of the planet. This calculation will provide a reference point, a fiducial value against which measured migration rates can be compared.

The encounter rate $R = n\sigma v_{rel}$ is dependent on the number density of the disk, the scattering cross-section of the planet, and the relative velocity of the planet-planetesimals. The number density can be expressed in terms of the density ρ as:

$$n = \frac{\rho}{m} \quad (5.1)$$

$$\rho = \frac{\Sigma}{2a_P i} \quad (5.2)$$

where Σ is the surface density of the planetesimal disk, with the planetesimal orbits having a typical inclination i and an individual planetesimal mass given by m (where all the planetesimals have the same mass). The term $2a_P i$ is the vertical height of the disk at the planet's semi-major axis a_P : similar to ae being the radial excursion of an orbit, ai would be the vertical excursion from the reference plane. The cross section of the planet is the area bounded by the Hill radius:

$$\sigma = \pi R_H^2 \quad (5.3)$$

The last chapter determined that the strongest scattering events occurred when a particle crossed the orbit of a planet, in that this population produced the highest angular momentum changes (see section 4.3). The section on wing structure (section 1.5.1) had also implied that such a scattering could be approximately compared to a planetesimal reaching peri/apocentre *at* the planet and then, after crossing the orbit, having its apo/pericentre at the planet. When the planet moves in response to this, it will be moving *into* the population from which that planetesimal began, and away from the other population. The population that stays within its initial wing may therefore be left behind, and may not be as important as the crossing population. For the fiducial calculation, the crossing scattering is what will be focused on, using

the approximation just described. The speed at pericentre for the planetesimal would be:

$$v_{peri} = \sqrt{\frac{GM_{Sun}}{a}} \sqrt{\frac{1+e}{1-e}} \quad (5.4)$$

where a is the semi-major axis and e the eccentricity. For the condition with the pericentre initially at the planet, $q = a(1 - e) = a_P$, this gives a speed of:

$$v_{peri} = \sqrt{\frac{GM_{sun}}{q}} \sqrt{1+e} \approx v_P \left(1 + \frac{e}{2}\right) \quad (5.5)$$

and a relative velocity v_{rel} compared to the planet's speed v_P of:

$$v_{rel} \approx \frac{e}{2} v_P \quad (5.6)$$

Taking these equations together for the encounter rate, with $R_H = \chi a$ where χ is the Hill factor, and $v_P = a_P n = a_P \frac{2\pi}{T}$, with T the orbital period gives:

$$R = \frac{\Sigma}{2ma_P i} \pi R_H^2 \frac{e}{2} a_P \frac{2\pi}{T} \quad (5.7)$$

$$R = \frac{e}{2i} \frac{\pi \Sigma a_P^2}{m} \chi^2 \frac{\pi}{T} \quad (5.8)$$

The angular momentum of a planetesimal of mass m is expressed as $L = m\sqrt{GM_{Sun}a}$. The assumed scattering event has $a_{initial} \approx q(1 + e)$ with $q = a_P$ to $a_{final} \approx Q(1 - e)$ with $Q = a_P$ and no change in e , so the change in angular momentum would be ΔL , with the angular momentum imparted to the planet being $\Delta L/M_P$:

$$\Delta L_P = \frac{m}{M_P} \sqrt{GM_{Sun}a_P} (\sqrt{1+e} - \sqrt{1-e}) \quad (5.9)$$

which simplifies to:

$$\Delta L_P \approx \frac{m}{M_P} \sqrt{GM_{Sun}a_P} e \approx L_P \frac{m}{M_P} e \quad (5.10)$$

However, figure 4.8 showed that the scatterings within the first synodic period definitely do not conserve e , and in fact change the eccentricity by several Hill factors.

The next synodic period sees scatterings on the order of a Hill factor, and for times much longer than a synodic period the eccentricity change does *on average* go to zero for the planetesimal population. For these initial scatterings, then, the change in eccentricity must be considered. The angular momentum change for a scattering that increases the planetesimal's eccentricity by Δe would be given by

$$\Delta L_P \approx L_P \frac{m}{M_P} (e_{init} + \Delta e) \quad (5.11)$$

and this would be negative for the opposite crossing of apocentre \rightarrow pericentre, but the magnitude would be the same and it is the magnitude that is desired for the fiducial estimate.

In a dynamically cold disk with $e_{init} \approx 0$, the angular momentum exchange is therefore proportional to Δe , which would be some multiple of a Hill factor. In a disk heated by a planet, the initial eccentricity may dwarf the change, or the change may average out to zero for the population, and so the more important factor would be e_{init} which would be some multiple of the planet's Hill factor. Either way, the term $e_{init} + \Delta e$ will be on the order of a Hill factor, and so we will replace it with $b_e \chi$ where b_e is some number close to one. This factor will be returned to in section 5.1.2 and will prove to be very important throughout this work.

The angular momentum exchange rate between planetesimals and the planet would be:

$$\frac{\Delta L}{\Delta t} = R \Delta L \quad (5.12)$$

and inserting equation 5.8 and 5.9 gives:

$$\frac{\Delta L}{\Delta t} \approx \frac{e}{2i} \frac{\pi \Sigma a_P^2}{m} \chi^2 \frac{\pi}{T} L_P \frac{m}{M_P} b_e \chi \quad (5.13)$$

The Hill factor χ cubed is proportional to the planet's mass, allowing several cancellations of masses:

$$\frac{\Delta L}{\Delta t} \approx \frac{e}{2i} \pi \Sigma a_P^2 \frac{\pi}{T} L_P b_e \frac{1}{M_P} \frac{M_P}{3M_{Sun}} \quad (5.14)$$

The angular momentum of the planet $L_P \propto a_P^{\frac{1}{2}}$ and so

$$\frac{\Delta L_P}{L_P} = \frac{1}{2} \frac{\Delta a_P}{a_P} \quad (5.15)$$

finally giving an expression for the migration rate of:

$$\frac{\Delta a_P}{\Delta t} \approx 2 \frac{e}{2i} \frac{M_{Disk}}{M_{Sun}} b_e \frac{a_P \pi}{T} \frac{\pi}{3} \quad (5.16)$$

where $M_{Disk} = \pi \Sigma a_P^2$. The factor $\frac{e}{2i}$ can be taken to be unity, as it is set initially and as it should remain in the main disk ([16]).

Removing the factors that are near to unity leaves the final fiducial migration rate for the planet:

$$\frac{\Delta a}{\Delta t} \approx \frac{2a}{T} \frac{M_{Disk}}{M_{Sun}} \quad (5.17)$$

which is off by only a factor of two from the migration rate predicted by IBLT [15]. Their prediction (equation 2.4) was based on a value for the angular momentum exchange that had been integrated over an actual scattering process in which every particle within the feeding zone was scattered once from zero eccentricity. This factor of two may also be related to the results of section 4.3 which showed that the population that scatters within the wing, and does not cross, provides a roughly equivalent angular momentum exchange with the planet as the population that crossed between the wings upon scattering. The IBLT result would have included this exchange.

5.1.1 Integrated $n\sigma v$

The result of equation 5.17 is the migration rate instantaneously at any given value of semi-major axis, but it can also be treated as a differential equation in a_P . It can therefore be integrated to give the form of the migration $a_P(t)$. Assuming that the surface density (a power law of index k) is set to be Σ_0 at a_0 , equation 5.17 can be expressed in our units as:

$$\frac{da}{dt} = \frac{2\pi\Sigma_0\left(\frac{a}{a_0}\right)^k a^2}{M_{Sun}} \frac{a}{a^{1.5}} \quad (5.18)$$

Setting $a_r = a/a_0$ this becomes:

$$\frac{da_r}{dt} = \pm \frac{2\pi\Sigma_0\sqrt{a_0}}{M_{Sun}} a_r^{k+1.5} \quad (5.19)$$

where the *plus/minus* tells the direction of migration, outwards or inwards respectively. Using the boundary condition $a_r(t = 0) = 1$ (ie. $a(t = 0) = a_0$) this is integrated to give:

$$a(t) = a_0 \left[1 \mp (k + 0.5) \frac{2\pi\Sigma_0\sqrt{a_0}}{M_{Sun}} t \right]^{\frac{-1}{k+0.5}} \quad (5.20)$$

This is the integrated $n\sigma v$ equation, the complete prediction of the fiducial calculation. In it, the term $\frac{2\pi\Sigma_0\sqrt{a_0}}{M_{Sun}}$ corresponds to $\frac{\left|\frac{da}{dt}\right|_0}{a_0}$, where $\left|\frac{da}{dt}\right|_0$ is the value of equation 5.17 at the initial semi-major axis a_0 . This term therefore represents the inverse of the timescale of the migration τ_{mig} . In the case where the following is true:

$$t < \left| \frac{1}{k + 0.5} \right| \frac{a_0}{\left|\frac{da}{dt}\right|_0} < \tau_{mig} \quad (5.21)$$

the integrated $n\sigma v$ equation can be approximated as:

$$a(t) \simeq a_0 \pm \left| \frac{da}{dt} \right|_0 t \quad (5.22)$$

which is a constant migration rate, or a 'linear' migration. When this condition becomes false, the migration will break from linearity. The break will occur after a long time for cases where $k = -1$, and earlier for cases with $|k| > 1$ or so. The timescale for the migration was longer than the duration of the simulation for most of the simulations of this chapter, and thus the migrations were well-represented by the linear approximation which is a constant migration rate given by equation 5.17 calculated at a_0 . For this reason, unless stated otherwise, equation 5.17 will be referred to as the fiducial migration rate, and not simply as an approximation.

5.1.2 The one-scatter limit

As discussed by IBLT [15], the planet can migrate fast enough that it only ever encounters its wing material once. In order to achieve this, the planet would have to migrate across a certain number of Hill radii in the time it takes to interact *once* with all of that material: one synodic period measured roughly at that distance. This can be expressed as:

$$\frac{da}{dt} = \frac{bR_H}{T_{syn}(bR_H)} = \frac{b\chi a_P}{\frac{2}{3b\chi}T_P} = \frac{3}{2}(b\chi)^2 a_P^{-\frac{1}{2}} \quad (5.23)$$

The fundamental difference between the first and second scattering events in a dynamically cold disk is that the first imparts a Δe of several Hill factors for a planetesimal that crosses the planet's orbit, while the next imparts an average $\Delta e \sim \chi$, as demonstrated by figure 4.8. The fiducial rate in equation 5.17 assumed the factor that described this, b_e , to be equal to one, but that is only the limiting case. Equation 5.11 gave the form for the angular momentum transfer with a change in eccentricity, and it was proportional to $(e_{init} + \Delta e)$. This means that if the disk is at zero eccentricity initially, but the average scattering event puts planetesimals at

$e \sim 2\chi$, then the angular momentum exchange would be twice that predicted by the fiducial rate as proposed.

The second scattering would have a higher e_{init} , a smaller Δe with some scatterings having a negative value, but there would be other differences as well. If we are concerned mainly with planetesimals that cross between the wings, with the fuel for inward migration being the population that crosses from the inner to the outer wing, then the second scattering would transfer that population *back* to the inner wing, partially canceling the first angular momentum transfer. However, the population would be at higher e , and therefore a lower scattering probability (as seen in figure 4.12), so much of it would be 'missed' on the second conjunction. Furthermore, if the planet had moved inwards in response to the first scattering, the population that had transferred to the outer wing would find itself at a larger value of C_T in the next encounter, and therefore at a yet lower scattering probability.

The main migration fuel from the wing, the population that crosses the planet's orbit, crosses mainly from the closest portion of the wing. This was discussed in section 4.1.3. The one-scatter limit will therefore be taken at $b \sim 2.2$, which is roughly the middle of the wing, and is a value that agrees well with figure 2.1 from IBLT, the results of section 4.3.1, and the results of the M0 run to be discussed in section 5.3. This means that the planet must migrate $2.2R_H$ within one synodic period measured at $2.2R_H$ to satisfy the limit. This is not a hard limit, so anything near this migration rate may experience these effects. The final equation to be used is therefore:

$$\left| \frac{da}{dt} \right|_{1scat} > 7.5\chi^2 a_P^{-\frac{1}{2}} \quad (5.24)$$

The exact result of having a migration rate below the one-scatter limit is uncertain,

as so many parameters will change between the first and second scattering. The conclusion from IBLT [15] was simply that the migration rate they predicted would not hold true unless it was above the limit. Here we will say for now that the migration rate will be *different* if it falls below the one-scatter limit. On the most basic level, it will likely be a much slower migration due to the partial cancellation in the second synodic period of the angular momentum transfer from scatterings within the first synodic period.

This rate will occur, for a planet migrating at a multiple f of the fiducial rate, at:

$$7.5 \frac{\chi^3}{\chi} a_P^{-\frac{1}{2}} = 2f \frac{M_{disk}}{M_{Sun}} a_P^{-\frac{1}{2}} \quad (5.25)$$

and using the definition $\chi^3 = \frac{M_P}{3M_{Sun}}$, this gives $M_P = 0.8fM_{disk}\chi = 0.2fM_{wing}$. Implying that the one-scatter limit will be crossed at a mass fraction M_P/M_{wing} just less than 1.0. As soon as the planet's mass begins to grow as large as the mass in the wing, the migration will be such that the planet is too slow to only scatter material once.

5.2 Resolution

Properly resolving the migration of a planet requires limits on several parameters. As already discussed the timestep is chosen to be 1-2% of the planet's initial orbital period in order to sample planet/planetesimal orbits many times per orbit. The output interval is also chosen so as to sample the planet's migration at least ten times as it crosses the disk. This interval is therefore dependent on the width of the disk as well as the migration³ rate of the planet. The migration rate is not known a priori so normal output intervals were 1000 years for slow migrators, down to 100

years for faster migrators.

The physical scattering of the planetesimal disk must also be resolved, placing constraints on planetesimal mass and number density. The planetesimal mass was kept to below $1/600^{th}$ of the planet mass in order to ensure that no individual scattering event was enough to substantially shift the planet's semi-major axis. Assuming a planetesimal with mass $m/M_P = 1/600$ and $e \approx \chi$, the scattering process in equation 5.10 would produce a semi-major axis change (from equation 5.15) of $\Delta a = 2a\chi/600$ which is $1/300^{th}$ of a Hill radius. This raises the question of how many planetesimals are within that Hill radius spacing of semi-major axis, as the planet should be passed from one to the next or - even better - be buffeted by many all at once. The normal number chosen was ≈ 1000 particles per R_H so that even scatterings not as strong as the assumption will tend to propel the planet into the next scattering. This number is also limited by the speed/size of a simulation, as for a disk of extent $a_P \pm 25R_H$ and power law surface density of $\Sigma \propto a^{-1}$ this produces a requirement of 5×10^4 particles, and going to 10,000 particles per R_H would increase the simulation time to a few days, and the size to several gigabytes. Simulations where the disk mass is greatly reduced, however, could produce mass fractions m/M_P much less than 10^{-3} , and would therefore require substantially more particles per R_H to ensure the planet is being evenly "passed along". These simulations also tended to require less disk extent as the migration was much slower, ensuring that the overall particle number could be held roughly constant. This was not always the case, however, as the disk extent could not be smaller than $a_P \pm 5R_H$ to avoid the planet feeling edge effects (see section 1.6 for the extent of the wing and the chaotic zone). Thus simulations with very low-mass disks tend to have very high particle number, in some cases prohibitively

high numbers.

Resolving the system in both mass and number was a challenge, especially in cases where the planet mass (and therefore its Hill radius) was varied widely. Cases where the particle number had to be reduced from the preferred value (beyond the buffer of reducing the disk extent) will be described individually. Unresolved migrations are noticeable for very stochastic and noisy lines of $a_P(t)$, but are not necessarily invalidated. They suffer more frequent reversals of the migration, and often do not show the same characteristics of change in the migration rate as properly resolved runs, but in very linear migration regimes they were occasionally sufficient.

Figure 5.1 shows a set of migrations where the particle number is varied from 5×10^3 to 4×10^4 by applying a factor f . The disk extent is $\pm 10AU$ centered on $a_P = 25AU$, with the planet's Hill radius being $R_H = 0.43$. This produces a mass fraction of $m/M_P = 1/(300f)$ and a particle-per- R_H of $215 \times f$. The migration (sampled every 1000 years) becomes seemingly resolved (smooth, and convergent with the higher-resolution runs) at a value of $f \approx 1$, with the a_P diverging by a few Hill radii after a time of 10^5 years. This shows that the limits for resolution chosen above are very safe for the average run, and while the effects of mass fraction and Hill radius density are not disentangled here, they should be self-reliant (best if both are satisfied, sufficient if at least one is). Indeed, the only fraction producing a strongly divergent migration is $f = 0.5$, a resolution seldom encountered in my simulations. Other cases where the resolution is varied, and the resulting impact on the migration and migration rate explored, are described in sections 5.3, 5.5, 5.7, and 6.3.

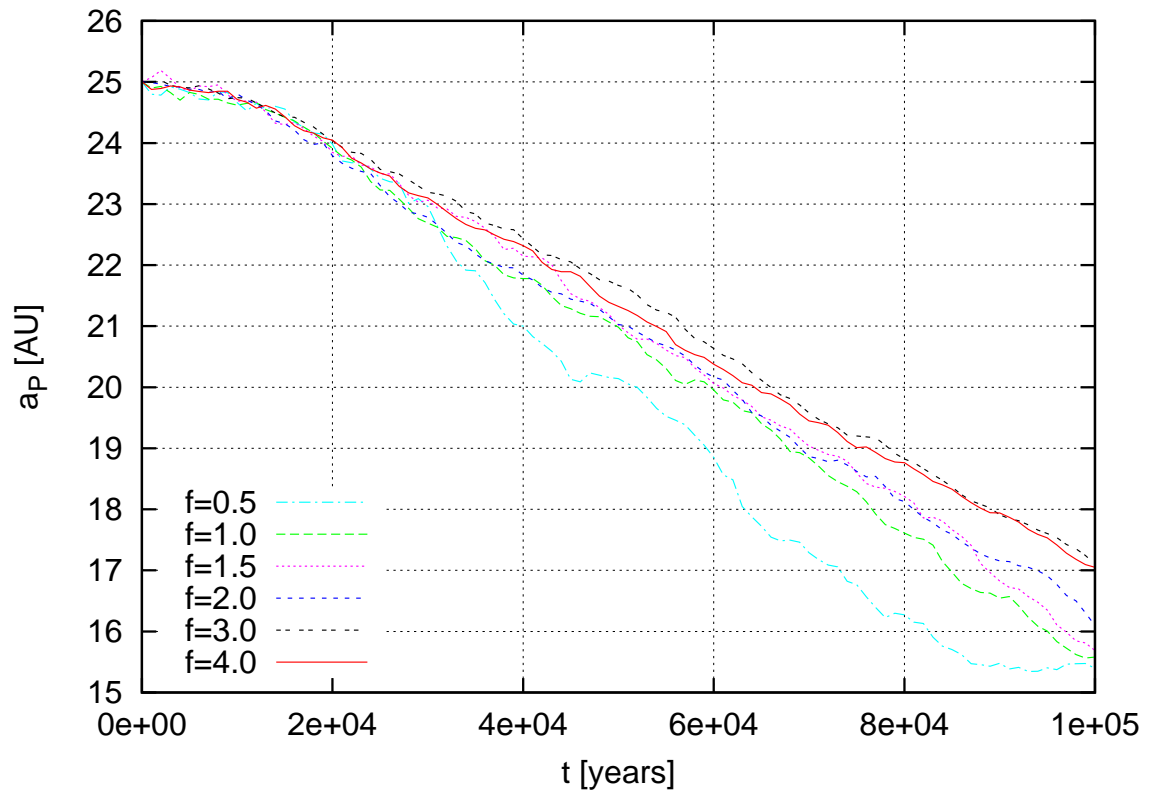


Figure 5.1: The factor f varies the planet/planetesimal mass fraction and the number of particles per Hill radius, increasing the resolution of the planet's migration from 25AU.

5.3 Planet mass

The preliminary set of simulations, called M0, involved varying the mass of the planet in a disk with all other characteristics held constant. Planetesimal number and mass fraction must be varied, however, to hold resolution constant, but this does not affect the mass of the disk. The planet mass was varied from 0.1 to 45 M_{Earth} , while the mass of the disk $\pi\Sigma a_p^2$ was held constant at approximately 230 M_{Earth} . Planetesimals were held to $1/600^{th}$ the mass of the planet, and were distributed over 10.5 AU on each side of the planet which was located at 25AU and therefore had an initial orbital period of 125 years. Surface density was proportional to a^{-1} , and thus the spacing between planetesimals was a constant determined by the number of planetesimals. The number of planetesimals was 8×10^4 for the 1 M_{Earth} runs, and went up to 4×10^5 for the 0.225 M_{Earth} runs, and down to 5×10^3 for the 18 M_{Earth} runs. Cases with lower and higher planet masses were treated differently.

The simulations with 0.1 M_{Earth} had a disk that was cut from being 10.5AU on either side of the planet to only 4AU outside and 7AU inside. The outer boundary was therefore $32R_H$ from the planet, too far to be felt, while the inner was $56 R_H$, and this allowed a good measure of the migration rate. Simulations with 18 M_{Earth} or higher had the resolution increased as they were pushing the limit by the original settings, increasing the particle number up to 1×10^5 , and this change was also explored.

The RMS eccentricity of the disk particles was set to 0.01, and individual eccentricities were chosen from a random sampling of a Rayleigh distribution about that value. Inclinations were done similarly, but with an RMS value of half the e_{RMS} , 0.005. The orbital angles were also chosen randomly, from zero to 2π .

Six simulations were done for each value of the planet mass, with the randomized

values (eccentricity, inclination and the angles of each planetesimal) being the only difference between the runs. Each simulation was run for at most 10^5 years, with an output interval of 10^3 years, and a timestep of 2 years. Simulations with faster migration were ended at earlier times, as the planet reached the end of the disk faster.

The migration of the planets, $a_P(t)$, showed a distinctly linear trend for the low mass planets. The first phase, occupying a few 10^4 years, found the planet roughly fixed, with oscillations occurring as material shifted back and forth across the planet's orbit and the wings grew. The next phase showed a constant acceleration up to a final velocity. This velocity remained constant until the very edge of the disk. Several examples of linear migration (constant velocity) are shown in figure 5.2.

The higher mass planets experience migrations that deviate substantially from linearity over time, and are far less smooth. The six highest mass planets' migrations are shown in figure 5.3. This rough migration is partially due to low number resolution, as the highest mass planets have the fewest particles by the resolution conditions set for this simulation set (which will be modified in the next paragraph, when the resolution becomes too low to be accepted). The wing mass in these runs is less than the planet mass, however, and this would imply that the planet would not be as easy to move through the disk. For all but the three highest mass planets, initially the migration rate is constant, and measurable.

The $18 M_{Earth}$ planet was resimulated at several particle counts, generating very different migrations with breaks at varied times and varied migration rates. Two runs each were done for counts of 2×10^4 , 4×10^4 and 10^5 particles, and all were smoother than the earlier version with only 5×10^3 particles. The break after 2×10^4 years remained similar, but the subsequent migration became slower. Within the higher

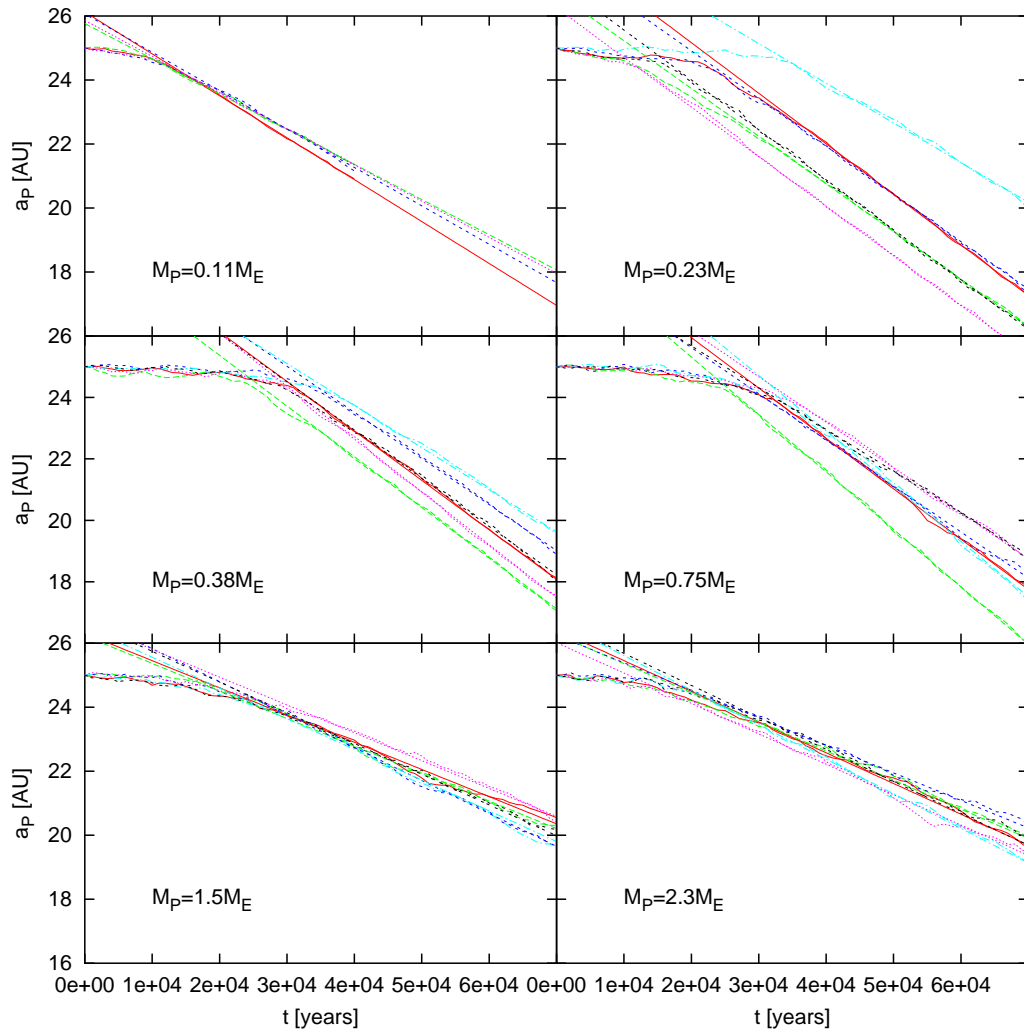


Figure 5.2: Migrations are shown for indicated planet masses in a constant-mass disk. Best-fit lines are also shown with the data to demonstrate the accuracy of constant migration rates.

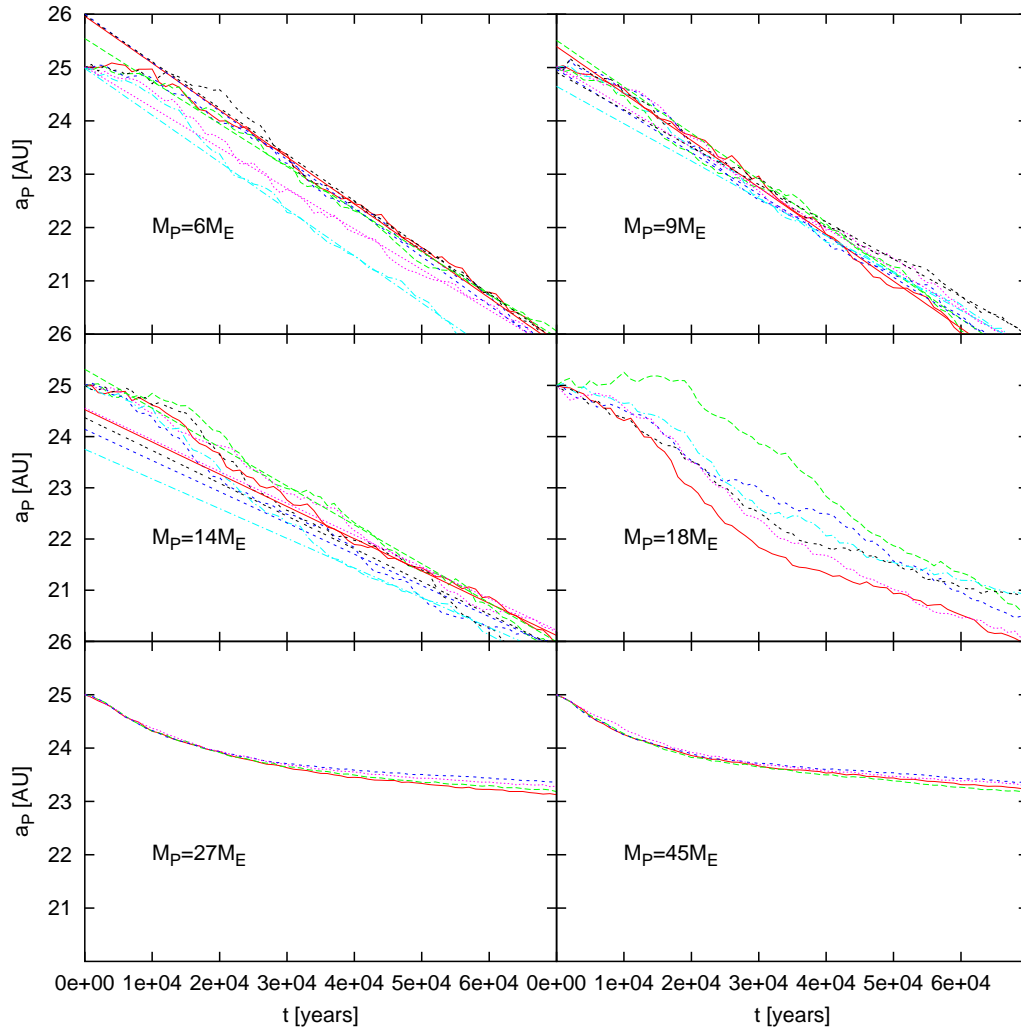


Figure 5.3: Migrations are shown for indicated planet masses in a constant-mass disk, along with best-fit lines.

resolution runs, one of the 10^5 runs resembled a 4×10^4 run, and the other 4×10^4 run resembled the 2×10^4 runs, which implies that the 2×10^4 particle count should be provide sufficient resolution and that the non-constant migration rate is not purely a resolution issue. For these runs, it is the resolved late-phase migration that provides the linear fit.

The highest mass planet, at $45 M_{Earth}$, was simulated initially at 5×10^4 particles, providing four very similar runs. The migration suffers the same break after 2×10^4 years, but the break is more gradual, seeming to be a deceleration, and the final migration rate is most likely not constant but rather damped. The last 2×10^4 years were nonetheless fit linearly in order to be compared to the previous runs.

The M0 runs can all be expected to have the same migration rate, that of the fiducial $n\sigma v$ rate given in equation 5.17, and the change from a smooth linearity seems to occur when the planet becomes bigger than the wing. These are therefore obvious reference points for characteristic migrations. The migration rate divided by the fiducial rate is plotted versus the planet-wing mass ratio for this simulation suite in figure 5.4. The migration rate drop-off at high planet mass is evident, even before the more drastic departures from linear rates for the two highest mass planets. At planet masses equivalent and slightly less than the wing mass, the migration is roughly constant at the fiducial rate, but it rises beyond the fiducial rate after $M_p/M_{wing} = 0.4$ and then turns down again at 0.2. This may be due to the change of \tilde{e} at this point, as the Hill factor drops below e_{RMS} at a mass ratio of 0.25, and discussion thus far has implied the migration rate may decrease due to increasing \tilde{e} . This may also be due to dropping below the one-scatter limit, which occurs at approximately the same point and has been indicated on the plot as given by equation 5.24. Crossing the

one-scatter limit may also account for the large dispersion in the migration rates at this point: whether or not the planet feels the limit will be very sensitive to the early conditions. These effects will be investigated further, and separately, in the following sections.

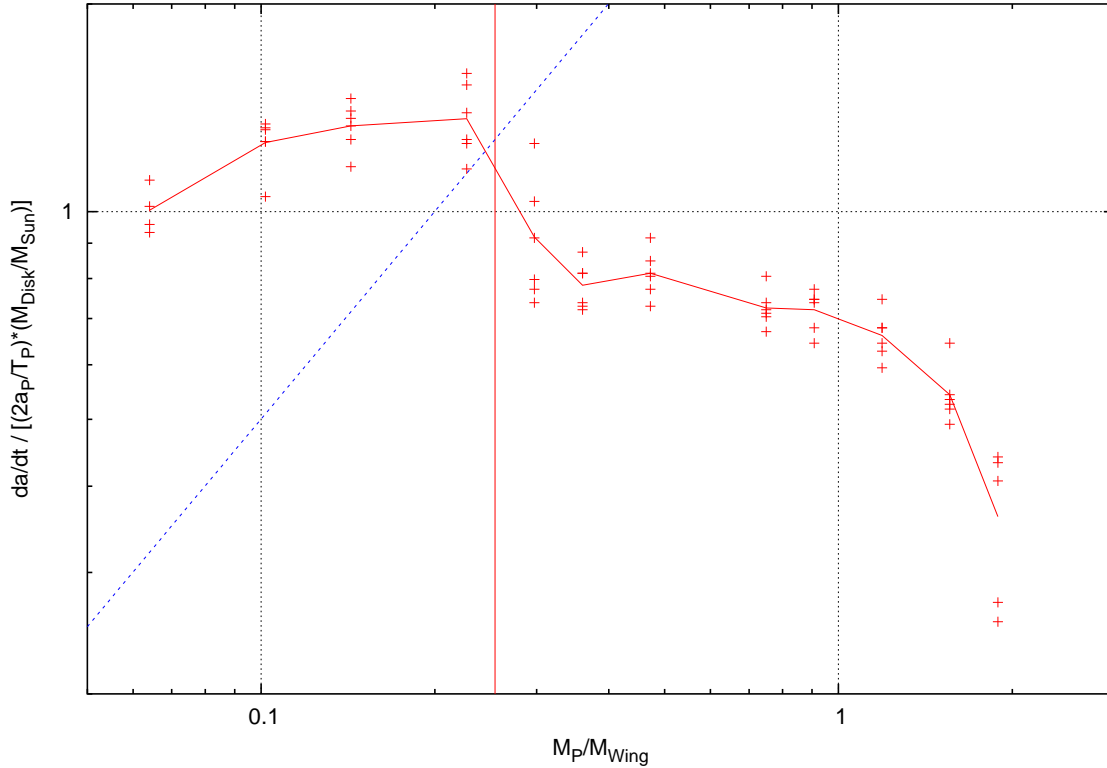


Figure 5.4: Four to six migration rates (in units of the $n\sigma v$ value) are plotted for each value of M_P/M_{Wing} , with a line drawn along the average values. The light red vertical line indicates the change from low \tilde{e} to high \tilde{e} . The blue line indicates the one-scatter limit, which is satisfied only on the left of this line.

Another interesting, and immediately apparent result from these runs is the length of time of the first phase of the migration where the planet does not migrate. While difficult to measure, the delay in migration commencing, if taken to be the time until the migration rate reaches its final value, seems to have a dependence on the planet

mass that is the same as the migration rate itself. For the high planet masses it is roughly 120 orbits, for planets around the top of the bump (at about $M_P/M_{wing} \sim 0.2$) the delay maximizes at 300 orbits, and then it decreases for lower values of M_P/M_{wing} to 100 orbits. This may be the time required for the planet to 'shed' its horseshoes and lose the inertial drag that they impose on it. Indeed, for $M_P/M_{wing} = \frac{1}{2}$ the number of particles in the horseshoe zone was seen to drop by a factor of 4 in the first 160 orbits, roughly the delay time, as the migration rate grew. This will be discussed further in sections 5.5 and 5.7 where the horseshoes are analyzed and excised.

5.3.1 The edges of the disk

In most of the simulations presented thus far, the run ended before the edge of the disk was reached. This section will pause from exploring mass trends to investigate what happens at sharp breaks in the surface density of the disk, including the inner and outer edges. In order to explore such breaks in the disk, and also to continue exploring the important populations of planetesimals, a series of runs was developed with gaps in the planetesimal disk about the planet. These runs, the MG runs, were under-resolved (only 50 particles per Hill radius spacing) and had a wing mass of about a third the planet's mass ensuring that any migration would be slow. The purpose of these runs was not to characterize migration, but simply to determine if any occurred.

A number of runs were done with a disk extending to $25R_H$ on either side of the planet, but with an emptied gap of nR_H directly on either side of the planet, with $n = 0, 1, 2, 3, 3.3, 3.6, 4, 5$. For the $n = 5$ run the semi-major axis of the planet varied by less than $0.15R_H$ over 5 million years, while the $n = 4$ run varied by $\sim R_H$ showing

that particles were beginning to feel the planet, but only a few. Clearly, a gap of five Hill radii on either side provides enough isolation for the planet to remain motionless over the relevant timescales. For this gap, the entire chaotic zone ($R_c \approx 4.89R_H$) is emptied, and so very little substantial stirring of the disk can occur. For $n = 3.6$ the planet began migrating (achieving the same rate as for $n = 0$) after a delay of 4 million years, while for $n = 3.3$ the delay was approximately half a million years and for $n = 3$ the delay was a few hundred thousand years. In these cases the planet was still well isolated initially, but was able to stir the chaotic zone enough to eventually bring planetesimals at apo/pericentre within the range of strong scatterings. For $n = 2$ and less, delays were less than ten thousand years, bringing us back to the normal mode of migration as if no gap had existed. These results fit with the extent of the planet's reach and the regions of strongest scatterings as discussed in chapter 4. In all cases where the planet reached the inner edge of the disk, migration halted. The planet stayed within a few Hill radii of the inner edge for the duration of these runs, sometimes for millions of years.

Several runs were also done with uneven gaps on the inside and outside, labeled by the number of Hill radii on either side (n_{in}, n_{out}). These are listed in table 5.1, with the delay time (time to move at least one Hill radius) and the direction of migration (no matter how slight) indicated. The continued inward migration seen for gaps with $n_{in} = 5$ demonstrates the bias towards inward migration even when very little inner planetesimals can be reached. This preference is only undone by the gap $(n_{in}, n_{out}) = (4, 2)$, which was rerun three more times to ensure the result was not simply random noise. In all four instances of the (4,2) gap the planet migrated outwards, eventually coming within a couple Hill radii of the outer edge of the disk

Table 5.1: Delay and direction of migration for a gap in the planetesimal disk of several Hill radii inside and outside of the planet's semi-major axis.

Inner	Outer	Delay	Direction
5	4	∞	in
5	3	∞	in
5	2	3×10^6	in
4	5	∞	out
4	3	3×10^6	in
4	2	8×10^4	out
3	5	4×10^6	in

at $a = a_P + 25R_H$. This was also interesting as a way to explore the outer edge effect. Near (not *at*) the outer edge the planet halted for times ranging from zero to a million or so years, and then reversed its migration and finally came to rest within a couple Hill radii of the *inner* edge of the disk at $a = a_P - 25R_H$. Only a slight bump was seen in the inward migration when the planet crossed the gap where it had originally begun. The original gap had of course been largely disrupted by the original stirring, so that it was no longer a true 'gap' at all.

Given that consistent outward migration is now a possibility, several runs were attempted with a planetesimal disk on only one side of the planet. The cases with an interior disk exhibit inward migration, as could be expected. The cases with an exterior disk proved surprising, however. In all three cases run, the planet migrated outwards by about a Hill radius before reversing and migrating *inwards* by several Hill radii. Given that thus far the interior wing has seemed to provide the fuel for inward migration, it would seem that the lack of an interior wing is only a temporary cause for outward migration. Once enough material has been scattered from the outer wing that an inner wing *exists*, the planet reverses. This shows the full power of the

inward bias: in cases where there is no inner fuel, the planet creates some.

The question of the (4,2) gap remains, however. Planetesimals on the interior of the planet are within the chaotic zone but outside of the wing (from which they could cross the planet's orbit). There they are pumped to higher eccentricities while forced to remain on the interior, causing them to lose angular momentum. In this sense, the inner chaotic zone is pushing the planet outwards, a repulsive force also seen in the slight outward migration for a gap of (4,5). This is as opposed to the attractive force usually associated with the inner disk which is in fact solely due to the wing particles in the feeding zone that can cross the planet's orbit. The difference between a gap of (4,2) and gaps of (5, 2) or $(\infty, 0)$ would then be that an additional source of angular momentum supply to the planet exists in the inner disk, upsetting the inward bias beyond what a pure exterior disk can provide.

The results of this section are largely qualitative instead of quantitative, and provide a useful comparison with the effects of disk populations as discussed in chapter 4. They also explain why a planet reaching the outer edge will migrate in, while a planet at the inner edge will simply stop. Trends in the migration rate as explored by the M0 runs will now be further examined.

5.3.2 Decreased eccentricity

The changes in migration rate in the M0 runs at the transition $\tilde{e} \sim 1.0$ implies the question: would the flat trend seen just above this transition point continue below it, if not for the \tilde{e} transition? To investigate this, a new simulation suite called M_e was generated with a lower e_{RMS} of $1e-4$, which was well below all values of the Hill factor for the planets in question. The i_{RMS} of the planetesimals was again half the e_{RMS} ,

but all other qualities of the disk were unchanged. As $\tilde{e} < 1.0$ for all the high mass planets in the M0 suite already, they were not resimulated. The lower mass planets, with $M_p = (0.1, 4.5)M_{Earth}$ were resimulated with four runs each, and a new run was added at a much lower mass of $M_p = 7.5 \times 10^{-3}M_{Earth}$ as well. The particle counts were treated as before for the resimulated runs, while the new run's disk was limited to 22AU to 25.5AU. The new planet had $R_H = 0.05$, so this gives the planet $60R_H$ inside its orbit to migrate through, and a $10R_H$ buffer between it and the outer edge of the disk. The particle mass ratio was also cut down to $1/400^{th}M_p$, which reduced the required particle number down to just over 1.3 million, still prohibitive enough that only one simulation with these parameters was performed.

The migrations in this cold disk retained the same look as for the M0 runs, and as they were at low mass there was no concern of breaks or nonlinearities in the late stages of the migration. Indeed, the 1.5 and 4.5 M_{Earth} runs, which satisfied $\tilde{e} < 1.0$ in the M0 suite as well as here, are basically unchanged. The change to the mass relation due to variation in \tilde{e} becomes clearer below those masses as the migration rate holds to the fiducial value down to below $M_p/M_{wing} = 0.2$. The migration rate does pick up to above the fiducial value below that mass, however, and then flattens once again all the way down to the lowest mass ratio. This data is shown in figure 5.5. The change in behaviour near the one-scatter limit is again apparent, with the migration rate going down from twice the fiducial rate to just under the fiducial rate as the actual migration rate encounters the limit. This implies that the bump in the trend of the M0 runs at the left of figure 5.4 is due to both the change in \tilde{e} *and* the one-scatter limit.

5.3.3 Increased eccentricity

To complement the M0 and M_e suites, another variation called M^e was imposed with $\tilde{e} > 1.0$. These runs were performed for the mass range $M_p = (0.1, 13.5)M_{Earth}$ and, like the M_e runs, changed only e_{RMS} (and $i_{RMS}=0.5*e_{RMS}$) by setting it equal to twice the Hill factor of the simulation's planet. Therefore, \tilde{e} was held constant at 2.0.

The resulting migration rates in units of the fiducial rate are shown along with the M_e runs in figure 5.5. The M0 simulation at $0.1M_{Earth}$ agrees well with the corresponding M^e simulation, and indeed this is the M0 run that also has the condition $\tilde{e} = 2.0$. The M^e runs for $M_P/M_{wing} < \frac{1}{2}$ are very close to the fiducial rate, and do not appear to react much to crossing into the one-scatter regime. This shows that one-scatter limit is probably only important in shear-dominated disks. The decrease in migration rate for high M_P/M_{wing} occurs for lower values of this mass fraction than in the M0 runs, most likely due to the high \tilde{e} causing an *effective* reduction in the wing mass due to planetesimals 'missing' the planet.

From this simulation set it is clear that the effect of $\tilde{e} > 1.0$ is to slow the planet's migration, and that the one-scatter limit is not inseparable from the effect of the eccentricity of the disk. The eccentricity will be further explored in the next section, while the discussion of the one-scatter limit will continue, especially in section 5.7.

5.4 Eccentricity

Several interesting variations were found in the mass trend for the M0 simulations owing to the eccentricity of the disk, as explored by the variations in the M_e and M^e runs. It is difficult to disentangle the mass and eccentricity trends, however, so a new

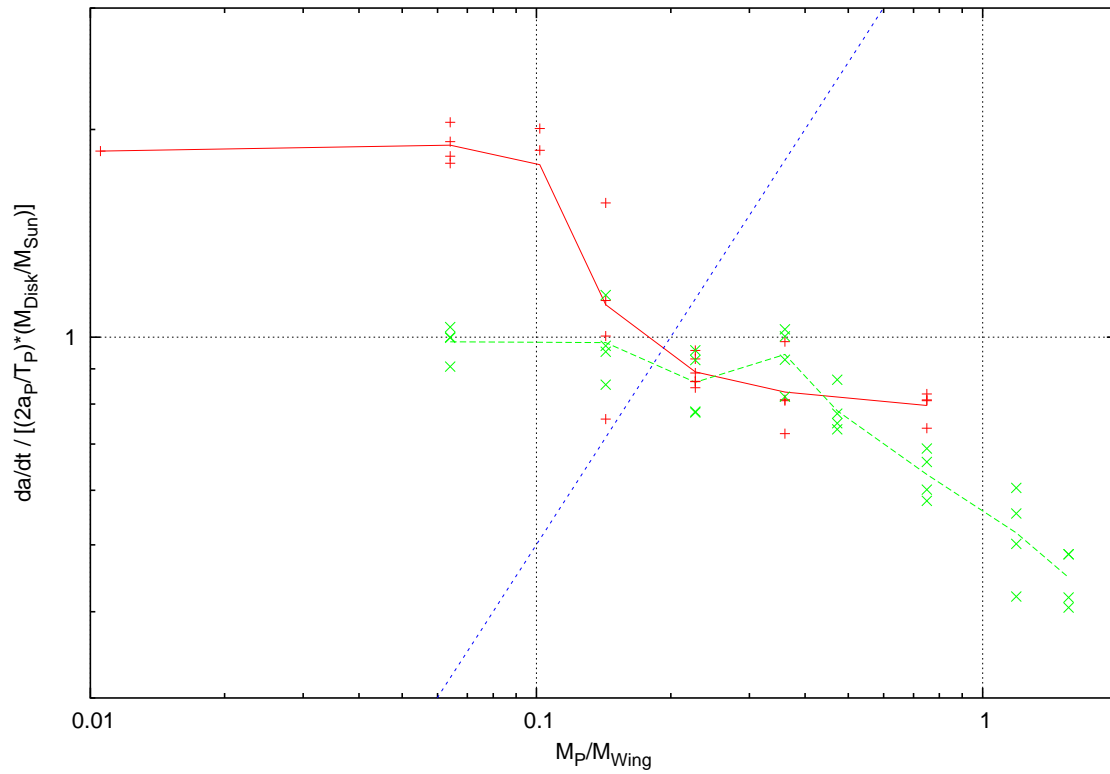


Figure 5.5: Migration rates in units of the fiducial rate for runs in which the disk root-mean squared eccentricity was set to 10^{-4} (red points) and twice the Hill factor (green points). The lines connect the averages for each value of the planet mass.

set of runs, the E0 runs, was generated to explore the effect of the disk eccentricity alone.

Simulations were run with root-mean-squared disk eccentricity varied from 10^{-4} to 0.1, with the planet's eccentricity set to a low value of 10^{-4} . RMS inclinations were half the RMS eccentricity, so it should be remembered that the simulations of this section include the effect of varying inclination along with eccentricity. In this simulation set, the planet's mass was 5 Earth masses at 25 AU, giving it a Hill factor of 0.017. The disk consisted of 5×10^4 particles spread over 25 Hill radii (0.43AU) on either side of the planet, with the planet being 1500 times the mass of each planetesimal, so that the wing mass was 1.3 times the mass of the planet. Four simulations were run for each value of the RMS disk eccentricity.

The resultant migration rates are shown in figure 5.6. The rates correspond within a constant factor to the nov result as long as the disk eccentricity is less than the Hill factor, ie. $\tilde{e} < 1$. For larger values of \tilde{e} the migration rate decreases. This is due to the fact that the timescale for interaction with $\tilde{e} > 1$ particles is longer than for circular orbits, reducing the effective mass of the wing per period. All runs were below the one-scatter limit, so this is unlikely to be a factor in the trend. The decrease in migration rate is only substantial for $\tilde{e} > 1$, and is well-fit in the given range by:

$$\frac{da}{dt} \approx \left. \frac{da}{dt} \right|_{e=0} \left[1 + \left(\frac{e_{RMS}}{3\chi} \right)^3 \right]^{-1} \quad (5.26)$$

where this result matches closely the prediction of IBLT in equation 2.5, which also used a relation between the average eccentricities and inclinations of $e \sim 2i$.

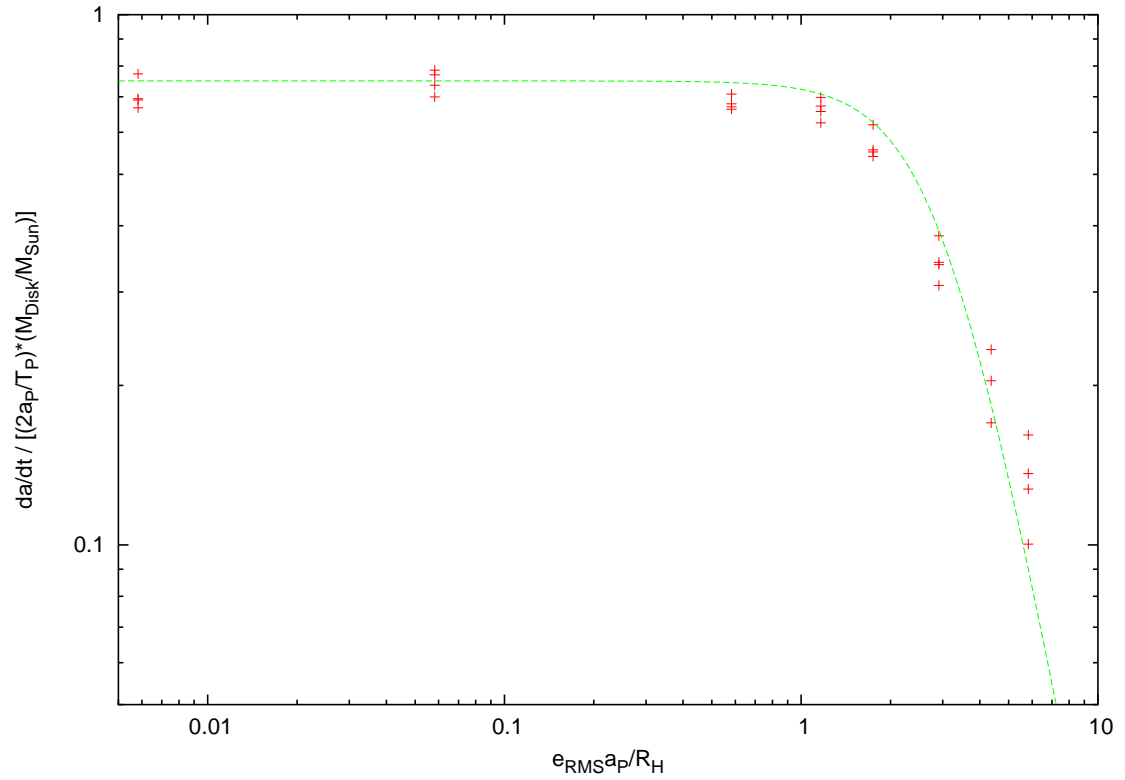


Figure 5.6: Migration rates in units of the fiducial value are shown for runs at multiple values of the root-mean-squared Hill eccentricity of the disk, with a fit provided by equation 5.26.

5.5 Horseshoes

The fraction of the disk that is orbiting within one Hill radius of the planet librates about the corotation resonance (section 1.7). These planetesimals experience stable horseshoe orbits which resonantly tie them to the planet. They are dragged along with the planet as long as it migrates slowly, and thus they effectively increase the inertial mass of the planet. This horseshoe-zone inertial mass is approximately equal to the wing mass, as it is the surface density integrated over a range of one Hill radius on either side of the planet, whereas a wing fills roughly two Hill radii on one side.

The horseshoe region is part of the region that will supply a planet with material as it accretes and grows from the core stage, and thus it can be expected to be emptied by the time the planet is massive enough to scatter planetesimals strongly. It will not be completely depleted, however, and the behaviour of a planet embedded in a horseshoe zone of varied mass can be important. The mass trends thus far investigated include horseshoes, and so to ensure that the final trend in mass is as simplified as possible, the effect of the horseshoes should be determined separately.

Simulations were run with a set planet mass of $4.5M_{Earth}$ at 25AU, in a disk of dynamically cold ($e_{RMS} = 10^{-4}$) planetesimals out to 25 Hill radii on either side, in a suite to be called the HS runs. The resolution in the horseshoe zone was increased to ten thousand particles, so that the mass ratio for planet to the planetesimals was 7500. For decreased horseshoe mass, the planetesimals mass was multiplied by a factor less than one, and the resolution only improved. To increase the horseshoe mass the number of planetesimals was increased by a factor greater than one, again not deteriorating the baseline resolution. This factor was then varied to give the total mass in the horseshoe region to be 0.01 to $10 M_P$. Neither the planet nor the rest of

the disk was altered. Four runs were done for each value of the factor.

The migration rates for a planet in a zone of a varied horseshoe zone can be seen in figure 5.7 as a function of the mass ratio of one wing to the entire horseshoe zone. All runs are slower than the one-scatter limit, so again that should not be large a factor. The planet mass in this case is a constant factor of 0.72 of one wing’s mass, so comparing the horseshoes to the planet or the wing is roughly equivalent. For a horseshoe mass of less than the wing mass, the effect is minimal and the planet attains the baseline migration rate given by equation 5.17. For horseshoe masses of more than the wing, the drag on the planet becomes evident, and the migration rate slows dramatically. For the highest factors, the migration also begins to wobble substantially on a timescale of about one synodic period at a distance of one Hill radius (5000 years), with an amplitude of about a quarter of a hill radius. An example of this can be seen in figure 5.8. This wobble reflects the strong damping of any attempted planetary migration on the timescale of the horseshoe zone’s ability to react to the planet’s migration.

A fit for migration rates as a function of horseshoe-wing mass ratio is found to be:

$$\frac{da}{dt} \approx \left. \frac{da}{dt} \right|_{M_{hs}=0} \left[1 + \left(\frac{M_{hs}}{2M_{wing}} \right)^2 \right]^{-1} \quad (5.27)$$

implying that the turnover is when the horseshoe mass is approximately equal to twice the wing mass. The reasoning for this may be that for particles crossing the planet’s orbit at zero eccentricity before and after a scattering (as the horseshoes approximately are), the angular momentum exchange with the planet is roughly proportional to the Δa of the crossing. For horseshoes, this $\Delta a \approx 2R_H$ whereas for wing particles the average spacing would be between the centres of the wings (at $\sim 2R_H$ from the planet) giving $\Delta a \approx 4R_H$. This implies that an individual wing particles has

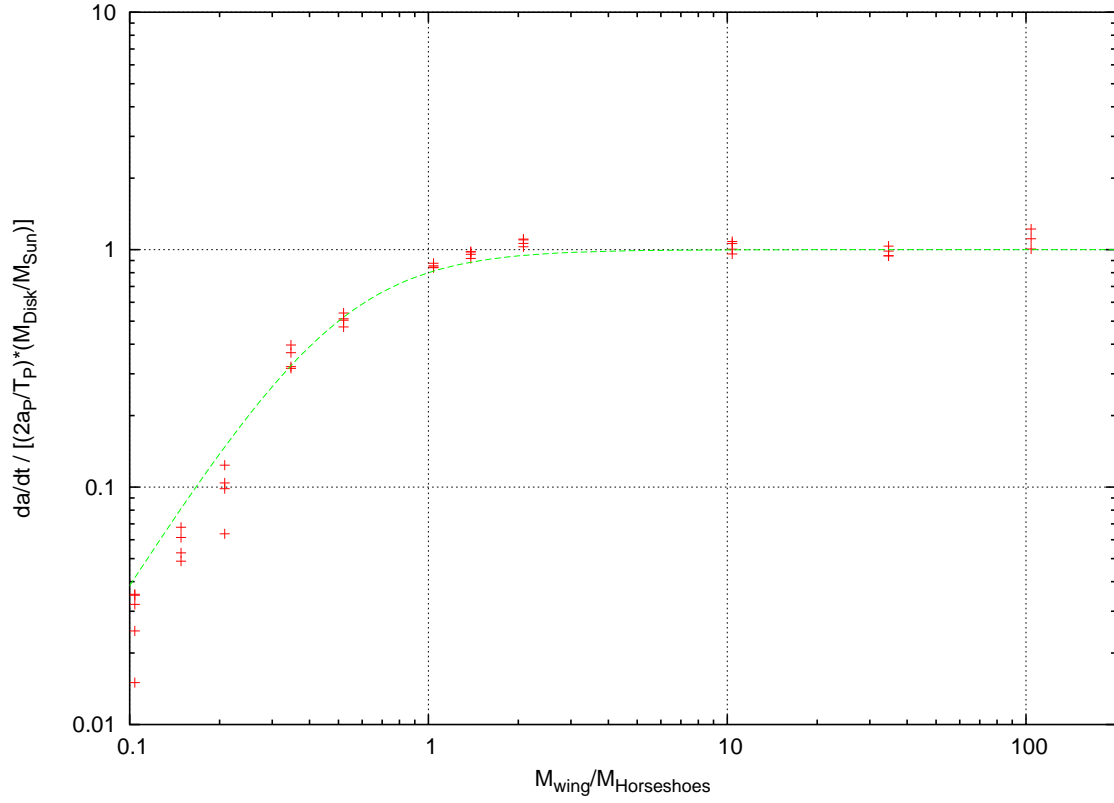


Figure 5.7: Migration rates in units of the fiducial rate as a function of the mass ratio between one Jacobi wing and the horseshoe zone, with a fit provided by equation 5.27.

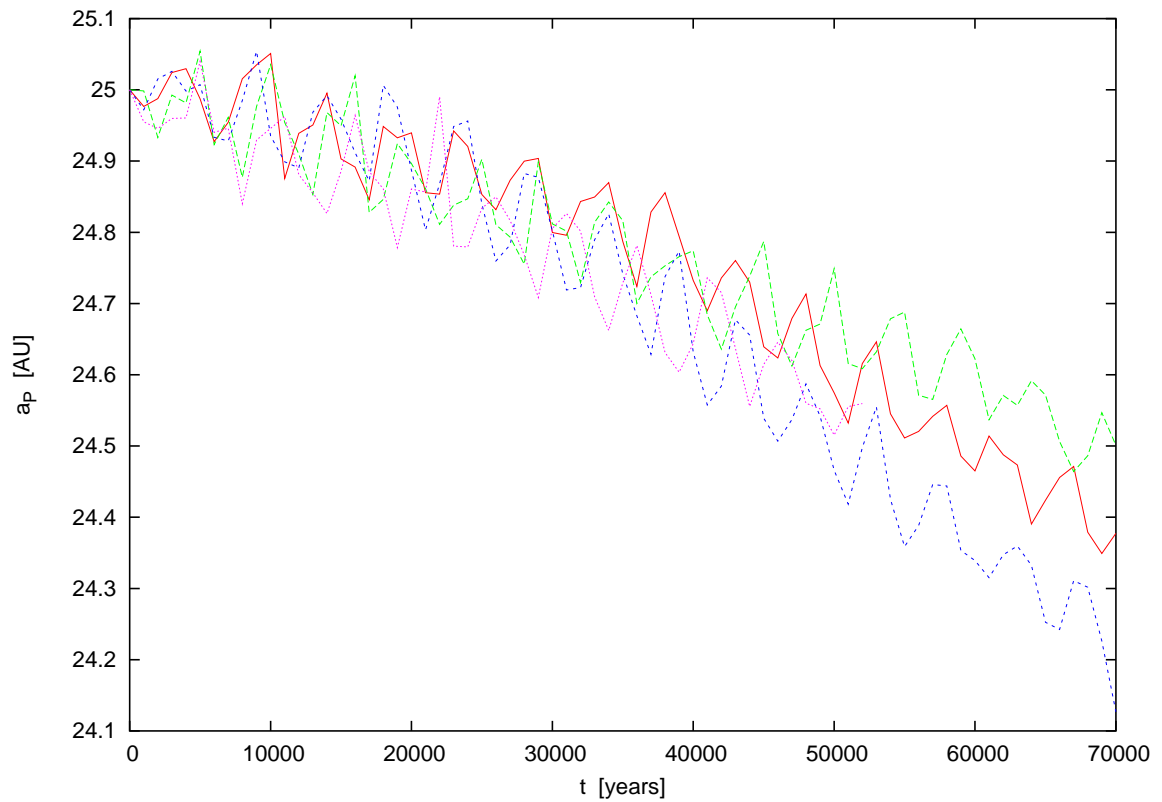


Figure 5.8: An example of horseshoe-damped migration, with an oscillation period of ~ 5000 years ($T_{syn}(1R_H)$), for the case with $M_{hs} = 4.8M_{wing} = 6.7M_P$, for four runs.

twice as much impact on the angular momentum exchange as a horseshoe particle.

The decrease is faster than linear with respect to M_{hs}/M_{wing} , which would be surprising if the zone acted as a constant inertial mass. Faster migrating planets will tend to 'miss' planetesimals (if faster than equation 5.23 with $b = 1$), migrating past their orbit between conjunctions, and thus the effective horseshoe mass will depend on migration rate just as much as it impacts that rate, producing a non-linear system. In the lower-horseshoe mass runs (the fastest migrators), almost all of the initially-horseshoe planetesimals fall out of that region by 2×10^4 years, reaching a steady state at a value of 90% mass loss. The trend is demonstrated in figure 5.9 for the fraction of the original horseshoe planetesimals that remain after 7×10^4 years. It is only the runs that affect a slowing of the planet that manage to retain a substantial mass in the zone. By retaining more mass, they are slowed more than other runs, and therefore retain more mass, and this cyclical argument results in the fast drop in migration rate seen in figure 5.7. Retention begins in earnest when the horseshoe mass is only half the wing mass, which is also approximately when the migration begins to slow.

Simulations up until this section have had even spacing of the planetesimals across the entire disk, giving roughly equal mass in one wing as in the entire horseshoe zone (each about $2R_H$ wide). In this case the reduction of the migration rate from the zero-horseshoe mode would be about 10%.

An interesting result in the M0 runs was that the time to begin migrating seemed to have the same dependence on mass scales as the migration rate. A possible reason for this is that it may have been related to the time to shed the planetesimals in the horseshoe zone. A run that had shown interesting qualities that have so far not been discussed was used to test this theory. The run had a planet of $4.5M_{Earth}$ at 25AU

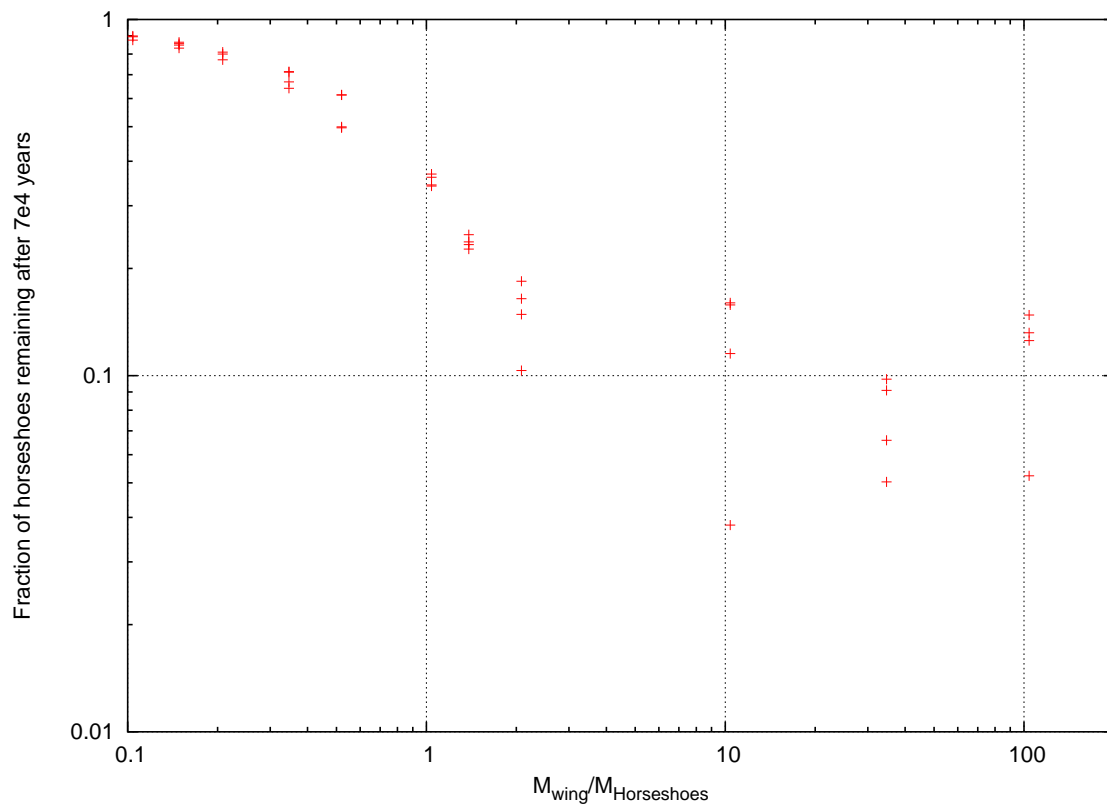


Figure 5.9: The fraction of the original horseshoe particles that remain in the horseshoe region after 7×10^4 years for the various values of M_{wing}/M_{hs} . Only the slowest migrators, dragged down by the highest horseshoe masses, manage to retain any particles.

which was about one-quarter as massive as the wing material. The planet required about 10^4 years to reach its final rate, but during that time it stayed relatively still and pumped planetesimals up the wings, until the centre-of-mass of the inner wing was about $5R_H$ inside the planet's orbit as figure 4.4 suggests should occur for a motionless planet. When the planet began migrating inwards, its semi-major axis eventually crossed this clumping of planetesimals and it halted. This was termed 'hitting' the wing.

Upon hitting the wing, the planet stayed motionless for a few thousand years, built new wings, and then began migrating *outwards*, until it again 'hit' a wing and reversed once more. The run had 215 particles per Hill radius and thus may have been under-resolved, so it was re-run with 1000 particles per Hill radius, and indeed the 'hit' vanished, and the planet migrated smoothly past the pumped particles, demonstrating the power of low resolution to incur large alterations in migration (500 particles per Hill radius were not enough to remove this effect). This setup was re-run with zero mass in the horseshoe zone, and it was seen to begin migrating *immediately*. This also meant no wings were grown, and no 'hit' occurred. This run seemed to indicate that the horseshoes are indeed the source of the migration delay seen in the M0 runs. Further exploring the system with no horseshoes will be a focus of section 5.7.

5.6 Initial semi-major axis

Before returning to the trend of migration rate with masses, another variable that impacts the Hill radius and the timescale of scattering will be investigated: the semi-major axis of the planet a_P . Seven values of the initial a_P were used from 10 to 80

AU, with four runs done for each value. The M0 runs showed that a wing mass of more than the planet’s mass allowed a constant-rate migration, so the wing mass was chosen to be $M_{wing} = 3.0M_P = 3.0M_{Earth}$. The disk was distributed over $25R_H$ on the inside of the planet, and $5R_H$ on the outside, with the horseshoe zone from $a_P - 1R_H$ to $a_P + 1R_H$ left empty, and the particle count was held constant at 28000 such that there were always 1000 particles per Hill radius. The planetesimal mass was therefore $1/600^{th}$ of the planet’s mass. The root-mean-squared eccentricities and inclinations were set to the low values of 10^{-4} and 5×10^{-5} respectively. The simulations were all initially run over 10^5 years with a timestep of one year and an output interval of 2000 years.

The resulting migration rates are all roughly 2.6 times the fiducial rate of $5.066 \times 10^{-4} a_P^{1.5}$, with scatter of about 10%. This is much faster than the very-close-to-fiducial rates of the last several sections, owing to the fact that all of these runs are faster than the one-scatter limit and, as discussed in section 5.1.2, surpassing this limit allows migrations faster than the fiducial by about that factor of 2.6. The time to for the migration rate to reach the final value was roughly 20 orbital periods, about one synodic period measured at the outer edge of the wing. With the finite migration distance provided by the width of the disk, this resulted in a total amount of time for the migration that was much shorter for the small- a_P runs. The migration of some of the smaller a_P runs was therefore undersampled, with only three outputs for $a_P = 10AU$. Most of these runs were redone with a higher sampling rate of 500 years, but the migration rates found from increasing the sampling rate was within scatter of those found from the less sampled runs anyway. Furthermore, the smaller a_P runs show slightly higher average migration rates as compared to the fiducial rate,

but under-sampling the migration would only decrease the observed migration rate, as it would be smoothed over more time.

The timestep was not adjusted for the innermost runs, so that the timestep for $a_P = 10AU$ was 3.2% of the initial orbital period, and 4.9% of the final orbital period. This is below the desired sampling rate of 1-2% of a period, so this simulation was run three more times with a timestep of 0.2 years, 0.6% of the initial orbital period. The resulting migration rates were all within the existing set of less-resolved inward migrations, and their average was only 1% off from the less-resolved average. The relatively large timestep was therefore not further considered as a problem for these runs.

Several of the migrations were also directed outwards, namely two at 10AU, two at 35AU, one at 40AU and two at 80AU. As the outer disk only extended $5R_H$ from the planet, these rates could not be measured, and were excluded from further study. The plot in figure 5.10 therefore shows four runs at each a_P that were inwards and properly resolved. The runs with $a_P < 35AU$ have an average rate of 2.70 times their fiducial value, while the larger-position runs are closer to 2.56, but this difference is roughly within scatter. The dependence of migration rate on initial semi-major axis is, within scatter, well predicted by the fiducial estimate except for a constant factor of ~ 2.6 . No trend in a_P was expected except for that predicted by the fiducial rate, so this is unsurprising.

5.7 Final mass trend

The trend of migration rate as a function of M_P/M_{Wind} was explored once more with no horseshoe orbiters and very low eccentricity, in a set of runs which will be referred

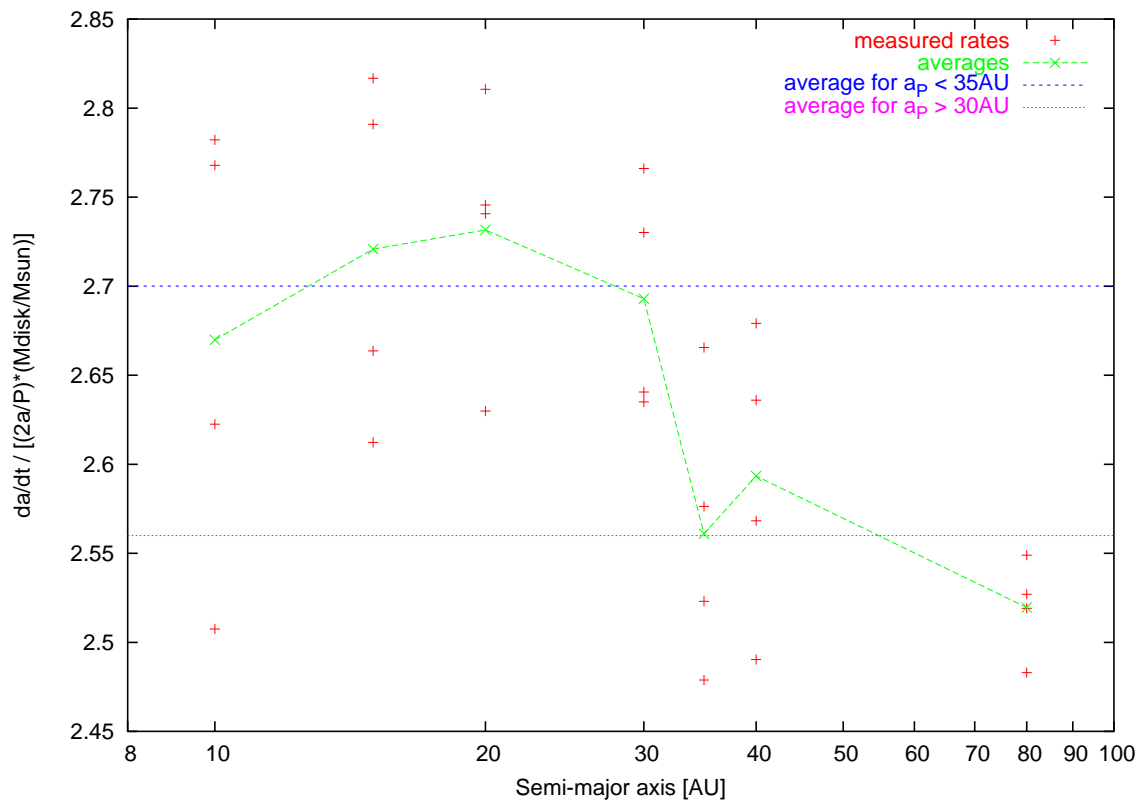


Figure 5.10: Migration rates divided by the fiducial rate for four runs at each studied value of the planet’s semi-major axis a_P . Averages for the first four and last three a_P values are separated, but no real trend is apparent (note the small vertical scale).

to as M1. These runs utilized a planet of $4.5M_{Earth}$ situated at $a_P = 25AU$ initially, in a disk with a mass varied such that the M_P/M_{Wing} fraction went from 0.1 to 100, distributed over $25R_H$ on either side of the planet. This is as opposed to the M0 runs where the planet mass was varied in a constant-mass disk. Also differing from the M0 runs is that the horseshoe region, the region within one Hill radius on either side of the planet (ie. from 24.57 to 25.43 AU) was devoid of any material. The disk RMS eccentricity and inclination were also reduced to a very low level of 10^{-4} and 5×10^{-5} respectively. These last two alterations were done to ensure no variation in the migration rate due to the variables discussed in sections 5.5 and 5.4.

The simulations were initially run over a time of 7×10^4 years, with some of the faster runs requiring less time and some of the slower runs requiring more time, with a timestep of 2 years. Four runs were done for each mass fraction. Similar to the method discussed in section 5.5, the variation in mass of the disk was achieved by decreasing the individual planetesimal's masses in order to decrease disk mass, or increasing the particle number to increase the disk mass. The reference point was at $M_P/M_{Wing} = 1.0$, where the number of planetesimals in the wing was 2000 (and a total planetesimal count of 48000) and the planetesimal mass was $1/2000^{th}$ of the planet's mass. Therefore the case with $M_P/M_{Wing} = 10.0$ had planetesimals $1/10^{th}$ as massive as the standard, but the same number of them, while the case with $M_P/M_{Wing} = 0.5$ had twice as many standard-massed planetesimals. The more extreme cases of disk mass increase (such as $M_P/M_{Wing} = 0.1$) increased individual planetesimal masses (up to $M_P/1000$) in order to save on particle number, and also reduced the range of the disk from the standard $a_P \mp 25R_H$ to $(a_P - 25R_H, a_P + 6R_H)$. Neither of these adjustments should affect the migration rate, as discussed in

section 5.2.

The migrations are shown for the high values of the mass ratio M_P/M_{wing} in figure 5.11, and for the low values in figure 5.12. The first thing to note is the variation of the scale on the y-axis: the extent of the migration is less than a Hill radius in 2×10^5 years for $M_P/M_{wing} = 10$, and less still for the higher fractions. Also noticeable is the 'bend' in the migration at $\sim 4 \times 10^4$ years, which is comparable to a synodic period measured at $2R_H$, for the high-ratio runs. Two rates have been measured for these runs: before and after the bend. The runs with $\frac{1}{2} < M_P/M_{wing} < \frac{5}{2}$ seem to exhibit an acceleration during their first synodic period, but most of them arrive at a rate that is measurable (and measured) before finally reaching a longer-lived (and smaller) constant migration rate. This last rate also tends to oscillate slightly about the linear fit. The runs with $M_P/M_{wing} < \frac{1}{2}$ show a very constant initial migration rate with only a very short acceleration phase, but eventually break at smaller semi-major axes to a slower migration. The three smallest mass fractions do not actually show this break, but it would likely occur at much smaller semi-major axes due to the reasons which will be outlined shortly. Also of note is that the 'delay' in the commencement of migration that was seen throughout the M0 runs is not present, for the most part. As mentioned in that section and in section 5.5, this may be due to the lack of horseshoe particles, which means the planet has no need to 'shed' these particles before it can attain a fast migration rate.

The slow migrators experience a very noisy migration. This may be due to the planet moving so slowly that the resolution chosen for the wing leaves it not resolved *enough*. For this reason, the resolution was increased for the run $M_P/M_{wing} = 100$ by a factor of 100, requiring the disk to be limited to $6R_H$ on either side of the planet.

The migration showed slightly less noise, but no significant change in the 'bend' at 160 orbital periods or in the average rates measured previously. This run is shown with the others in figure 5.11 with a black line to differentiate it.

Two sets of migration rates were taken from each mass fraction where at all possible: the lowest mass fractions exhibit only one rate, and several of the fractions close to 1 have an initial rate that is exhibited for too short a time to be disentangled from the acceleration phase. These migration rates are shown in figure 5.13 in units of the fiducial rate as a function of the mass fraction. Also shown is the one-scatter limit, which shows that for this simulation suite everything with a mass fraction less than one is under the limit. Runs that are close to but above the limit are the runs which exhibit an initial migration rate that is twice the fiducial rate, but eventually drop below the limit (which is proportional to $a_P^{-\frac{1}{2}}$) and slow to being approximately equal to the fiducial rate. This matches with observations of the M0 run, where migrations faster than the one-scatter limit were at ~ 2.5 times the fiducial rate, and migrations slower than the limit were at ~ 1 times the fiducial rate.

The runs that are always below the one-scatter limit ($M_P/M_{wing} > \frac{1}{2}$) are not *actually* below the limit within the first synodic period. This is because, by definition, within one synodic period the planet has only scattered most of the planetesimals *once*. Within the first synodic period, then, the planetesimal will accelerate as it scatters material, and will reach a rate that is some fraction of the fiducial rate set by the trend with M_P/M_{wing} . Once it begins to re-encounter material, however, the angular momentum transfer with the disk will reduce by a factor of ~ 2.5 and the migration rate will drop correspondingly. This is what causes the gap between the two curves in figure 5.13 that is approximately the same difference in rate for all runs

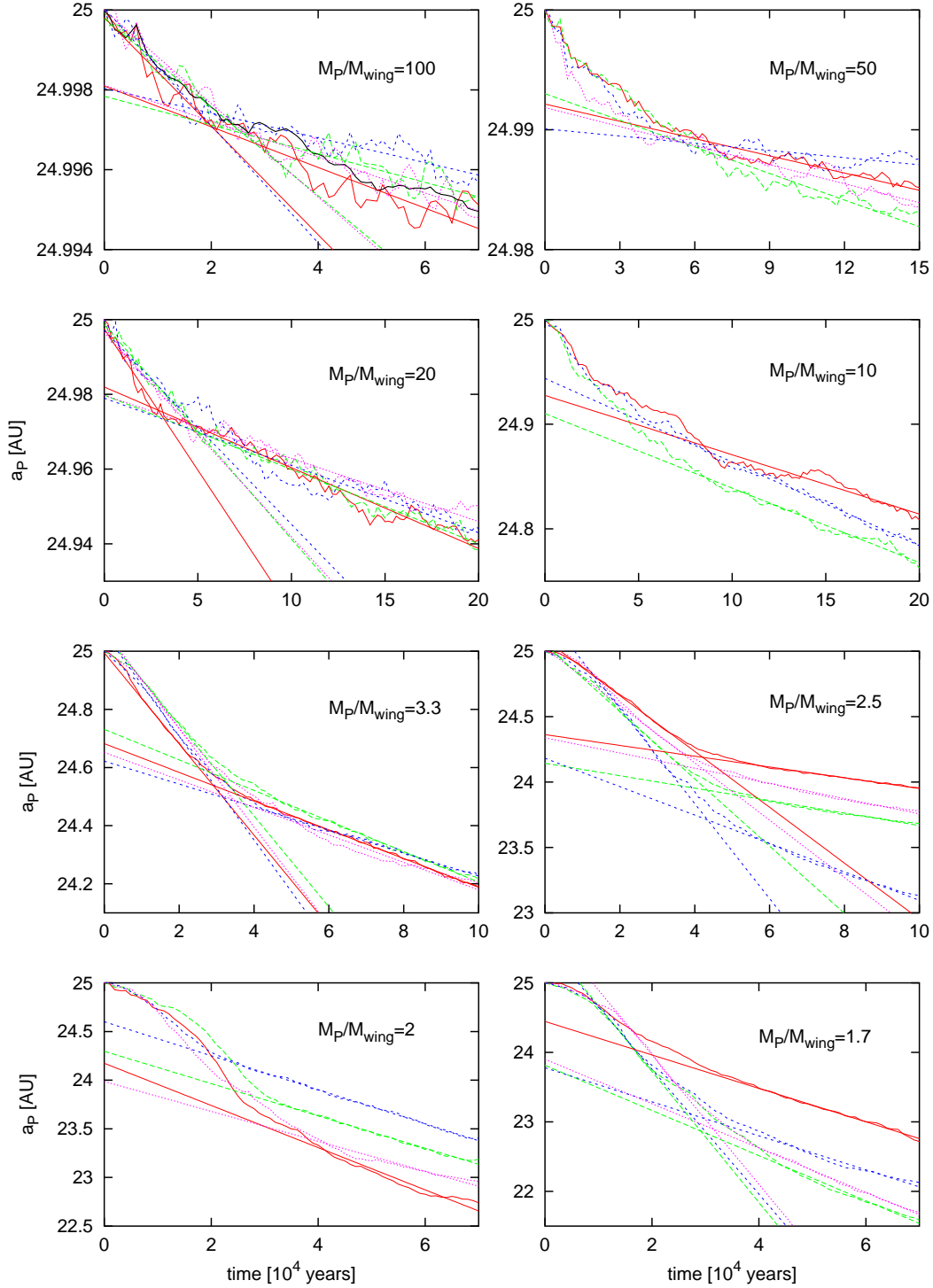


Figure 5.11: Migrations are shown in a dynamically cold disk with no horseshoe particles, with a planet of mass $M_P = 4.5 M_E$, for a varied mass disk (indicated by the value of M_P/M_{wing} in the upper corner of each migration). When possible, two constant-rate fits have been applied to the first and second phase of the migration, as described in the text. One higher resolution run is shown for $M_P/M_{wing} = 100$ in black.

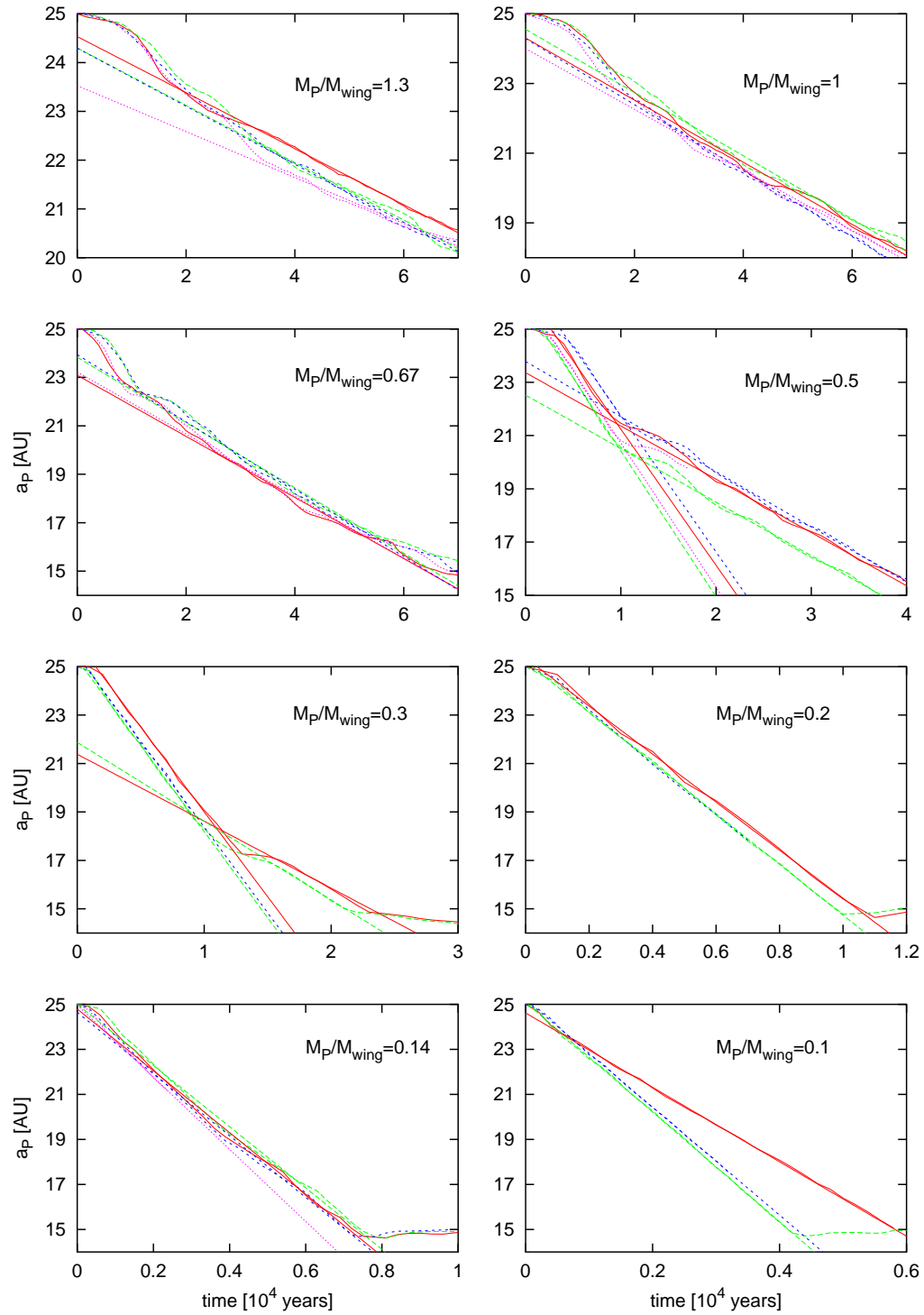


Figure 5.12: More migrations are shown, now with values of M_P/M_{wing} close to or less than one.

that have two rates measured. The fit shown is given by:

$$\frac{da}{dt} \approx \frac{\left| \frac{da}{dt} \right|_{fiducial}}{1 + \frac{1}{5}(M_P/M_{wing})^3} \quad (5.28)$$

which will be discussed more in section 5.9.

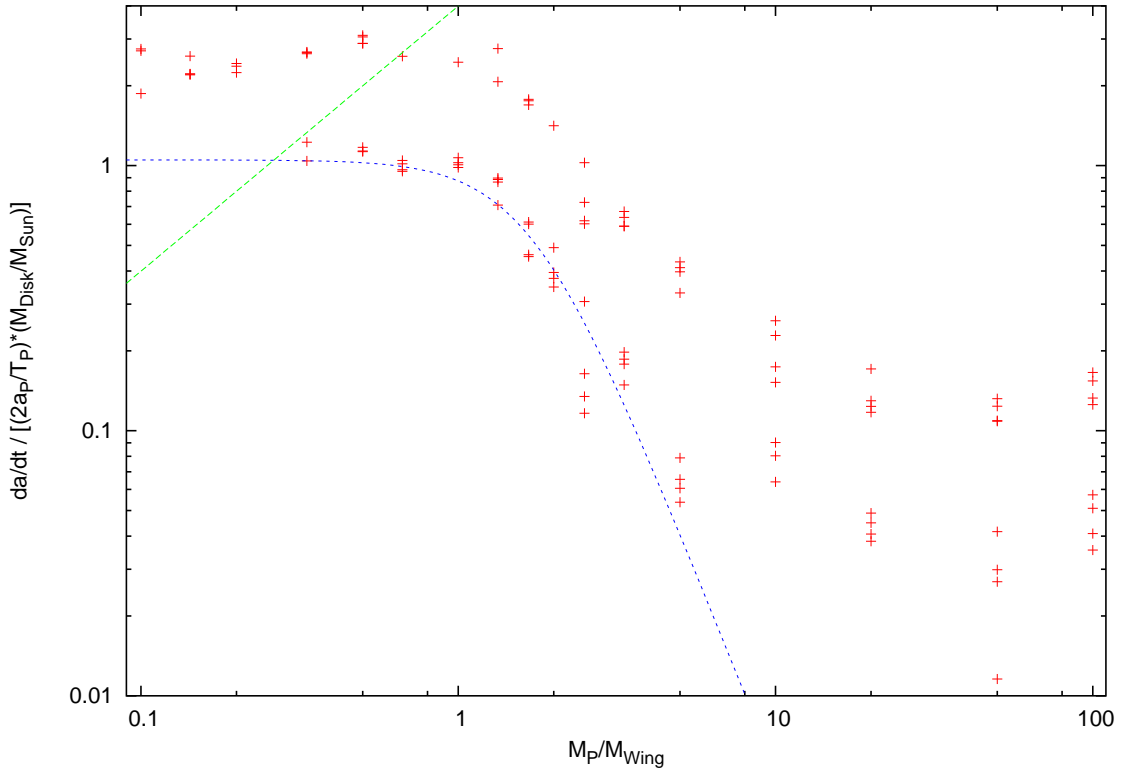


Figure 5.13: Migration rates in units of the fiducial rate for several runs at each of various values of the planet’s mass to the wing mass. These runs include no horseshoes, and a dynamically cold initial disk. Most runs have early (and short-lived) migration rates that are faster than the later rate, and in those cases both values are shown. High planet mass cases are estimates, as the migration is unlikely to be well-described by a constant rate.

The slow migrators, namely the cases with $M_P/M_{wing} > 1$, do not have enough fuel to propel their migration into a region with a fresh source of fuel. This ensures that they cross the one-scatter limit before even moving a few Hill radii. It also

implies that a constant migration rate is unlikely to be an appropriate fit for long times, although it should still be useful as an 'instantaneous' measure of the migration rate. In fact, the migration is likely to be exponentially damped, by the following logic. The planet's source of fuel is $2R_H$ wide. If its migration does not move it $2R_H$ in one synodic period, then its next synodic period will have less 'fresh' fuel, and it should therefore move less. This would provide even less fresh fuel, and this continuing pattern that should give exponential damping. The migrations shown do not immediately show strong departures from linearity, even over 200,000 years in the case of $M_P/M_{wing} = 20$. A run was therefore extended to 500,000 years for the case $M_P/M_{wing} = 5$ and is shown in figure 5.14, and in fact the constant-rate fits are shown on figure 5.13 in units of the fiducial rate. Once again the departure from linearity is small, even though it takes 3×10^5 years to move one Hill radius. The linearity of these high mass ratio runs will remain one of the more difficult questions of this work.

5.8 Planet mass growth

While the planet's semi-major axis is varying, its other physical parameters are also changing, most importantly its mass. The scattering process not only propels planetesimals across the orbit of the planet, but it sometimes delivers them directly to the planet, where they collide and are accreted to the planet. Thommes, Duncan and Levison (2003) [30] present a formula for the mass growth rate:

$$\frac{dM_P}{dt} \approx 3\pi \frac{\Sigma}{h} R_P^2 \left(1 + \frac{v_{esc}^2}{v_{rel}^2} \right) v_{rel} \quad (5.29)$$

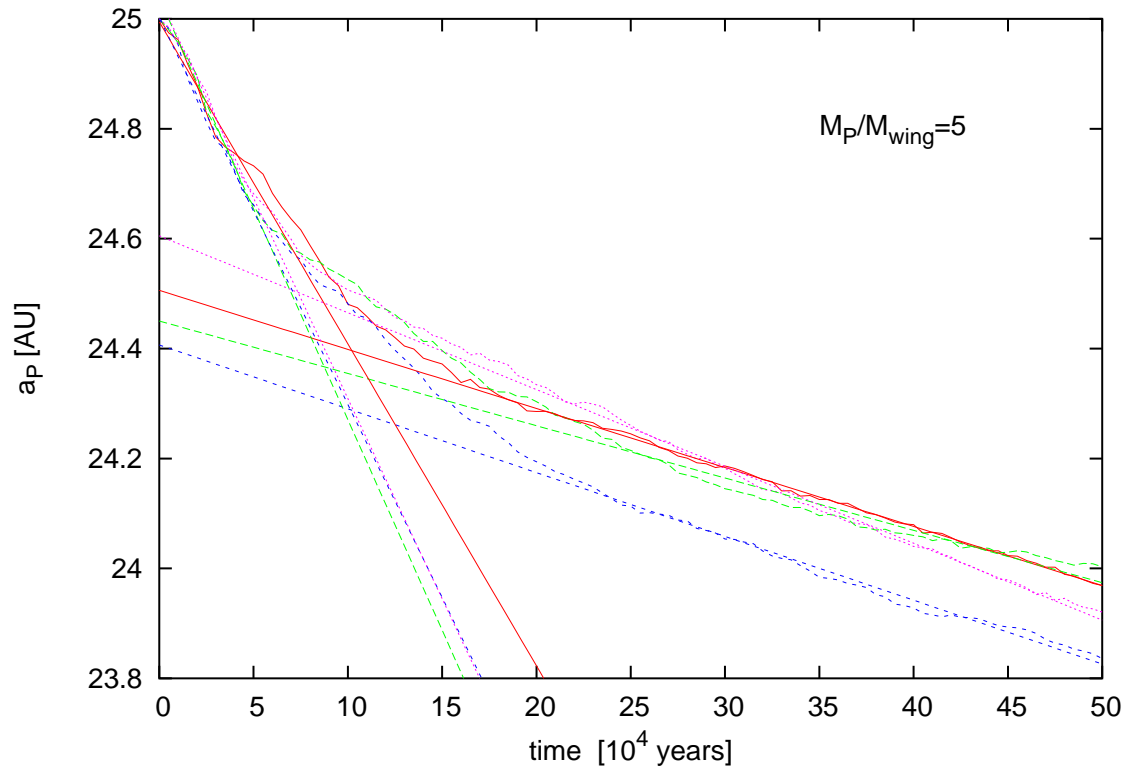


Figure 5.14: Migration for the case $M_P/M_{wing} = 5$, extended to 5×10^5 years, with constant migration rate fits displayed.

where h is the scale height of the disk, R_P is the radius of the planet, and the velocities are the relative velocity and the escape velocity from the surface of the planet. In the oligarchic regime several assumptions can be made for these values, finally giving a mass growth rate dependent on the planet's mass and semi-major axis, and the surface density and RMS eccentricity of the disk. There is no explicit dependence on the migration rate, but like the fiducial migration rate it should be valid at any instant in the disk for planets of the size considered in this study. The fact that, unlike the fiducial migration rate, this result is dependent on the planet's mass as well as the semi-major axis means that it is not as simple to integrate.

Planetary accretion is not the focus of this work, but as demonstrated by figure 5.13 the planet's mass will determine its migration rate in the case where it outmasses its wing. In this regime, however, the fraction of the wing that the planet accretes will not be a substantial fraction of the planet's mass, and therefore the planet's mass will not grow significantly. In either regime $M_P/M_{wing} > 1$ or < 1 , then, the accretion will not *at the beginning of the run* be an essential part of the migration process. The next section will briefly discuss how the accretion can cause a change from one regime to the other during the migration.

Several examples of the planet's accretion are shown in figure 5.15, for the M1 runs, and are marked by their M_P/M_{wing} ratio for comparison. In the high ratio runs the mass gain levels off towards the end due to the planet having already accreted most of the easily accessible material, and slow migration not providing any further material. For the $M_P/M_{wing} < 1$ cases, the planet is reaching the edge of the disk by the time the curves are cut off, and is roughly accreting its own mass in planetesimals, increasing its mass by a factor of 2.2 for all three shown. This correspondence can

be seen as the migration (and therefore the inverse of the accretion time available) being proportional to Σ , and the accretion rate being proportional to Σ , so that the total accretion by the edge of the disk is independent of Σ . Accretion continues at the edge of the disk where the planet stops, but slows down as in the relatively stationary $M_P/M_{wing} > 1$ cases.

5.9 Variation in the Hill radius and wing mass

The process of planetesimal accretion also changes the Hill radius ($R_H \propto M_P^{\frac{2}{3}}$) and the planet-wing mass ratio. The M0 and M1 runs demonstrate what happens when this ratio grows to values larger than 1.0, which is a slowing of the migration from that predicted by the fiducial rate by up to an order of magnitude. The ratio is also dependent on semi-major axis, and therefore will change even if no accretion occurs. The dependence is $M_P/M_{Wing} \propto M_P^{\frac{2}{3}}/a_P$ and so an inward migration will see an increase of the ratio due to the migration, as well as due to the accretion. This means that during a simulation, the position of the planet on the x-axis of figure 5.13 will change, and so will the migration rate.

Low mass ratios enjoy an independence of the migration rate on the M_P/M_{Wing} ratio itself, and thus can move along the x-axis without changing the migration rate. Mass ratios higher than one, however, will decelerate further as the ratio increases. The higher mass ratios will not tend to change their planet mass much, as they already outweigh their food supply as discussed in the previous section, but also do not change their a_P much. Indeed, the very highest mass ratios do not seem to have much of a dependence on M_P at all, in figure 5.13 showing the M1 runs. This means that only the runs with $M_P/M_{Wing} \sim 1$, which migrate over many Hill radii in 10^5

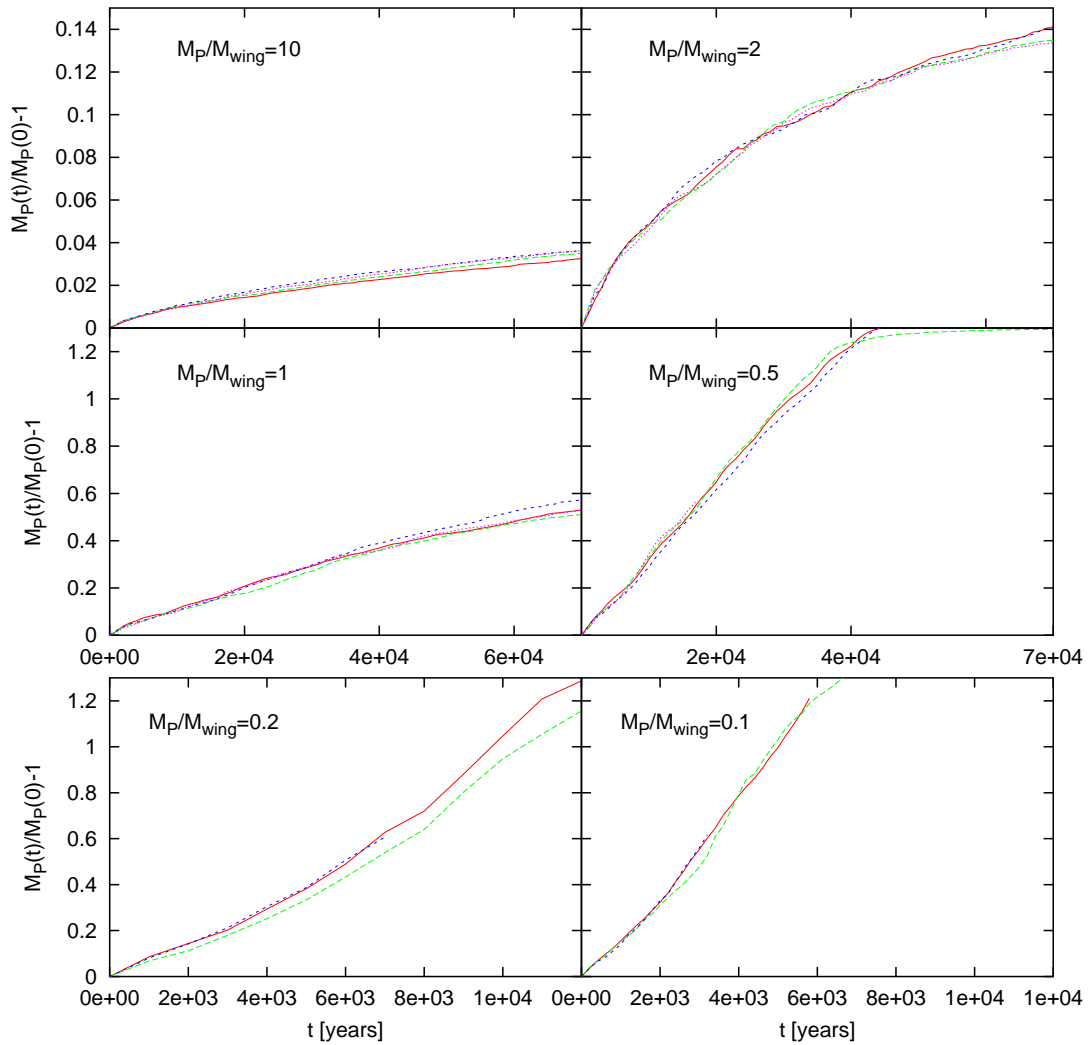


Figure 5.15: Change in the planet’s mass, relative to its initial mass of $4.5M_E$, for six values of M_P/M_{wing} taken from the M1 runs. The faster migrators, at the bottom, reach the edge of the disk before the end of the simulation.

years, will be able to vary their mass ratio by a substantial amount. This is where, in figure 5.13, the strongest trend is seen, and it may explain the faster-than-linear drop in the migration rate as a function of the mass fraction. This may also explain the oscillations seen in the migrations of these runs in figure 5.12, as the migration rate is continuously 'reset' by the ever-changing value of the mass fraction.

5.10 Self-heated initial conditions

The gap in the disk for $1R_H$ on either side of the planet in section 5.7 can be seen as modifying the initial conditions of section 5.3 (a smooth, dynamically cold disk) to reflect the sweeping up of material by the planet expected in the planet's formation stage. In this sense, however, the modification is incomplete, as the planet would not only accrete material, but it would excite material up the Jacobi wings and in the resonances (producing a dynamically hotter disk). Furthermore, several simulations thus far have shown a change of the migration phase after a few synodic periods, or upon leaving the initial gap region (see the M1 runs with $M_P/M_{Wing} \approx 1$). This is likely to be due to the M_P/M_{Wing} ratio changing after a short phase of accretion/migration, but especially in these runs the affect of the initial conditions is likely to be strong.

In order to remove the artificial situation of embedding a planet into a dynamically cold disk, a set of simulations to be referred to as M2 was run to duplicate the M1 runs of $M_P/M_{Wing} = (2, 1, \frac{2}{3}, \frac{1}{2}, \frac{1}{3})$ where the planet had self-heated the initial conditions. The initial setup was identical to the corresponding M1 runs (up to the randomized variables) except that the particle mass was reduced by a factor of 10^{-60} , with the Hill radii and physical radii therefore reduced by a factor of 10^{-20} . These 'massless'

simulations were run for 2×10^4 years (160 planetary orbits), the approximate relative synodic period (section 1.9) at the centres of the wings. The final output was then restarted with the proper mass (and Hill/physical radii) for the particles. Since particles were accreted or ejected during the massless phase, the actual initial particle number for the massive phase was lower than the corresponding M1 run by up to a thousand. The newly massive runs were then followed from the new time zero for 7×10^4 years, as in the M1 runs. Four runs were done for each mass ratio.

The resulting migrations are shown in figure 5.16, with the corresponding M1 runs accompanying them. The runs are for the most part indistinguishable, with two exceptions. The $M_P/M_{Wing} = 2$ runs show a slightly longer phase of initial migration, with the effect being that the planet penetrates further in to the disk before slowing. This may be due to the fact that, during the massless phase, the planet accreted ~ 300 particles that, had they been accreted during the massive phase, would've contributed $\sim 7\%$ more mass to the planet. As the planet was slightly less massive, it attained a faster/longer initial migration. This is also the case, but even more slightly, for the $M_P/M_{Wing} = 1$ runs. The second major difference is that more outward migrations were found for among the M2 runs than in the M1 runs. This is likely due to the wing mass imbalance being closer to the equilibrium value that the planet sets up. As in the M1 runs, the outward migrations are found at the high values of M_P/M_{Wing} (in fact the three highest are all 1 for 4 in this regard).

In case the initial heating phase was not long enough, one further run was generated for the $M_P/M_{Wing} = \frac{2}{3}$ case with a heating time of 10^5 years. The resulting migration once the particle mass was reset is also shown in figure 5.16: it is also indistinguishable from the M1 runs. This extra heating time was mostly unnecessary

as the approximate maximum $\tilde{\epsilon}$ in the Jacobi wings only increased from ~ 9 to ~ 12 during this time.

5.11 Surface density power law index

The inward migration of the planet is mostly predicated on the imbalance of scattering on either side of the planet, but this is also dependent on the particular power law that the disk's surface density follows. The majority of this work has focused on a surface density power law with $\Sigma \propto a^k$ where the index $k = -1$, but it is of interest to determine if changing the index can bring about an outward migration, and how the index is related to the actual migration rate.

Inevitably, changing the index will change several factors along with it. For very steep indices, the density will drop sharply over long migrations and this will also affect the particle resolution. Even the initial state is harder to define with regard to wing mass and disk extent. The decision was made to start from a given set of initial conditions and hold fixed the initial surface density at the planet's location, and the total mass of the disk. This means that the extent of the disk, and the exact local wing mass will vary. Furthermore, the mass of particles does not vary through the disk, and so particle resolution will be altered as the disk thins out. This thinning will occur on the side of the disk where there is less mass, however, and it is expected that the planet will generally migrate towards the other side, effectively increasing the particle resolution beyond the already-satisfied requirements.

The initial conditions chosen place a planet of mass $1.5 M_{Earth}$ at 35AU, with a disk mass of $M_{Disk}/M_{Sun} = 3.34 \times 10^{-3}$, such that for an index of $k = -1$ the disk extends $50R_H$ on either side, from 14.2AU to 55.8AU. The particle count was 1.5×10^5 , so the

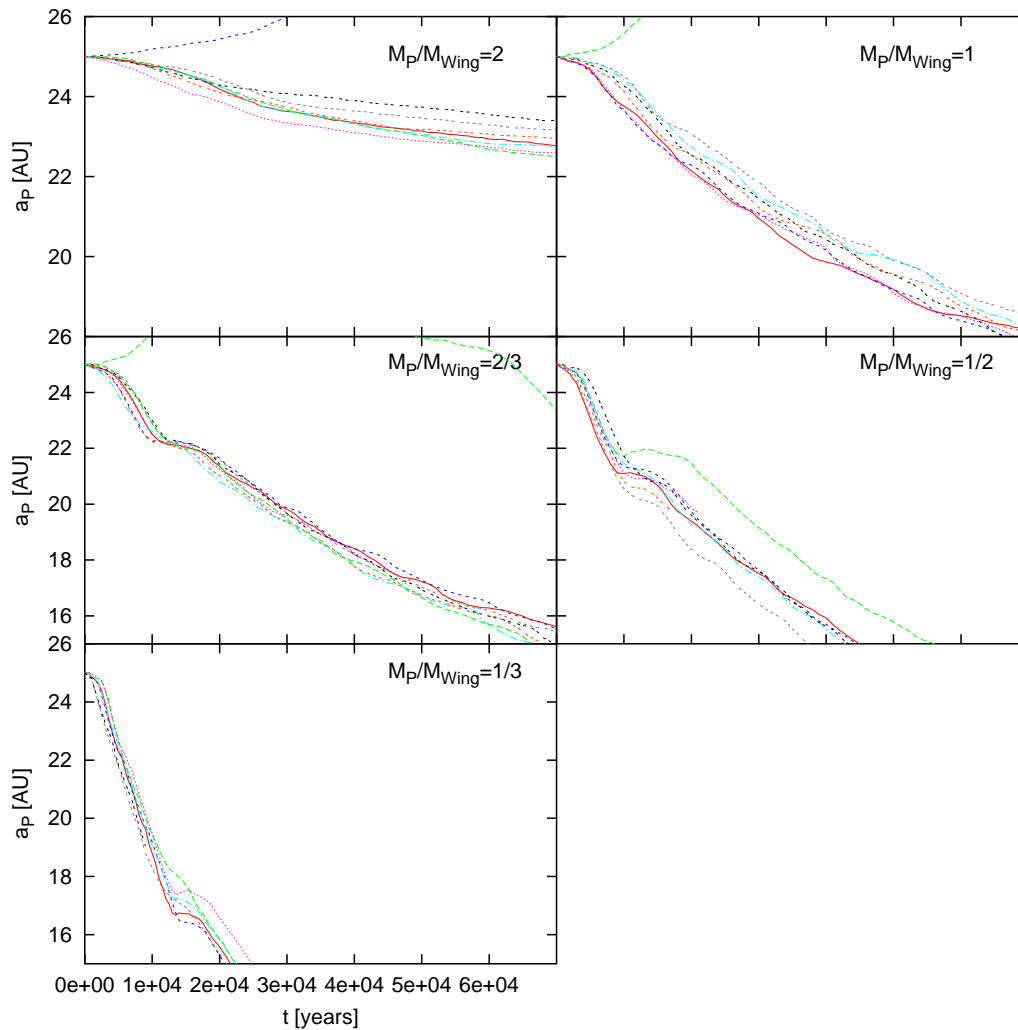


Figure 5.16: Migrations shown for the M2 runs, replicating M1 runs except for a period of massless heating before the migration was begun. The M2 runs are shown in red, green, blue and pink, while the M1 runs are shown in black, grey, orange and light blue. The inward green line for $M_P/M_{Wing} = \frac{2}{3}$ was heated for five times longer.

number per Hill radius in the $k = -1$ case was 1500, while $M_P/M_{\text{Wind}} = \frac{1}{5}$. This mass fraction would allow for a very linear migration in a $k = -1$ disk. The eccentricity and inclinations were set low, and the horseshoe region $\pm 1R_H$ was artificially emptied. The timestep chosen was 2 years, 1% of the planet's initial period. The simulations were run for 6×10^4 years, with an output interval of 1000 years. Four simulations were run for each value of the index, with that value varied from $k = -3 \rightarrow 4$.

In order to vary the index, the initial surface density was defined to be a power law of the form:

$$\Sigma = \Sigma_0 \left(\frac{a}{a_P} \right)^k \quad (5.30)$$

where the planet is initially located at a_P , and the surface density there is Σ_0 . Thus the total mass of the disk, extending from some inner semi-major axis a_1 to an outer semi-major axis a_2 , would be:

$$M = \int_{a_1}^{a_2} 2\pi a \Sigma da = \int_{\alpha_1}^{\alpha_2} 2\pi \Sigma_0 a_P^2 \alpha^{k+1} d\alpha \quad (5.31)$$

where α is a semi-major axis in units of a_P . This gives:

$$m_f = \frac{M}{\pi \Sigma_0 a_P^2} = \int_{\alpha_1}^{\alpha_2} 2\alpha^{k+1} d\alpha = \frac{2}{k+2} (\alpha_2^{k+2} - \alpha_1^{k+2}) \quad (5.32)$$

The next requirement is that the surface density at the planet be kept the same by keeping m_f on either side of the planet equal. Changing the limits of integration and equating the two sides, the last result becomes:

$$\frac{2}{k+2} (1 - \alpha_1^{k+2}) = \frac{2}{k+2} (\alpha_2^{k+2} - 1) \quad (5.33)$$

$$\alpha_2^{k+2} = 2 - \alpha_1^{k+2} \quad (5.34)$$

Putting this back into the result for m_f gives:

$$m_f = \frac{4}{k+2} (1 - \alpha_1^{k+2}) = \frac{4}{k+2} (1 + \alpha_2^{k+2}) \quad (5.35)$$

Defining $\frac{1}{4}m_f(k+2) = x$ allows us to solve for the limits of the disk that will satisfy these conditions:

$$\alpha_1 = (1 - x)^{\frac{1}{k+2}} \quad (5.36)$$

$$\alpha_2 = (1 + x)^{\frac{1}{k+2}} \quad (5.37)$$

The semi-major axis a_i of a particle i is then determined against their fractional position in the list of particles $i = 0..N$:

$$a_i^{k+2} - a_1^{k+2} = \frac{i}{N} (a_2^{k+2} - a_1^{k+2}) \quad (5.38)$$

thus laying them down between a_1 and a_2 . As mentioned earlier this means that the particle number is not equal on the two sides of the disk, and neither is the resolution. However, the planet generally migrates toward the higher resolution (and higher mass) side for cases where the resolution is strongly asymmetric (*i.e.* high- k values).

The migrations for indices of $k = 1$ and lower were primarily inwards, with a few exceptions, but for higher indices the migrations were entirely outwards. The migrations were clearly not linear (*i.e.* non-constant migration rates), except for the index $k = -1.5$, as could be predicted from the calculations of section 5.1.1. Nonetheless the initial fit employed was a simple line, fit from after the migration had started (~ 5000 years), until (at most) half of the migration timescale over which departure from a linear migration would be evident. The resulting migration rates in units of the fiducial rate showed a linear trend with the index, hinting that the simple linear fit is not good enough to estimate the migration rates even at their beginnings.

More accurate migration rates were determined by fitting directly with equation 5.20, with a single parameter multiplying the expected initial migration rate,

such that the equation takes the form:

$$a(t) = a_0 \left[1 \mp f(k + 0.5) \frac{\left| \frac{da}{dt} \right|_0}{a_0} t \right]^{\frac{-1}{k+0.5}} \quad (5.39)$$

and the expression $\frac{\left| \frac{da}{dt} \right|_0}{a_0}$ is that predicted by equation 5.17 as usual. This factor f is therefore the migration rate in units of the fiducial rate, the same factor that has generally been plotted. The rates are shown in figure 5.17 after least-squares fitting for this parameter for every migration. The average values of the factor f are shown for the inwards and outwards rates (although averaging all the values assumes there is no dependence on k) to be 2.8 and 2.1 respectively. The f factor being ~ 2.5 fits with previous cases where the migration is above the one-scatter limit, as all of these runs initially are.

The inward migrations are faster in general than the outward migrations by $\sim 34\%$, and are predominant when the surface density index is less than $k \sim +1$, with the outward migrations becoming the favoured direction at larger values. This is likely due to the asymmetry in the wing scattering, as discussed in section 4.5. Increasing the surface density index increases the relative mass in the outer wing as compared to the inner wing, which would change the relative mass of material scattered inwards or outwards by the planet. To explore the variation in the asymmetry with the index, the approximate initial masses of the planet's two wings were calculated for each index by counting the particle mass in zones interior and exterior to the planet's initial orbit. The inner zone was chosen to extend from $a_P - 1R_H$ to $a_P - 3R_H$. As can be recalled from section 1.8, a displacement of $3R_H$ interior corresponds to (from equation 1.26) approximately $3.2R_H$ exterior in order to find particles with identical Jacobi constants (and therefore scattering qualities). The mass in the outer zone was

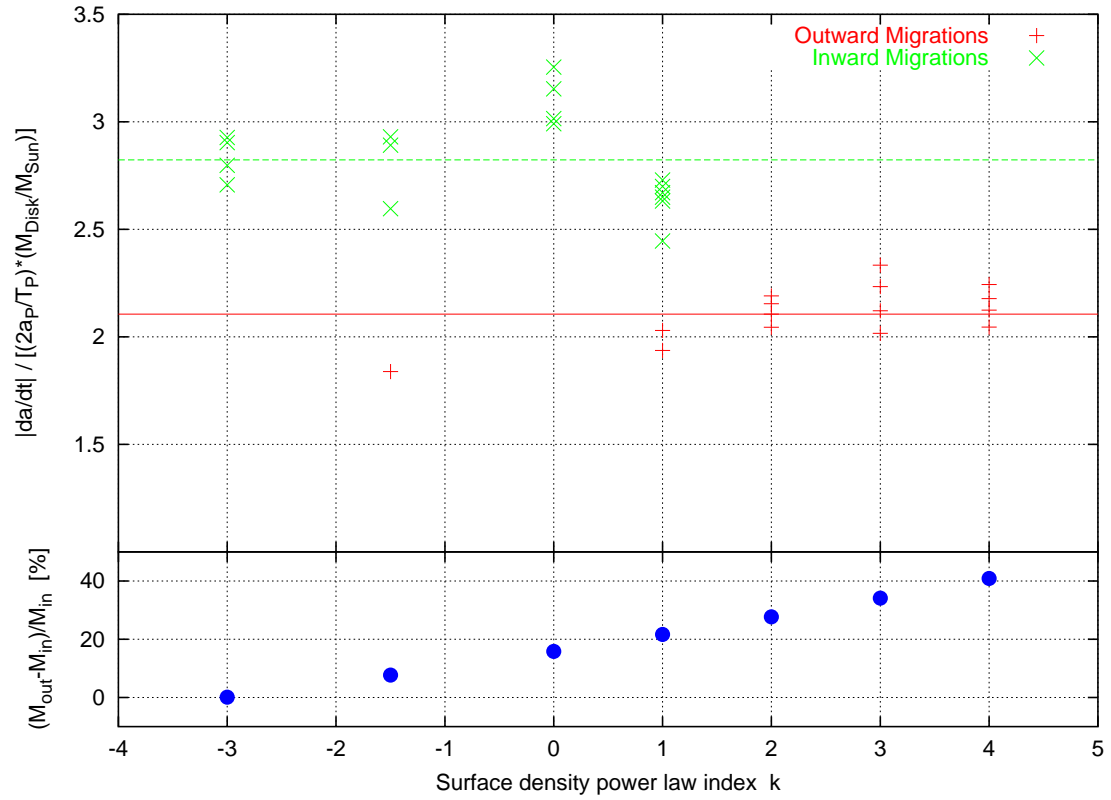


Figure 5.17: Migrations were fit with equation 5.39, using least-squared methods to determine the factor f . The factors are shown separately for the outwards and inwards migrations as a function of the surface density index k . The averages for each group are also shown as horizontal lines. The bottom panel also shows the initial mass difference between the wings as a function of k .

therefore measured from $a_P + 1R_H$ to $a_P + 3.2R_H$. The percentage difference between these two masses is also shown in figure 5.17.

The wing mass asymmetry that a planet of this mass would attain at equilibrium as identified in section 4.5 is around 20-30%, and this asymmetry is passed at around $k \approx +1$. As found in section 5.10 the planet migrates inwards even if the disk is initially heated to this asymmetry level. Evidently increasing the asymmetry beyond the equilibrium level overcomes the planet's preference to migrate inwards. Furthermore, the large asymmetry will remain throughout the migration for these high indices, making reversals of the direction unlikely. A run with $k = -1$ that lacked any material on the inside of the planet would suffer this asymmetry instantaneously, but migrating outward into the disk even slightly the asymmetry would quickly reverse, and so too would the migration direction itself. This is why previous simulations with the planet encountering the inner edge would normally see the planet remain stationary or wiggle, but would seldom see the planet migrate back out.

The migrations with the best fit to equation 5.39 are shown in figure 5.18 and figure 5.19. Also shown are two runs for $k = 3$ that were set up with an outer disk edge at 55AU and 65AU, requiring 235,536 and 535,536 particles respectively to keep all other conditions the same, but allowing much longer migrations. These runs further demonstrate the departure from linearity and the accuracy of the integrated- $n\sigma v$ calculation even for widely varied indices.

Bumps in the migration were seen in all the inward migrations for the indices $k = 0, 1$ at around 23AU and 25AU respectively. This was more than just the curvature predicted from the integrated- $n\sigma v$ calculation, and was likely due to the planet reaching the one-scatter limit at this point. The migration falls below the rate

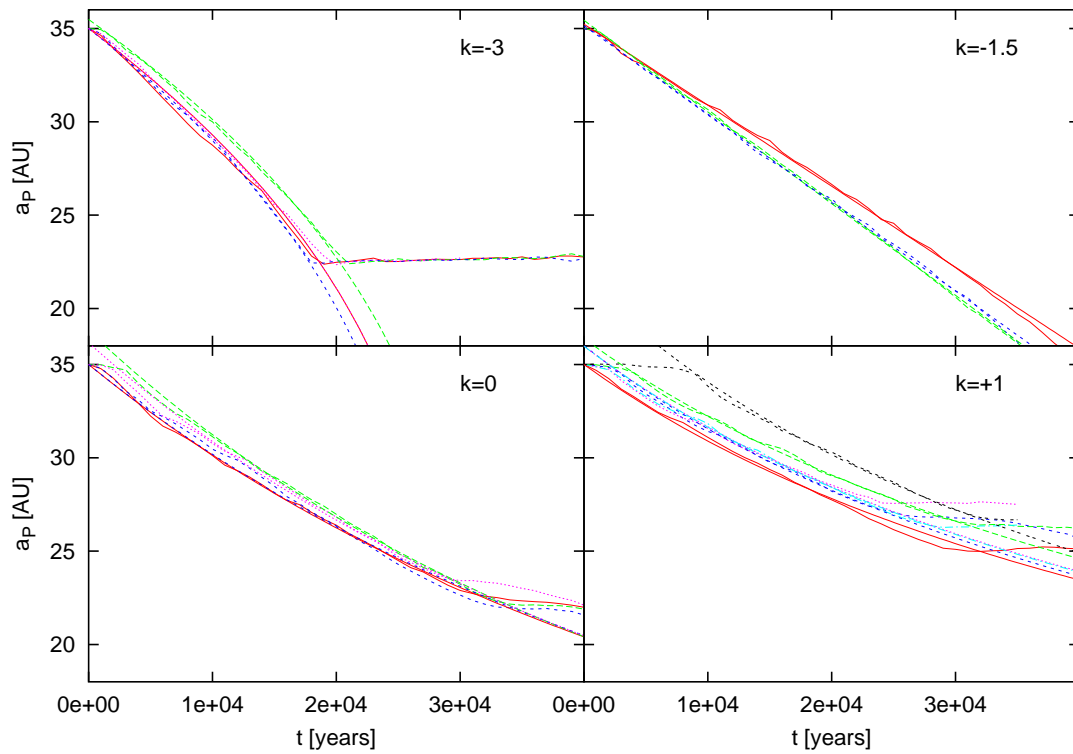


Figure 5.18: Migrations shown are for the inward-migrating cases with surface density power law index k indicated, and the best-fit line from equation 5.39 also shown. The $k = -3$ case breaks at the edge of the disk, while 'bends' are visible in the $k = 0$, $k = +1$ cases which are likely due to the migrations following below the one-scatter limit.

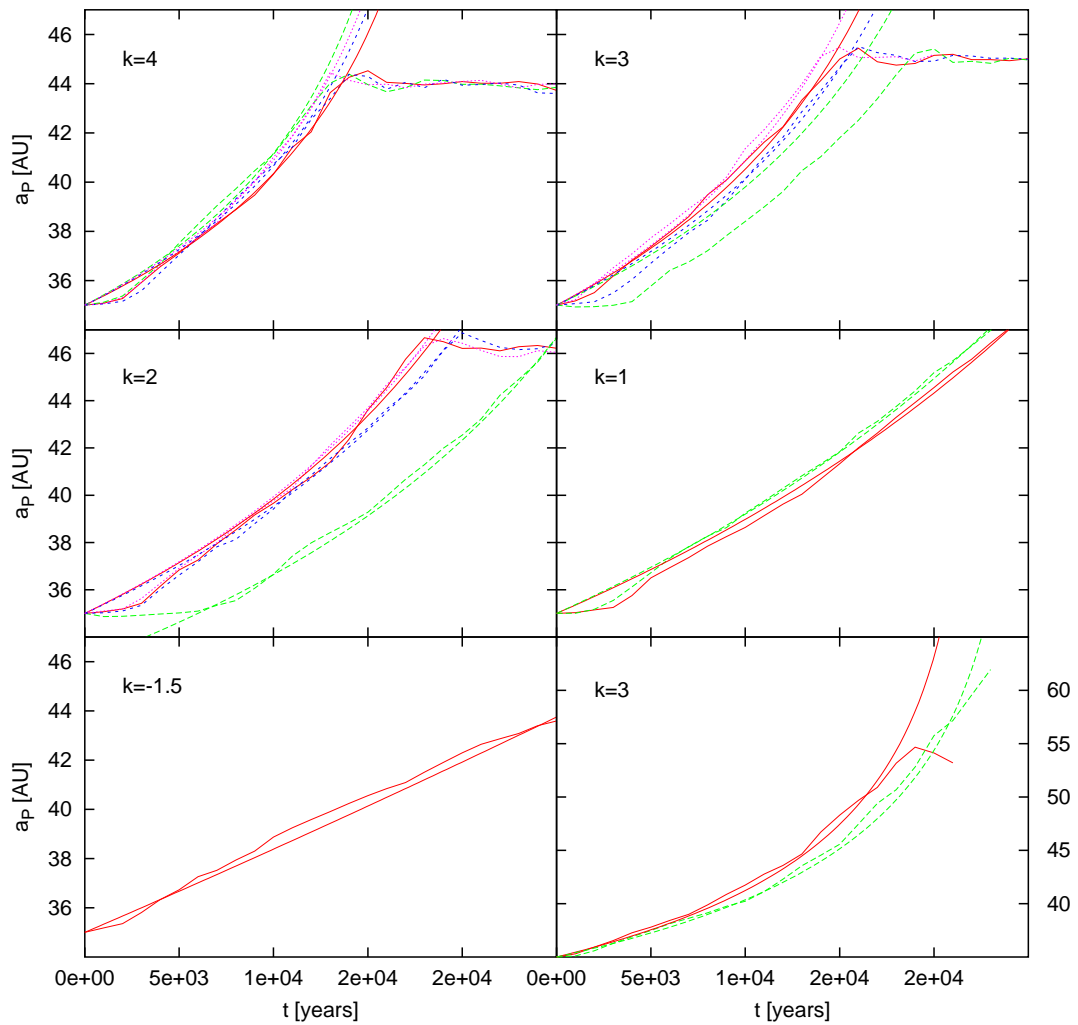


Figure 5.19: Migrations shown are for the outward-migrating cases with surface density power law index k indicated, and the best-fit line from equation 5.39 also shown. All breaks are due to the planet reaching the edge of the disk. The bottom-right panel shows two runs for $k = 3$ which had expanded disks to allow longer migrations.

required to scatter planetesimals only once a few thousand years before the break in the observed migration in both sets of runs. Another limit is also being reached near these breaks, however, as the M_P/M_{Wing} ratio is approaching 1 (it is close to 0.75 at the break) and this may be affecting the migration rate. The trend from the M1 runs (roughly fit by equation 5.28) implies that migration slows from the fiducial rate only once the mass ratio is *greater* than one, and so the bumps are likely due to crossing the one-scatter limit. All the other runs are faster than this limit throughout their migrations.

The M_P/M_{Wing} ratio for the outward migrations shows a substantial decrease over time, going down by a factor of 3.3 during the $k = 4$ runs. This is due to a dependence on planet mass and semi-major axis of $M_P/M_{Wing} \propto M_P^{\frac{2}{3}}/a_P^{2+k}$. It can therefore be expected that outward migrations for $k > -2$ would closely follow the prediction of the integrated- $n\sigma v$ calculation (as expected when $M_P/M_{Wing} < 1$) until the very edge of the disk, or some other interruption. This in contrast to the inward migrations in most cases, which see the M_P/M_{Wing} ratio rise, which would eventually slow or cease the migration entirely.

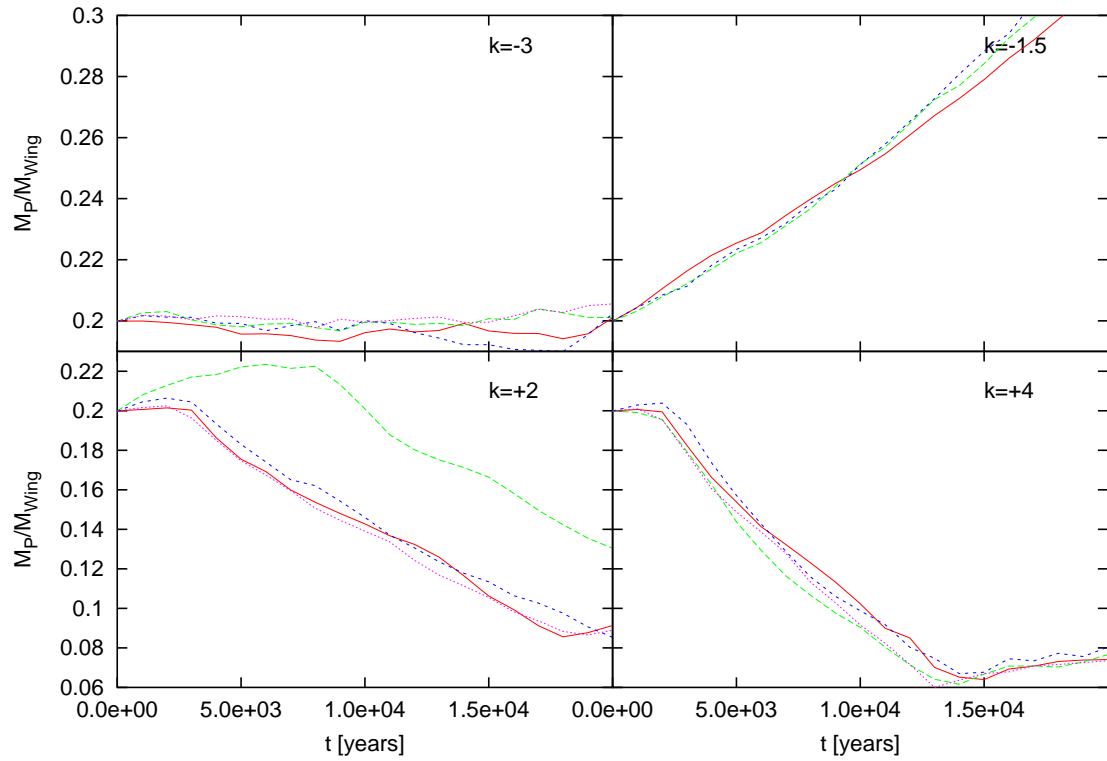


Figure 5.20: The ratio of the planet mass to the wing mass (calculated using $M_{wing} = 4\pi\Sigma_0 R_H a_P (a_P/a_0)^k$ for several runs with different surface density power law indices k . An increase in this fraction beyond 1 would tend to slow/damp the migration.

Chapter 6

Discussion and conclusions

Results have been discussed as they were developed throughout this work, especially for the various simulation sets. This chapter will summarize those results and restate the most important discoveries in an effort to give a complete picture of the migration of a planet in a planetesimal disk. The essential trends of the migration rate as a function of various physical quantities will be summarized starting with the simulations of last chapter. Next, several concepts that have reappeared throughout this work will be summarized, namely the resolution requirements of planetesimal scattering, the direction of migration that a planet will take in a given situation, and the effect of the one-scatter limit on migration. Lastly, future work that may focus on the numerous unsolved questions of migration will also be discussed.

6.1 Trends

Using several simulation sets, a wide parameter space was covered in the planetary migration problem, focusing on the variables identified in the fiducial rate of

equation 5.17 and its derivation: mass, eccentricity, semi-major axis and the surface density power law index. The fiducial rate itself is given by:

$$\left| \frac{da}{dt} \right|_{fid} = 2 \frac{M_{disk}}{M_{sun}} \frac{a_P}{T_P} \quad (6.1)$$

The results will be summarized now.

The masses in the problem turned out to be best expressed in three variables: $M_{disk} = \pi \Sigma a^2$ as an expression of the mass in the planetesimal disk; M_P/M_{wing} the ratio of the planet's mass to the mass in the planet's Jacobi wing, the fuel supply; and M_{wing}/M_{hs} the ratio of the wing mass to the mass in the horseshoe region. Three regimes were determined that linked the disk mass to the planet-wing mass ratio in the M1 simulation set in section 5.7. For high mass disks, or low mass planets, when the ratio is below 1.0, migration rate *does not* depend on the planet's mass, and is very constant at $\sim 1 - 2.5$ times the fiducial rate depending on if the migration is slower/faster than the one-scatter limit. This does not mean, however, that the migration *rate* is constant: it is proportional to the local disk mass. Therefore, as long as the planet is less massive than the material it can 'reach', in two bands of width $\sim 2R_H$ on either side of it, it will migrate near the fiducial rate.

When the planet is slightly more massive than its Jacobi wing, or $1 < M_P/M_{wing} < 10$, the migration rate is reduced from the fiducial prediction by a factor given by an approximate fit to be $\left(1 + \frac{1}{5} \left(\frac{M_P}{M_{wing}}\right)^3\right)$, but will nonetheless migrate over a substantial range. This drop in the migration rate bottoms out when the mass ratio comes close to $M_P/M_{wing} \sim 10$, at roughly $1/20^{th}$ the fiducial rate. At this speed, the planet was seen to migrate less than a Hill radius in 1600 orbits. Given billions of years it may move a few Hill radii, but the fact remains that even if it directly tossed *all* the available mass out of the system, it would be unable to move much more. The

exact form of this migration, be it at a constant rate (which it seemed to be over the simulation time) or exponentially damped, was not completely resolved over a migration timescale. Again it should be remembered that the actual migration rate was not a constant; lower mass disks produced slower migrations, but it was roughly constant in units of the fiducial rate.

The third variable, that of the mass ratio of the wing and horseshoe zones, was explored separately in the HS runs in section 5.5. For these runs only the mass in the horseshoe zone was varied. This was slightly unphysical, as a more reasonable regime has the two zones being roughly equal with the horseshoe zone perhaps more depleted from the actual formation process of the planet. The migration rate in units of the fiducial rate was found to be reduced by a factor of roughly $\left(1 + \left(\frac{M_{hs}}{2M_{wing}}\right)^2\right)$. When the ratio was approximately 1.0 the rate was therefore reduced by a factor of $\sim 10 - 20\%$, but in the most physical regime of a heavier wing, the horseshoe zone did not affect the migration strongly. It did delay the start of the migration by several synodic periods, however, an effect not seen in the M1 runs which had no horseshoes.

The root-mean-squared eccentricity e_{RMS} of the disk is also an important variable, as it can move the system from a shear-dominated to a dispersion-dominated regime, and in the latter case the migration rate has a definite dependence on e_{RMS} . The E0 runs explored this effect in section 5.4 by varying e_{RMS} (and setting the disk's root-mean-squared inclination to half of that value) for an otherwise unchanged system. The inclination was not investigated separately, but a heated disk should have $e \sim 2i$ in any case, and the effect of the two is tied as well (Ida and Makino, 1992 [16]). The migration rate was found to be reduced by a factor of $\left(1 + \left(\frac{e_{RMS}}{3\chi}\right)^3\right)$ where χ is the Hill factor, and therefore the critical variable is actually the Hill eccentricity. This

is roughly what was predicted by IBLT [15]. Therefore in the dispersion-dominated regime ($e/\chi > 1$) the migration rate will be reduced quite strongly.

In retrospect, the M0 runs of section 5.3 were tainted by having a constant eccentricity, meaning that the Hill eccentricity varied as the planet's mass was being varied. The one-scatter limit was also crossed at about the same mass ratio as $e/\chi \sim 1$, further confusing the issue. This created a bump in the trend (where the M1 runs had a flat line) at $M_P/M_{wing} < 1$ where the migration rate went up by a factor of ~ 2.5 as the planet mass was decreased and the migration crossed the one scatter limit, and then the rate reduced due to the higher values of e/χ at even lower planet masses. This suite does stand as a good example of several of these effects all varied together. Another interesting result from this suite which did not occur in the M1 suite (where there no horseshoe particles) was that the delay in migration beginning (*i.e.* the instantaneous rate reaching the final measured rate) had roughly the same dependence on the mass ratio as the migration rate itself did. This was presumably due to the loss of horseshoes required (and caused by the same scattering process as the migration itself) before the planet reached its final rate, but was not closely investigated.

Another critical parameter, the initial semi-major axis of the planet a_P , was investigated in section 5.6. This sets the timescale of scattering and migration, among other things, but it was found that the fiducial rate was an excellent descriptor of its contribution to the problem over a wide range of semi-major axes from 10AU to 80AU. However, the semi-major axis of the planet also influences the planet-wing mass ratio, and the one-scatter limit, meaning that it does have a more subtle effect than just that predicted from the fiducial rate, as it can push the planet into a different regime. This was seen especially in the M1 runs with a very high mass disk,

when breaks occurred in the migration as the one-scatter limit was crossed due to the change in a_P . The changing value of a_P is also extremely important in disks with a surface density that varies as a power law in semi-major axis, the index of which was explored in section 5.11.

The power law variation proved to be one of the more interesting analyses, as it crossed into the regime where the *instantaneous* value of the fiducial rate varied strongly within a migration timescale, and the fiducial value had to be integrated to give the actual form of the migration over the relevant timescale. The migrations were shown to fit very well to the predictions of the fiducial rate and the one-scatter limit, with the additional benefit of demonstrating reliably *outward* migrations could occur for steep enough power laws. Specifically, section 4.5 showed that the planet asymmetrically scatters particles to the outer wing, producing a mass imbalance. When the surface density was varied strongly enough to *overcome* this imbalance, placing more particles in the outer wing, the planet could not help but respond to the now-larger amount of mass crossing inwards by migrating outwards. As one of the few cases where outward migration was reliably obtained, this also allowed the determination that outwards migrations are slower than their inwards equivalents by $\sim 34\%$. This likely reflects the continuing preference of the planet to scatter material outwards, so that it is just as hard to migrate out as it is to *start* migrating out. Nonetheless, the form of the migration was remarkably well fit by the fiducial model, even for very steep surface densities, which again demonstrates the accuracy of the fiducial model to the variable a_P .

6.2 The interpretation of the fiducial rate

The success of the fiducial rate was at times very surprising: it is an extremely simple and approximate model to describe such varied circumstances. In this section the components of that toy model will be addressed once again in an effort to explain *why* it works so well, as well as what it means that it does.

The fiducial rate is fundamentally an *n σ v* calculation, saying that the planet sweeps out a zone as it orbits the sun and scatters the material in that zone. It assumed an angular momentum transfer with the planetesimal disk that was mostly based on scattering of particles on one side of the planet (the side it migrated towards), and causing them to cross to the other side. Along with only assuming an angular momentum exchange with *one* wing, it also assumed a scattering event that had no significant change in planetesimal eccentricity, and switched apocentre \rightarrow pericentre at the planet. As figure 1.2 showed, the apo/peri switch will underestimate the Δa of the crossing, and therefore the angular momentum change. Despite underestimating the Δa and the Δe , and ignoring the wing particles that don't cross and *completely* ignoring the other wing, the rate comes out to be within a factor of three of the actual rate for all observed cases where the wing (the fuel) outmassed the planet.

The success despite these approximations is likely due to the fact that the scattering has been underestimated, but the cross-section (taken from the Hill sphere) has also been underestimated, and does not include gravitational focusing. The wing the planet is not migrating towards can possibly be mostly ignored *because* the planet is moving away from it, and will probably miss many particles due to that, and will reduce the probability of strong encounters (which falls off with distance) as it moves. Meanwhile, particles that stay in the inner wing during an interaction will be moving

closer to the planet during the interaction simply due to its migration, and therefore will increase the probability of being strongly scattered.

The fact that the fiducial rate is proportional to the surface density makes intuitive sense, as the more mass there is in the disk the faster the planet should migrate. The fact that it is proportional to a_P/T_P is also not surprising, as this is the ratio of the length scale to the time scale. That it is not dependent on the planet mass is surprising, however, and is mostly due to the various quantities that scale with the Hill factor managing to make up for what otherwise would have been an inverse dependence on the planet's mass. Regardless, the simple calculation that is the fiducial rate has proved its worth not only as a hand-wavy estimate, but as a very close approximation. It will certainly be very useful for all future studies of planetesimal-driven planet migration.

6.3 Resolution

Previous work in planetary migration, as discussed in chapter 2, tended to use much lower resolutions than the standards that this work attempted to hold to. This was due to a lack of computer power, as well as the much longer timescales that they simulated. Nonetheless, resolution was shown to be a very critical issue throughout this thesis, as insufficient resolution caused very significant changes in migration rates, distances, and even the form of the migration itself.

Section 5.2 described the standards that were preferred for use in this thesis: about a thousand particles per Hill radius; and planetesimals less than $1/600^{th}$ the mass of the planet. While these standards were not always held to, they were very safe, and soft limits. The simulations in that section demonstrated that sub-resolution runs

as defined in this manner could often be very noisy, and might have bends in the migration not seen otherwise. Section 5.3, the M0 runs, demonstrated this when planets mass was varied in disks that were not being altered to accommodate the larger Hill radius, and were thus becoming unresolved in terms of particles per Hill radius. The resulting unresolved migrations did not bend enough after several synodic periods, and had greater dispersion in the measured migration rate. In section 5.7, the M1 runs, the very high values of M_P/M_{wing} showed very noisy migrations. These runs were 'resolved', but the planet was moving so little that the baseline resolution was not enough to completely characterize the wings, which would be required if a very smooth migration is at all possible in this situation. In section 5.5 an example was discussed where, in a low-resolution disk of only a couple hundred particles per Hill radius, the planet 'hit' its wing once it began migrating, an effect which was not seen once the disk was better-resolved. This was a very large effect indeed, reversing the migration direction after a few thousand years of the planet not migrating at all. This dramatically different result occurred despite the migration not appearing very noisy. Furthermore, 215 particles per Hill radius would not immediately *seem* to be a terribly unresolved value. Apparently the effects of low resolution can be surprisingly potent.

If large changes in the form of migration are possible in only *slightly* unresolved systems, than this draws into question the 'excursions' seen in previous, largely under-resolved works such as Gomes, Morbidelli and Levison (2004) [8]. These were migrations of $\sim 30AU$ in a million years or so, but they were overlaid on a much slower migration mode. This was the Solar System model, however, where a slower mode of migration may be due to the effect of Jupiter on the other planets. Indeed, a

quick calculation shows that the excursions match within an order of magnitude the prediction of the fiducial rate for their disks. The disk in this situation had only ~ 175 particles per Hill radius, with a value of $M_P/M_{wing} \sim 4$, so they are under-resolved, but as they extended over 40 million years it would be difficult to do them any better to confirm these excursions as real. This means that, while the migration itself is likely within the predictions of this thesis, whether or not it would have *begun* migrating in a well-resolved disk is a valid question. Another simulation set they presented showed a planet migrating outwards which experienced repetitive and short-lived pauses. This may have been a variation on wing hitting as described in the last paragraph, which may be eliminated with higher resolution.

The stringent requirements of resolution are difficult to match in a variety of mass and time regimes, and are sure to be a touchy subject in future studies of planetesimal-driven migration. Nonetheless, this work has shown that it is often surprisingly important to have a fully-resolved system.

6.4 Migration direction

Throughout this thesis, planet migrations almost always tended to draw the planet *closer* to the sun. Indeed, only a few special cases managed to reverse the direction of migration. Previous work had not assumed that any direction would be preferred for an isolated planet, and indeed the Solar System model, with a Jupiter-mass body inside the orbits of the other migrating planets, tend to produce outward migrations. The Solar System case became the default, and thus the consistently-inwards migrations of this thesis are a surprise.

Section 4.5 showed that a bias exists in the circular restricted three-body problem

such that more particles end up in the outer wing than in the inner wing over many synodic periods. Initially, a bias exists due to the outer wing being wider and therefore containing more mass, but the final asymmetry in wing mass triples the initial value. As the strongest angular momentum exchange is with planetesimals that cross the planet's orbit, and the planet will move in the direction opposite to the crossings, this means that the planet will move inwards if the planetesimals have any mass. The asymmetry was shown to grow with the planet's mass (and therefore its Hill radius and wing extent). Therefore while very small planets may be able to be perturbed and migrate outwards due to, say, only having a 1% difference bias, larger planets have a stronger bias and for the Earth (with a 10% bias) to migrate outwards, a very strong perturbation would have to occur, and this is unlikely to occur physically in a one-planet system (although it could commonly occur in an unresolved simulation). Even when started from a disk that has already been dynamically heated by the planet (section 5.10), the strong bias remains, although the perturbation required to push it outwards appeared to be smaller (outward migrations occurred more frequently than usual in these runs).

The bias will not only be present at the planet's initial position, but at all points along its migration. This means that it would have to overcome the bias not once, but consistently. In under-resolved simulations where the planet did start migrating outwards, it often turned around, but not always. Once it starts migrating, it is likely that the bias is actually reduced by the motion of the planet towards the wing that is acting as fuel. After it initially overcomes the bias, it is closer to the outer wing, giving those particles a higher probability of crossing, and this may self-consistently allow the migration to continue outwards. However, the simulations of section 5.11,

where the surface density power law was varied, show that in cases with outward migration, the outwards rates were $\sim 34\%$ less than what the inward rate would be. This shows that the bias is indeed still there at every instant, and while the planet may be able to continue migrating in the face of it, there will be a price paid in migration rate.

The bias also explains what will happen at the edge of the planetesimal disk, or at gaps in the disk, as discussed in section 5.3.1. For a planet at the inner edge of a disk, with planetesimals only on the outside of its orbit, it often stays put instead of migrating outwards. This may be because, while it will be perturbed outwards, it may just as quickly turn back, and in the end it may not be able to migrate far from that inner edge. However, examples were seen with the planet rebounding from the inner edge after migrating inwards, so this situation is slightly more complex than it appears. For example, it may be that some cases with very fast migration have the planet virtually thrown from the disk, moving too far inside to effectively reach many planetesimals. At the outer edge of the disk, however, it is safe to say that the planet will eventually migrate inwards. Similar logic could be applied to gaps opened up about the planet, as that section showed. An interesting case, meriting further study, was discovered where a gap of $4R_H$ on the inside of the planet (*i.e.* no interior wing) and $2R_H$ on the outside caused the planet to migrate consistently outwards. This simulation was under-resolved, but an interesting departure from predictions.

The exact cause of the bias remains somewhat of a mystery. A simple ratio of synodic periods (as discussed in section 4.5) does not match the results. Indeed, if it was simply due to relative synodic periods then the outer wing (which is farther from the planet on average) would tend to have more frequent conjunctions than the inner

wing, and this could create *outwards* migration if every conjunction produced a strong encounter. However, the outer wing moves to a higher e than the inner, and at high e the actual scattering *probability* per conjunction is reduced. Thus the interaction timescale is longer in the outer wing (see figure 4.6), despite having a shorter synodic period. The increase of timescale may cause a pile-up of material in the outer wing. This hypothesis is difficult to test analytically, as the synodic period is a function that varies across the wing and over time, even for individual particles, and the effect of e on the interaction timescale is not easy to characterize either. Nonetheless, the result remains: an isolated planet is biased to inwards migration.

6.5 The one-scatter limit

A migration rate was suggested by IBLT [15] and explored in section 5.1.2, above which the planet only scatters material once. For this to occur, it would have to cross the scattering region ($\sim 2R_H$ wide) within the synodic period at that maximum distance, giving: $\left.\frac{da}{dt}\right|_{1scat} \approx 7.5\chi^2 a_P^{-\frac{1}{2}}$. This rate came to be an important quantity, causing two distinct migration modes in most of the M1 runs and partially creating the bump in the M0 trend. However, it did not seem to have much of an effect beyond reducing the migration rate from ~ 2.5 times the fiducial value when *above* the limit to ~ 1.0 times the fiducial value when *below* the limit.

In section 5.3.3, the M^e runs where the eccentricity of the disk was raised to $e \approx 2\chi$, the trend of migration rate with planet mass showed no change at the one-scatter limit, unlike the case with $e \ll \chi$. This implies that the one-scatter limit is only important in shear-dominated disks.

Below the one-scatter limit a planet will interact more than once with a fraction

of its wing planetesimals. How large a fraction depends on how far below the limit it migrates (indeed, there could be a two-scatter limit, and a three-scatter, and so forth). As the second interaction will tend to transfer crossed particles *back across* to their original wing, undoing much of the effect of the first scattering, this implies that the higher the fraction, the slower the migration would proceed. Therefore, slowing of the migration caused by crossing the limit could feed back on itself, and damp the migration rate. This was not seen, however, as runs under the limit seemed to continue at a constant migration rate.

After the first synodic period, planetesimals will be at higher e than in the first (assuming an initially cold disk; this is not necessarily true in an initially hot disk). Assuming the planet has migrated due to scattering across its orbit the population of interest, they will also have been left behind, and therefore at a larger C_T . Both of these factors reduce the probability of scattering in the second synodic period. However, at the planetesimals' larger distances, the 'second' synodic period is in fact much shorter than the first originally was. Perhaps, then, the simple reduction in the constant migration rate is due to the fact that only some of the planetesimals manage to have a second scattering event after their first, and this fraction will be sustained self-consistently by the migration and scattering of the planet.

Crossing the one-scatter limit changes the planet's scattering in a complex way, but changes the actual migration rate in a simple way. This is an intriguing piece of the puzzle of planet migration that will remain incompletely understood for now. The next section will discuss several other such pieces, and how this puzzle will continue to be of interest for some time to come.

6.6 Future work

This thesis has presented a parameter space survey of planetary migration in planetesimal disks, primarily focusing on the regime where the planet migrates in a very smooth and stable manner. For low-mass disks or high-mass planets, where $M_P/M_{wing} \gg 1$, the migration is very noisy, and small, and we are still not certain what the exact form is for the long term behaviour of the migration rate. Part of the problem is that the largest migration in this regime occurs in the first synodic period, where the mode is certain to be different. The regime of interest, after everything has been scattered once, does not produce much migration and therefore it is difficult to fit. To investigate this further, longer migrations at very high resolution will be required. An analytic prediction for migration slower than the one-scatter limit, possibly an exponential, would also be useful. The slow-migration regime is therefore the most important mode of migration remaining relatively unsolved in the isolated planet case.

The cause of the dominance of inward migration, what has been referred to as a bias, imbalance or asymmetry throughout this work, is also not completely understood. This will require more analytic work, likely combined with the simulation results of chapter 4 for massless particle scattering. A complete understanding of the mechanism that determines the migration direction is obviously critical.

Taking this work to a level that is perhaps more applicable in the physical sense would require the introduction of multiple planets. In particular, the Solar System model would be useful to study in the context of the results of this paper, but as discussed previously it is difficult to properly resolve this very long-timescale case. The effect of a second planet of varied mass and placement on the migration of

another planet would be a fascinating study, as would the more general effect of multiple planets all migrating together. Previous works have found interesting effects from strong interactions among the planets (*e.g.* Thommes *et al.*, 1999 [29], Tsiganis *et al.*, 2005 [32]), and it has already been seen in the Solar System model that Jupiter is a strong influence and can funnel planetesimals to and from the other planets (Safronov, 1969 [27]), but what of similar-mass protoplanets interacting at long range during migration? Could this be factored into the simple fiducial model?

The epoch of this migration would also be interesting to vary: protoplanets are forming while there is still much planetesimal-planetesimal interaction of interest, and while there is still a gas disk. Adding gas drag on the planetesimals, and perhaps gas-phase migration to the planets, would add a new level of applicability to the concepts presented here. Adding fragmentation and non-uniform masses to the planetesimals would also be useful in this regard.

Many questions remain in planetesimal-driven planet migration, and not all of the regimes investigated in this work are yet completely understood, so future work in this area should have much to choose from in terms of focus. This process is an essential phase of planetary system formation, and while this work has brought it to a much higher level of resolution and understanding in the case of a single planet, there is still much that can be learned.

Bibliography

- [1] A. P. Boss. Formation of Planetary-Mass Objects by Protostellar Collapse and Fragmentation. *ApJ L.*, 551:L167–L170, April 2001.
- [2] A. Carusi, G. B. Valsechi, and R. Greenberg. Planetary close encounters - Geometry of approach and post-encounter orbital parameters. *Celestial Mechanics and Dynamical Astronomy*, 49:111–131, 1990.
- [3] M. J. Duncan, H. F. Levison, and M. H. Lee. A Multiple Time Step Symplectic Algorithm for Integrating Close Encounters. *AJ*, 116:2067–2077, October 1998.
- [4] J. A. Fernandez and W.-H. Ip. Some dynamical aspects of the accretion of Uranus and Neptune - The exchange of orbital angular momentum with planetesimals. *Icarus*, 58:109–120, April 1984.
- [5] B. Gladman. Dynamics of systems of two close planets. *Icarus*, 106:247–+, November 1993.
- [6] P. Goldreich and S. Tremaine. The dynamics of planetary rings. *Annu. Rev. Astron. Astrophys.*, 20:249–283, 1982.
- [7] R. S. Gomes. The origin of the Kuiper Belt high-inclination population. *Icarus*, 161:404–418, February 2003.

- [8] R. S. Gomes, A. Morbidelli, and H. F. Levison. Planetary migration in a planetesimal disk: why did Neptune stop at 30 AU? *Icarus*, 170:492–507, August 2004.
- [9] J. M. Hahn and R. Malhotra. Orbital Evolution of Planets Embedded in a Planetesimal Disk. *AJ*, 117:3041–3053, June 1999.
- [10] K. E. Haisch, Jr., E. A. Lada, and C. J. Lada. Disk Frequencies and Lifetimes in Young Clusters. *ApJ L.*, 553:L153–L156, June 2001.
- [11] C. Hayashi. Structure of the Solar Nebula, Growth and Decay of Magnetic Fields and Effects of Magnetic and Turbulent Viscosities on the Nebula. *Progress of Theoretical Physics Supplement*, 70:35–53, 1981.
- [12] M. Henon. Numerical exploration of the restricted problem, V. *Astron. Astrophys.*, 1:223–238, February 1969.
- [13] M. Henon. Numerical exploration of the restricted problem. VI. Hill’s case: Non-periodic orbits. *Astron. Astrophys.*, 9:24–36, November 1970.
- [14] G. W. Hill. Researches in the lunar history. *Am. J. Math.*, 1:5–26,129–147,245–260, 1878.
- [15] S. Ida, G. Bryden, D. N. C. Lin, and H. Tanaka. Orbital Migration of Neptune and Orbital Distribution of Trans-Neptunian Objects. *ApJ*, 534:428–445, May 2000.
- [16] S. Ida and J. Makino. N-body simulation of gravitational interaction between planetesimals and a protoplanet. I - Velocity distribution of planetesimals. *Icarus*, 96:107–120, March 1992.

- [17] S. Ida and J. Makino. Scattering of planetesimals by a protoplanet - Slowing down of runaway growth. *Icarus*, 106:210–+, November 1993.
- [18] E. Kokubo and S. Ida. Orbital evolution of protoplanets embedded in a swarm of planetesimals. *Icarus*, 114:247–257, April 1995.
- [19] R. Malhotra. The Origin of Pluto’s Peculiar Orbit. *Nature*, 365:819–+, October 1993.
- [20] M. Mayor and D. Queloz. A Jupiter-Mass Companion to a Solar-Type Star. *Nature*, 378:355–+, November 1995.
- [21] D. McNeil, M. Duncan, and H. F. Levison. Effects of Type I Migration on Terrestrial Planet Formation. *AJ*, 130:2884–2899, December 2005.
- [22] C. D. Murray and S. F. Dermott. *Solar System Dynamics*. Cambridge University Press, Cambridge, UK, 1999.
- [23] N. Murray, B. Hansen, M. Holman, and S. Tremaine. Migrating Planets. *Science*, 279:69–+, January 1998.
- [24] E. J. Opik. Collision probability with the planets and the distribution of planetary matter. *Proc. R. Irish Acad. Sect. A*, 54:165–199, 1951.
- [25] E. J. Opik. *Interplanetary encounters : close-range gravitational interactions*. Amsterdam ; New York : Elsevier Scientific Pub. Co., 1976., 1976.
- [26] J. B. Pollack, O. Hubickyj, P. Bodenheimer, J. J. Lissauer, M. Podolak, and Y. Greenzweig. Formation of the Giant Planets by Concurrent Accretion of Solids and Gas. *Icarus*, 124:62–85, November 1996.

- [27] V. S. Safronov and E. V. Zvjagina. Relative Sizes of the Largest Bodies during the Accumulation of Planets. *Icarus*, 10:109–+, January 1969.
- [28] P. Saha and S. Tremaine. Symplectic integrators for solar system dynamics. *AJ*, 104:1633–1640, October 1992.
- [29] E. W. Thommes, M. J. Duncan, and H. F. Levison. The formation of Uranus and Neptune in the Jupiter-Saturn region of the Solar System. *Nature*, 402:635–638, December 1999.
- [30] E. W. Thommes, M. J. Duncan, and H. F. Levison. Oligarchic growth of giant planets. *Icarus*, 161:431–455, February 2003.
- [31] S. Tremaine. Resonant Relaxation in Protoplanetary Disks. *AJ*, 116:2015–2022, October 1998.
- [32] K. Tsiganis, R. Gomes, A. Morbidelli, and H. F. Levison. Origin of the orbital architecture of the giant planets of the Solar System. *Nature*, 435:459–461, May 2005.
- [33] G. W. Wetherill and G. R. Stewart. Formation of planetary embryos - Effects of fragmentation, low relative velocity, and independent variation of eccentricity and inclination. *Icarus*, 106:190–+, November 1993.
- [34] J. Wisdom and M. Holman. Symplectic maps for the n-body problem. *AJ*, 102:1528–1538, October 1991.

Appendix A

Supplementary information

A.1 Maximum eccentricity change

The distribution of eccentricity changes in figure 4.8 showed a peak and an upper limit at $\Delta e \sim 6\chi$ that seemed to reflect a maximum possible eccentricity change. To explore this, several dynamical results from the literature will be used. To begin, the planetesimal being scattered will be assumed to keep its pericenter fixed at the planet $q = a(1 - e) = a_P$, and this gives an eccentricity of:

$$e = 1 - \frac{a_P}{a} \tag{A.1}$$

and so the change in eccentricity will be:

$$|\Delta e| = a_P \Delta \left(\frac{1}{a} \right) \tag{A.2}$$

The energy change in an orbit, from Öpik (1976) [25] is proportional to the change in $1/a$, which can be expressed as:

$$\Delta \left(\frac{1}{a} \right) \approx \frac{2U}{a_P} \sin \gamma \tag{A.3}$$

where U is a dimensionless relative velocity that can be expressed as (from Cursi *et al.* 1990 [2]) $U = \sqrt{3 - C_T}$, and γ is a scattering angle. To obtain the highest relative velocities, the particles farthest from the planet are desired. Using the value of the Tisserand parameter at approximately the maximum extent of the feeding zone, from Henon (1969 [12], 1970 [13]):

$$C_T^{max} \approx 3 + 3^{\frac{4}{3}} \mu^{\frac{2}{3}} \quad (\text{A.4})$$

where μ is the mass ratio of the planet to the sun. This gives the highest relative velocity:

$$U_{max} \approx 3^{\frac{2}{3}} \mu^{\frac{1}{3}} \quad (\text{A.5})$$

Now, for the strongest scattering, the angle $\gamma \sim \frac{\pi}{2}$ which finally gives

$$|\Delta e| \approx 2 \frac{a_P}{a_p} 3^{\frac{2}{3}} \mu^{\frac{1}{3}} = 6\chi \quad (\text{A.6})$$

which approximately matches the observed maximum eccentricity change.